Predictability and Dynamics of Potential Vorticity Streamers and Connections to High Impact Weather

Arwen Fay Twitchett

Submitted in accordance with the requirements for the degree of
Doctor of Philosophy

The University of Leeds
School of Earth and Environment
January 2012

Declaration of Authorship

The candidate confirms that the work submitted is her own, except where work which has formed part of jointly-authored publications has been included. The contribution of the candidate and the other authors to this work has been explicitly indicated below. The candidate confirms that appropriate credit has been given within the thesis where reference has been made to the work of others.

Section 6.4 contains work from the publication Wiegand, L., Twitchett, A., Schwierz, C. & Knippertz, P., 2011. Heavy precipitation at the Alpine south side and Saharan dust over central Europe: A predictability study using TIGGE. *Weather and Forecasting* **26**: 957:974. Section 4 and 5c of the paper was prepared by A. Twitchett (including Figure 4) the remaining text and figures were done by Wiegand, L. with comments from all co-authors.

Section 6.3 contains work from the publication Schlemmer, L., Martius, O., Sprenger, M., Schwierz, C. & Twitchett, A., 2010. Disentangling the forcing mechanisms of a heavy precipitation event along the Alpine south side using potential vorticity inversion. *Monthly Weather Review*, 138: 2336-2353. Section 3b of the paper was prepared by A. Twitchett while the majority of text and figures were done by Schlemmer, L. with comments from all co-authors.

The right of Arwen Fay Twitchett to be identified as Author of this work has been asserted by her in accordance with the Copyright, Designs and Patents Act 1988.

Acknowledgements

I would like to express great thanks to my supervisors Conny Schwierz (for getting me started) and Peter Knippertz (for keeping me going) during my time at Leeds. Their continued guidance and support throughout the production of this thesis was sincerely appreciated. Additionally, I would like to thank Doug Parker and Michael Morgan for their help and support over the past few years.

Thank you very much to Olivia Martius and Heini Wernli for data input and use of their existing programs. I would also like to acknowledge the NERC for the funding support they provided.

To all the members of the department in Leeds who always made coming in to work so enjoyable, in particular Helen, Laura, Matt, Tom, Rosey, Cathryn, Tor, and Verity, thank you all for the many fun times we had.

I would like to say a very special thank you and dedicate this work to my family, Barry and my parents who have helped along the way, supported and encouraged me and especially to Caitlin and Jamie who were both born during this PhD and had to give up a lot of "Mommy time" so that I could finish my work!

Abstract

Narrow potential vorticity (PV) intrusions across the tropopause (PV streamers) are interconnected with surface high- and low- pressure systems and frequently present during high-impact weather in the mid-latitudes. They often form during the breaking of Rossby waves (observed as large meanders of the jet stream), and occur at the end of the wave life cycle. Extreme weather events are likely to increase in the future due to global warming and climate change, so, enhanced knowledge about the main influences on these events is crucial for early warning systems.

This thesis explores the location and relationship between upper- (troughs and PV streamers) and lower- (cyclones and anticyclones) level features impacting the United Kingdom during heavy precipitation days. It then investigates the genesis of preceding Rossby waves and initiation of PV streamer formation related to heavy precipitation cases. Finally, the predictability of these features is analysed through an assessment of forecasting skill in the European Centre for Medium-Range Weather Forecasts (ECMWF) deterministic models as well as the THORPEX Interactive Grand Global Ensemble (TIGGE) prediction system through the use of a novel feature-based error method.

Stratospheric PV streamers were found to be present during UK heavy precipitation cases 88% of the time in summer, 85% in autumn, 72% in spring and 63% in winter. They are the dominant influence on heavy precipitation for the UK in summer as well as in autumn in combination with cyclones. Cyclones are located to the north-west of the UK during all of the seasons with highest frequency in winter and least in summer. Anticyclones also have an impact on UK precipitation by steering systems further north in the winter. The results vary regionally, with western and northern areas characterized by orographic influences. Eastern Scotland has the most consistent pattern of stratospheric streamer involvement, and the combination of upper-level and orographic effects create uplift of moist air leading to heavy precipitation events. Remarkably, spring has the most variance in the distribution of upper- and lower-level features with evidence of a distinct east/west split across the country. Cyclone and anticyclone pairings dominate in the west, while stratospheric and tropospheric streamer coupling enhances precipitation in the east.

Rossby waves preceding the events are triggered from 3 to 7 days in advance, with some seasonal variations. The trigger points range from the Pacific Ocean basin, throughout North

America to the western Atlantic Ocean. The waves then proceed across the North Atlantic, where PV streamers are initiated. Triggers located to the west (or behind) the PV streamer lead to enhanced ridges and LC1 or anticyclonic streamer types, while triggers to the east (ahead of the streamer) increase the likelihood of LC2 or cyclonic streamer types. Influences to the east are the most common form of trigger closely followed by streamers forming from recirculated stratospheric air (for example when a parcel of air re-attaches to the stratosphere).

PV streamers are generally represented well in short forecast lead times (1-2 days) with a growth in structural and location errors as lead time increases. An interesting result of the feature-error method was the identification of significantly lower PV mean and maximum amplitudes (by as much as -3.5PVU) especially in the upper eastern flank of the streamer. This could be due to insufficient influx of high PV air into the streamer and would benefit from further investigation. In associated heavy precipitation forecasts, TIGGE ensemble members with more accurate rainfall prediction have consistently better PV streamer representation than those who under-predicted the precipitation. The evidence indicates that improved understanding and prediction of PV streamers can lead to better predictability of heavy precipitation and thus an enhancement in early warning systems.

Contents

List of Figures

List of Tables

Chapter 1

Introduction

1.1 Background and focus

Atmospheric Rossby waves propagate along the potential vorticity (PV) gradient at the tropopause and are observed as large-scale undulations of the mid-latitude jet stream. As the waves propagate, ridges and troughs form which are associated with high and low pressure systems, contributing to daily weather. Wave breaking corresponds to PV streamer formation (stratospheric air extending southward or tropospheric air extending northward (Appenzeller and Davies, 1992)) and this can lead to high-impact weather such as heavy precipitation events (Martius et al., 2006a).

Rossby waves have been studied ever since the 1940's when Carl Gustav Rossby first identified them and explained their movement. Since then, a variety of aspects of the waves have been investigated such as waveguides, propagation, energy diagnostics, and breaking. By further studying the dynamics of the waves a greater understanding of how they are triggered, how they propagate, and when the waves break and form streamers, can be discovered. This information can then be implemented into forecast models in order to aid in the prediction of the waves and the subsequent streamers. The main aim of this project is to further understand dynamical features of Rossby waves such as triggers and links to heavy precipitation events and to better predict Rossby wave breaking and streamer formation in forecast models and the high-impact weather events they induce.

1.2 Motivation

Extreme weather events are becoming more frequent due to the effects of climate change with increased loss of life and economic consequences (Field et al., 2011) The ability to predict when and where extreme events will occur is important for early warning systems. High-impact weather events occur across the globe, and many of these events are linked to upper-level circulation dynamics. Enhanced wave activity can cause downstream cyclone development or create large-scale ridge-trough patterns which trigger weather patterns leading to flooding or drought conditions. For instance, the extratropical transition of Typhoon Tokage caused a deep trough to form over the northwestern United States which was responsible for heavy coastal rains and mountain snows in California on the 20th of October 2003 (Hakim, 2005). Similarly, enhanced upper-level troughs have been linked to heavy precipitation events in Spain and the Mediterranean (Romero et al., 1999; Jacobeit, 1987).

Severe storms occur when meteorological conditions contain certain features such as enhanced moisture in the lower troposphere, vertical stratification which is suitable for deep convection and a mechanism for prompting and sustaining that convection (Massacand et al., 1998). Several studies for Alpine regions (Massacand et al., 1998; Fehlmann et al., 1999; Martius et al., 2006b; Hoinka and Davies, 2007) have concluded that these conditions are met when an elongated stratospheric intrusion is present over Western Europe. The stratospheric intrusion extending down to the troposphere contains air high in potential vorticity and so is termed a PV streamer (Appenzeller and Davies, 1992). The presence of a PV streamer has also been linked to storms in Israel (Krichnak et al., 2004) as well as to flooding in Algeria (Tripoli et al., 2005). The amplitude and region where the precipitation occurs is affected by the moisture of the air and the local air circulation (Gheusi and Davies, 2004), and the internal structure of the streamer can determine the locality of the precipitation maximum (Fehlmann and Quadri, 2000). The streamer can reduce the static stability of the atmosphere (Juckes and Smith, 2000) and induce, enhance and sustain moist convection (Griffiths et al., 2000; Hoinka and Davies, 2007).

Cloud-diabatic heating effects were found to influence the formation of a PV streamer, leading to heavy precipitation over the Alps, by creating a negative PV anomaly at tropopause level downstream of the heating event (Massacand et al., 2001). The advection of upper-level PV anomalies occurring before the onset of streamers was also studied by Fehlmann and Quadri

(2000). They analysed the predictability of such features by looking at heavy precipitation events that had large forecasting errors and found that poor forecasts occurred when large PV values were present over northern Europe. Dirren et al. (2003) also found errors in forecasting PV amplitude and substructures. Although accurate precipitation forecasts, with associated PV streamers, have been observed at short lead times of 1 to 2 days (Jenkner et al., 2008), improvements in longer forecasts (3-5 days) would be beneficial in order to increase early warning systems. Further investigation into the role of PV streamers in heavy precipitation events, the dynamical processes leading to formation as well as the representation of streamers in forecasts could aide in prediction of extreme weather events.

1.3 Main research questions

Studying the onset, location, structure and forecasting of PV streamers could aid in the prediction of heavy precipitation events. Based on the research carried out in the past, and uncertainties still remaining, the following questions will be addressed in this thesis:

United Kingdom heavy precipitation:

- What are the main synoptic influences on heavy precipitation in different parts of the UK?
- What are the differences in heavy precipitation days with and without an overlying PV streamer?
- Is there an archetypal stratospheric PV streamer that occurs on the heavy precipitation day?

Triggers and PV streamer formation:

- Where are the main trigger localities to precursor Rossby waves?
- Where do the dominant influences on PV streamer formation occur?

Predictability of the waves:

- How well are PV streamers predicted in forecast models?
- Do the errors in PV streamers have a relation to the heavy precipitation forecasts?

1.4 Thesis Structure

The key concepts related to Rossby waves and PV streamers are discussed in Chapter 2. A description of diagnostic tools used throughout the thesis are then outlined in Chapter 3. Several different aspects relating to PV streamers are studied in this thesis and as the data sets and methods are varied, these will be described at the beginning of each subsequent chapter. Chapter 4 presents a study of the role of streamers and synoptic features in heavy precipitation events in the UK. The heavy precipitation cases are readdressed in Chapter 5 with the analysis of the onset and triggers to the PV streamers. Further case studies are also discussed including an Alpine precipitation case and a sensitivity study using the adjoint to the MM5 and NOGAPS models. The forecasting capabilities of the PV streamers are then discussed in Chapter 6 by a feature-based comparison with the ECMWF deterministic and ensemble models. Finally, a main summary of the results and key implications for future work are presented in Chapter 7.

Chapter 2

Literature Review

2.1 Rossby Waves

Atmospheric circulation is driven by uneven heating between the equator and the poles. Excess solar radiation at the equator is transported to the poles in a series of circulatory cells. The large scale flow on Earth is dependent on several balanced forces. The pressure gradient force (PGF) is directed from high to low pressure and works to even out pressure variations. Due to the rapidly rotating nature of planet Earth the Coriolis force (the effect of the Earth's rotation on a free-moving object) causes a turn to the right in the Northern Hemisphere. The magnitude of the PGF is similar to the Coriolis force and creates a west-to-east component called geostrophic wind. In the vertical direction, decreasing pressure with height imposes an upward force (the PGF) which is balanced by the gravitational force due to the mass of the atmosphere above (known as hydrostatic balance). Hydrostatic balance combined with geostrophic balance results in thermal wind, where a change in temperature over distance sets the wind in motion. Along the geostrophic westerlies, at a height of around 10km, there are narrow bands of high-speed winds called jet streams. These fast streams of air are caused by large temperature contrasts at the surface that create steep pressure gradients overhead (Lutgens and Tarbuck, 2004). Westerlies and the jet streams follow wavy paths with long wavelengths known as Rossby waves, named after Carl Rossby (Rossby, 1939, 1940).

The basic properties of a wave can be described by how it oscillates and propagates in space and time. The main characteristics of a wave include the period (duration of one cycle of the wave), wavelength (distance between wave crests), wavenumber (the number of waves per

unit distance in a series of waves), amplitude (distance between a peak and trough), phase (the position of a wave in a cycle of amplitude change or how far to the left or right the wave moves in time), and frequency (the amount of peak and trough occurrences over time or the rate of phase change). The wavenumber can be found by dividing the length of the spatial domain by the wavelength, and is also expressed as the number of times a wave has the same phase over the spatial domain (Hennon, 2007).

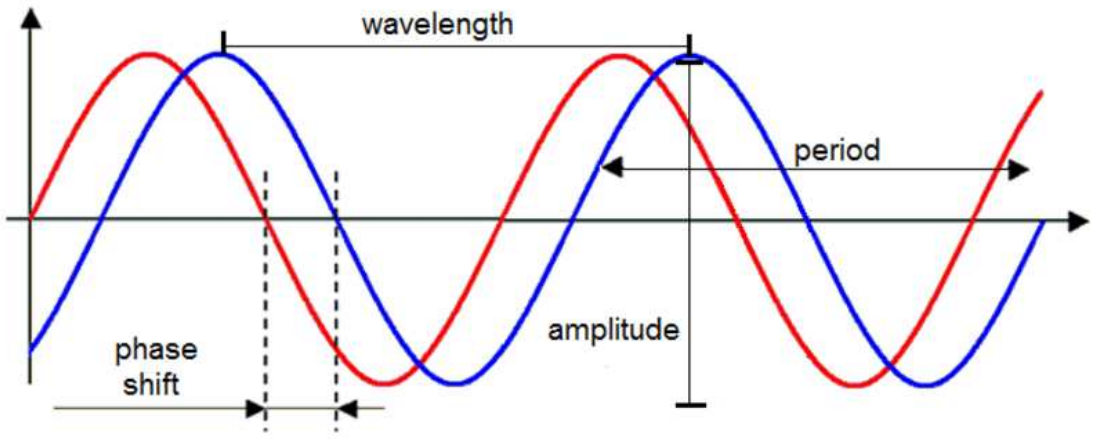

FIGURE 2.1: Components of a wave, modified from Hennon (2007)

Rossby waves are planetary waves as the zonal wavelengths are on the scale of the earth's radius. In a barotropic (atmospheric conditions where the density depends only on the pressure) or quasi 2-d environment, they are chiefly governed by the variation of the Coriolis force with latitude. This can also be termed planetary vorticity, or the spin due to the rotating Earth (Bigg, 2003). Absolute vorticity is defined as a sum of the relative vorticity (η) (the vorticity relative to the axes fixed to the Earth), and the Coriolis parameter (f) (the vertical component of the earth's rotation in space):

$$\eta = \zeta + f. \tag{2.1}$$

In other words, it is the vorticity of the Earth at a specific point plus the vorticity of the air relative to the Earth. Rossby found that the vertical component of absolute vorticity was the most important aspect for atmospheric flow on a large scale (Hoskins et al., 1985).

2.2 Potential vorticity

Potential vorticity (PV) is the absolute circulation of an air parcel between isentropic layers (Hoskins et al., 1985). Ertel (1942) defines PV as the product of absolute vorticity ($\zeta_{a\theta}$) and static stability ($-g\frac{\partial\theta}{\partial p}$) (the stability of the atmosphere in the vertical direction with respect to vertical displacements). In an isentropic coordinate system:

$$PV = (\zeta_\theta + f) \times (-g\frac{\partial\theta}{\partial p}). \tag{2.2}$$

where ζ_θ is the vertical component of the relative vorticity on an isentropic surface, f is the Coriolis parameter, g is acceleration due to gravity and θ is the potential temperature. The atmosphere is considered to be stably stratified if the potential temperature (θ) increases as a function of height. When this occurs monotonically, potential temperature (θ) may be used as an independent vertical coordinate (Holton, 2004).

Potential vorticity is expressed in PVU (potential vorticity units) which are derived from typical midlatitude synoptic scale flow. PV normally equals 0 PVU ($1PVU = 10^{-6}m^2Ks^{-1}kg^{-1}$) close to the equator (in the Northern Hemisphere) and increases polewards and upwards (Hoskins, 1991). Tropospheric air normally has values of PV up to 1.5 PVU and once the tropopause is reached (around 1.6 to 2 PVU) the values rise due to an increase in static stability. Large values of PV are found in the stratosphere which can exceed 10 PVU (Bluestein, 1993). Isentropic surfaces vary with latitude and display a slope toward the ground from the poles to the equator. High PV air is found at lower heights at the poles than near the equator (Hoskins, 1991).

2.2.1 Principles of PV

The main advantages to using PV are the properties of conservation and invertability. When a closed material contour is located in a frictionless, adiabatic atmosphere it will remain on the same isentropic surface and its circulation will be conserved. In this same frictionless and adiabiatic atmosphere PV will be conserved on an isentropic surface by 2-D motion. Assuming a horizontally uniform reference state and a constant Coriolis parameter then the reference state always has a constant PV on each isentropic surface (Ertel, 1942). Also PV is

conserved between isentropic layers unless the layers transect the surface of the Earth (Haynes and McIntyre, 1987). For this reason, PV can be used as a tracer of motion and significant features within the atmosphere (synoptic scale weather systems) can be identified and followed in space and time. As PV is conserved in the absence of diabatic processes and friction (Hoskins et al., 1985), when these processes occur, PV can be created and destroyed. When there is a sudden increase or drop in PV, it signifies that diabatic heating or friction is involved, so can aide in the identification of these processes.

The Lagrangian markers necessary to identify a parcel of air are: potential temperature, specific humidity and potential vorticity (in adiabatic, frictionless flow). The invertability principle is an important tool as it is possible to determine the flow field (wind, pressure and temperature fields) from the distribution of PV when potential temperature at the surface is known (Eliassen and Kleinschmidt, 1957; Hoskins et al., 1985).

2.2.2 PV anomalies

PV anomalies are viewed as displacements along the isentropic potential vorticity (IPV) surface or θ gradient. In the upper-levels, a lowering of the tropopause is called a positive PV-anomaly while a raised tropopause is a negative PV-anomaly (Hoskins et al., 1985). They are caused by wind fields created by neighbouring IPV and surface θ anomalies or can be generated by active moist processes diabatically. For instance latent heating associated with precipitation can alter the absolute vorticity and static stability and can lead to the generation or destruction of PV (Brennan et al., 2007). The rate at which this occurs is established by the latent heating gradient and the background absolute vorticity (Stoelinga, 1996).

Typical flow structures induced by either positive or negative IPV anomalies in a statically stable reference state can be deduced. In a positive PV anomaly (Figure 2.2, left) isentropes have higher values than surrounding areas and the height of the tropopause has a local minimum. Corresponding pressure is low and the wind fields display a cyclonic circulation. In a negative PV anomaly (Figure 2.2, right) isentropes have lower values than surrounding areas and the tropopause has a local maximum. Associated pressure is high with an anticyclonic circulation in the wind fields (Hoskins et al., 1985). The same types of fields occur for low-level disturbances near the earth's surface (Thorpe and Emanuel, 1985). PV anomalies occurring at low-levels

do not have a stratospheric origin, but instead are produced in strong baroclinic zones where latent heating takes place (Stoelinga, 1996).

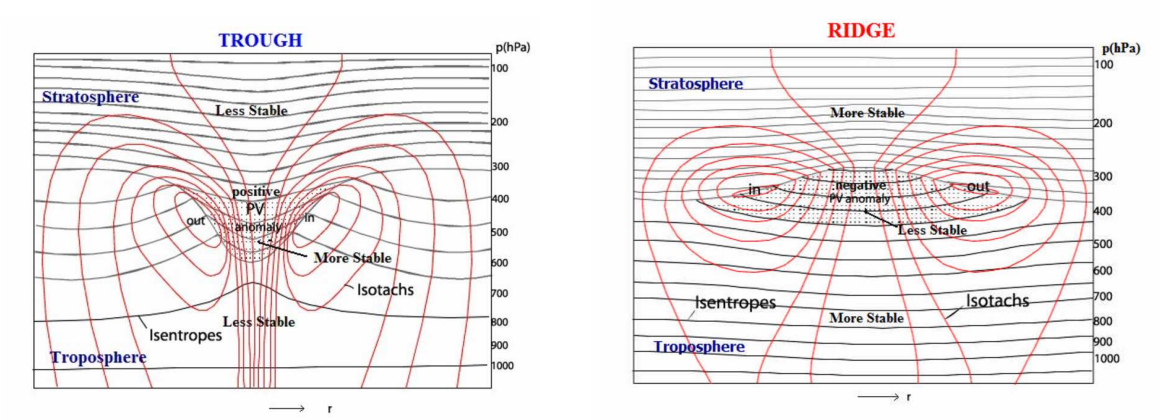

FIGURE 2.2: The circulation around a positive (left) and negative (right) PV anomaly. A trough causes statically stable air to intrude into the troposphere and cyclonic circulation is formed. A ridge induces less stable tropospheric air to push into the stratosphere creating an anti-cyclonic vortex. Adapted from Hoskins et al. (1985).

PV anomalies can grow or decay depending on how they interact with other PV anomalies (on lower, higher or the same IPV level). The circulation caused by each anomaly can help to induce greater velocities, by mutual amplification, if the phase difference has an optimum value. Similarly, if the phase difference is not in sync, the circulations can decay (Hoskins et al., 1985). An example of this is observed in the process of cyclogenesis. If a significant synoptic-scale upper-level PV anomaly develops, the induced wind field can traverse the entire troposphere and produce cyclonic rotation at the earth's surface. If the PV-anomaly moves over a baroclinic band (such as a low-level surface front) the cyclonic rotation at the upper level is induced in the lower level. The low-level circulation causes warm advection ahead leading to a low-level positive temperature (or PV) anomaly. This new PV anomaly is associated with a cyclonic vortex of its own and has a positive feedback on the upper-level circulation, amplifying the pattern and strengthening the anomaly. Within the increased flow, higher PV values are advected southward to the west of upper-level PV anomaly while lower PV values are advected northward to the east. The eastward movement of the PV anomaly is thus decreased and the interaction between the lower and upper-level circulations will continue to strengthen until the system matures (Martin, 2006).

2.3 Propagation of Rossby waves

The propagation of Rossby waves are similar to that of PV anomalies and are reliant on the existence of the PV gradient. Rossby waves travel along this band of enhanced PV gradient at the tropopause (Schwierz et al., 2004). The waves form as a result of vertical squeezing and stretching of the column of air as it is perturbed (for instance while passing over a mountain barrier). Northward displacement of air causes negative vorticity perturbations, associated with anticyclonic rotation (Plumb, 2003). Positive anomalies (southward perturbations) are associated with cyclonic rotation as illustrated in Figure 2.3:

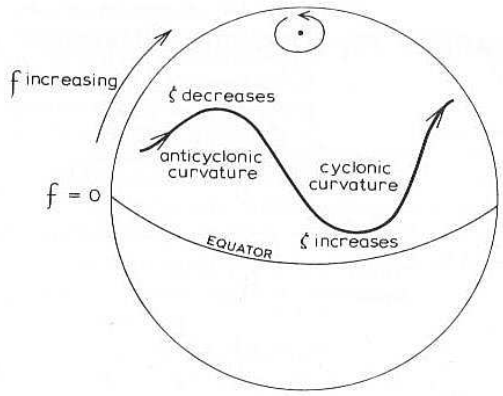

FIGURE 2.3: A schematic illustration of the mechanism of long-wave development in the tropospheric westerlies, from Barry and Chorley (2003).

As the column of air is squeezed the vorticity (or measure of spin) decreases, this has the effect of creating a clockwise turning (anticyclonic circulation) in the Northern Hemisphere so the air turns equatorwards. When the column of air is stretched (on the lee side of the mountain barrier) vorticity increases resulting in an anticlockwise turning (cyclonic circulation) and the air moves poleward (Holton, 2004).

Once the wave has been initiated it is maintained by the need to conserve absolute vorticity (equation 2.1). The Coriolis parameter is at a minimum at the Equator with a maximum value at the poles. As air moves poleward the Coriolis parameter increases, so in order to maintain absolute vorticity the atmospheric vorticity decreases. By decreasing the vorticity, as the airstream moves poleward, it increasingly becomes anticyclonic and eventually the air turns equatorward again. The circulation creates oscillation back and forth creating a propagating vorticity field which is the Rossby wave. The downstream oscillation continues until the

airstream is perturbed again or is influenced by other factors (for instance surface temperature patterns) (Barry and Carleton, 2001).

Rossby waves are dispersive, hence the pattern of the wave changes with time. The dispersion relation for a barotropic Rossby wave can be viewed as:

$$w = \bar{u}k - \frac{k\beta}{k^2 + l^2}, \tag{2.3}$$

where $\bar{u}$ is the mean westerly flow, k is the zonal wave number, l is the meridional wave number and $\beta = \partial f / \partial y$ (or the variation of the Coriolis force with latitude). The phase speed, or velocity of the wave, is determined by how fast the constant phase segment of the wave (or a single wave peak) propagates. The zonal phase speed is:

$$c = \frac{w}{k} = \bar{u} - \frac{\beta}{k^2 + l^2}. \tag{2.4}$$

When $\bar{u}$ is set to zero, the zonal phase speed is negative, so the Rossby wave phase moves westward relative to the background flow. The phase speed is also a function of wavenumber so longer waves travel westward faster than shorter waves. Short waves with slow phase velocities propagate to the east, long waves propagate westward and stationary waves occur when the frequency is zero (Plumb, 2003).

The dispersive nature of the waves implies that a collection of waves (or wavepacket) moves at a different speed than the phase speed. The group velocity is the rate at which changes in amplitude (or the observable disturbance carrying the wave energy) propagate over time (Hennon, 2007). The wave's group velocity (associated with the energy flux) is calculated as:

$$c_g = \frac{\partial w}{\partial k} = \bar{u} + \frac{\beta(l^2 - k^2)}{(k^2 + l^2)^2}. \tag{2.5}$$

The group velocity is always positive and so moves in an eastward direction. Although Rossby waves move to the west relative to the mean flow, the localised perturbations (or interference patterns of several waves) move to the east (Holton, 2004)

Baroclinic Rossby waves allow for variations in the flow with height, such as horizontal temperature gradients, and are three dimensional in nature. The phase speed is then in the x, y

and vertical directions and the components of the phase velocity are defined in the equations below:

$$c_x = \frac{\omega}{k_x} = \bar{u} - \frac{\beta}{k_x^2 + k_y^2 + (f_0^2/\bar{\sigma_0})k_p^2}, \tag{2.6}$$

$$c_y = \frac{\omega}{k_y} = \left(\bar{u} - \frac{\beta}{k_x^2 + k_y^2 + (f_0^2/\bar{\sigma_0})k_p^2}\right)\frac{k_x}{k_y} = c_x\frac{k_x}{k_y}, \tag{2.7}$$

$$c_p = \frac{\omega}{k_p} = \left(\bar{u} - \frac{\beta}{k_x^2 + k_y^2 + (f_0^2/\bar{\sigma_0})k_p^2}\right)\frac{k_x}{k_p} = c_x\frac{k_x}{k_p}, \tag{2.8}$$

c_x is the component of the phase velocity in the x direction, c_y is the phase velocity in the y direction and c_p is the phase speed along the vertical pressure axis which has the units $hPa\ s^{-1}$. k is the wavenumber, $\bar{u}$ is the mean westerly flow of the air current, f is the coriolis parameter and σ is the static stability (Zdunkowski and Bott, 2004).

Rossby waves are generated by topographic forcing such as flow over large-scale mountain ranges, thermal forcing from heating differences associated with land and sea distributions, and forcing from interactions with smaller scale circulations such as extra-tropical cyclones (Lynch and Cassano, 2006). Vortices are induced by each of these features which impact the flow of the wave downstream, depending on the amplitude and position of the vortex. The effects are similar to the cyclogenesis example in section 2.2.2. Another example is the interaction between waves and topographic features. Depending on the phase of the wave (whether a ridge or trough passes over the mountain) the wave responds by gradually increasing or decreasing in amplitude. A steady state occurs when the westward propagation of the wave coincides with forcing from the topographic vortex. (Schwierz et al., 2004).

Waves can also interact with each other. Barotropic (y axis) and Baroclinic (z axis) instability occurs when two or more Rossby waves coincide. They can either be above each other (z) or beside each other (y). The cyclonic and anticyclonic circulation, and the induced velocity field of each wave (observed as the effect of the PV structures or PV anomalies), overlaps and impacts the other. The effect can be an increase in amplitude (when the velocities are in phase and added together) causing growth and leading to propagation against the basic zonal flow. This often creates a situation where the patterns are "phase-locked" and stationary against

the basic zonal flow. The energy of one wave can also be transferred to the other, causing growth and increased propagation for one wave, and decay in the other (Hoskins et al., 1985).

2.4 PV streamers

The wave flow at the tropopause moves horizontally and vertically, and when the fluctuations in the horizontal direction reach an irreversible state wave breaking occurs (McIntyre and Palmer, 1983). When Rossby waves break, elongated tongues of high PV air may form, termed PV streamers (a special type of PV anomaly - see Section 2.2.2). These are made up of stratospheric air extending equatorward or tropospheric air extending poleward. They only have a thin connection to the main body of air from which they are drawn. In this study, stratospheric PV streamers are denoted as having a PVU content greater than 2 and tropospheric PV streamers have a PVU content less than 2 (as the climatological PV-tropopause lies around 1.6PVU (Wernli and Sprenger, 2007)).

PV streamers tend to form in areas where the climatological isentropic PV gradients (and jets) are weak. Changes in the distribution and frequency of streamers are related to changes in the strength and location of the jet (Postel and Hitchman, 1999). They are key elements in mid-latitude flow structures and a stratospheric intrusion normally occurs when low-pressure systems develop and a cold front is at the ground. In this situation, a tongue of stratospheric air subsides towards the equator to the west of the front. The streamer of stratospheric air can be deformed by large-scale flow or by the PV band itself (Appenzeller and Davies, 1992). Near tropopause streamers can be influenced by diabatic PV anomalies and by underlying topography. It may respond to these effects by rolling up or splitting at the tip of the streamer forming smaller PV streamers or filaments, or by breaking up into vortices. Once the streamers break up, the process is irreversible, and so is associated with quasi-isentropic mixing. Cut-offs may break up and decay quickly, but they do not always decay completely (Wernli and Sprenger, 2007).

2.4.1 Streamer life cycles

Several studies have been done of cyclonic life cycles related to baroclinic shear and two main life cycles have been described - LC1 as anticyclonic and LC2 as cyclonic (Thorncroft et al.,

1993). These groups are applied to streamers as shown in Figure 2.4 where the LC1 streamer is depicted in red while the LC2 is shown in blue. In the LC1 life cycle, the upper-level wave changes in the final stage and anticyclonic shear on the southern edge of the jet creates elongated filaments, which often break up into cut-off vortices. During the LC2 life cycle, there is a significant difference in that the breaking wave remains broad and does not create cut-offs, but instead wraps up cyclonically as it is influenced by the cyclonic shear of the jet. These differences are also reflected in how the upper-level development affects synoptic evolution of surface cyclones, anticyclones and fronts. The breaking of the wave is a major characteristic leading to the different types of baroclinic wave life cycles (Martius et al., 2007).

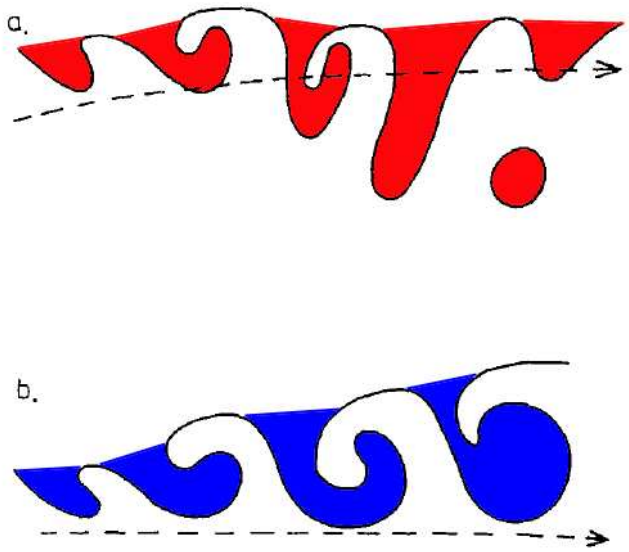

FIGURE 2.4: Schematic of a PV-theta contour with an a) LC1 life cycle and b) LC2 life cycle adapted from Thorncroft et al. (1993).

Changes in the location of the baroclinc wave in relation to the subtropical, polar and arctic jets have a crucial impact on the life cycles of the waves (Shapiro et al., 1998). The meridional position of the jet itself also influences the wave's life cycle (Akahori and Yoden, 1997). Cyclonic wave breaking occurs more often when there is a narrow strong jet, while anticyclonic breaking is more favourable in weak and broad jet conditions (Esler and Haynes, 1999). Cyclonic breaking waves form when the jet is shifted southward, whereas the opposite is true for anticyclonic breaking waves. Advection of low PV, caused by strong upstream jets, also enhances anticyclonic wave breaking. There is a change with height of the frequency of cyclonic and anticyclonic streamers and there is spatial separation of maximum cyclonic and anticyclonic frequency on the 310K level (Isotta et al., 2008). Cyclonic streamers are

located on the Pacific and Atlantic storm track on this level while anticyclonic streamers are downstream from the cyclonic maxima over Europe (Martius et al., 2007).

2.4.2 Impacts of PV Streamers

PV streamers have an influence on high-impact weather such as precipitation and winds. Flooding can occur to the east of a PV streamer due to poleward transport of moisture (Tripoli et al., 2005). The location and orientation of a streamer as well as its meridional extent can influence heavy precipitation patterns (Martius et al., 2006a). This is enabled by the magnitude and position of the streamer modifying the moisture flux into a region. The internal structure including the amplitude of PV can also alter the location of the precipitation maximum (Fehlmann and Quadri, 2000). Mesoscale PV structures within the streamer have an influence on convective available potential energy (CAPE) and thus convection (Schlemmer et al., 2010). While in the lower latitudes PV streamers can aide in the initiation and intensification of tropical convection (Slingo, 1998). Although not all streamers produce heavy precipitation, there is a link between longer lived streamers and higher amounts of accumulated precipitation. Longer lasting streamers have a higher probability of creating more intense events - ie 10 mm/day of precipitation (Martius et al., 2006b).

High winds, generated by PV streamers, can lead to dust emission, transport and deposition. This occurs when PV streamers west of the Alps extend into Africa and initiate Saharan dust storms (Knippertz and Fink, 2006). The dust can then be transported into the Mediterranean and deposited on Alpine glaciers (Sodemann et al., 2006) and central Europe (Wiegand et al., 2011).

At the final stage of the PV streamer life cycle strong deformation may create cut-offs of high-PV air. Appenzeller et al. (1996) showed that the vortex created can then instigate or modify the development of weather systems and cyclogenisis. The break up of the streamer may lead to stratospheric air (rich in potential vorticity, ozone and deficient in water vapour and fluorocarbons) mixing with tropospheric air, causing exchange of chemical constituents and leading to radiative effects. Aerosols are also transported into a domain where their residence time may be very different and can have an effect on variations in ozone trends (Appenzeller and Davies, 1992).

2.5 Predictability

An objective for understanding the dynamical processes related to Rossby waves and PV streamer formation is the ability to represent these features accurately in numerical weather prediction systems, and in particular, to improve forecasts of extreme weather events. Rossby waves and wave trains have been identified as important features which can impact the predictability of mid-latitude weather systems (Shapiro and Thorpe, 2004). Precursor Rossby wave trains leading to heavy precipitation in the Alps have been identified up to 8 days in advance (Martius et al., 2008) and as much as 10 days for a case of flooding in Germany (Grazzini and Van der Grijn, 2003). Forecasting errors propagate on the same time-scales as Rossby wave trains and when these synoptic-scale systems are forecast correctly, the downstream high-impact weather events also have higher than average predictability (Szunyogh et al., 2011). Grazzini (2007) investigated precursor wave trains within typical flow patterns leading to heavy precipitation in the Alps and found they were well represented in ECMWF forecasts. This signifies that identifying flow patterns and precursor wave trains leading to high-impact weather in other locations may also improve forecasts in these regions. To this end, a diagnosis of wave initiation and the downstream wave trains which lead to PV streamer formation and heavy precipitation in the United Kingdom are investigated.

Recent studies have found that forecasts of heavy precipitation events have good skill once a PV streamer has formed (Jenkner et al., 2008), however, aspects of PV streamers such as the exact location and amplitude are still not resolved well, even in more recent models. Dirren et al. (2003) found that the correct phasing and orientation of streamers were not captured accurately, which in turn led to misforecasts of associated severe weather events. Specific locations of PV anomalies also have an impact on forecasting skill, as small changes to the PV distribution can make significant differences in the position and strength of forecast cyclones over the North Atlantic (Rosting and Kristjansson, 2008). It is not understood how well the structural aspects of PV streamers are represented in numerical weather prediction models and the relation these differences have to heavy precipitation events are studied in this thesis.

Chapter 3

Diagnostic Tools

3.1 Identifying PV streamers

The first step in analysing PV streamers is to define what constitutes a "streamer". In general, a streamer is a body of stratospheric air descending equatorwards (or tropospheric air extending polewards) that retains a connection to the main body of stratospheric (tropospheric) air. The method introduced by Wernli and Sprenger (2007) and Martius et al. (2006b) is utilised in this study and attempts to demarcate a streamer based on its size and width. The tropopause is projected onto isentropic levels using the 2PVU contour. Working along the 2PVU tropopause, points are checked for a distance across the contour of $\leq$800km (between the two white endpoints in Figure 3.1 including the root point) so as to remove larger troughs. The total contour length (from endpoint to endpoint around the length of the contour including the southernmost point) must also be $\geq$1500km so that only significant features are captured and not small variations on the 2PVU tropopause. When these conditions are met, the area enclosed by the contour is identified as a streamer (shaded grey area of Figure 3.1).

The orientation of the streamer is calculated by using a horizontal line through the root point. The angle of the orientation axis (a line connecting the root point to the southernmost point) to the horizontal line is determined as the angle of the streamer. Streamers with angles less than 75° are in the anticyclonic group and streamers with angles greater than 105° are in the cyclonic group. These two groups make up about 4/5ths of all the streamers and the rest are categorised as meridional (with an angle between 75 and 105°). Other streamer features are also diagnosed such as the elongation and width. The elongation is defined as the distance

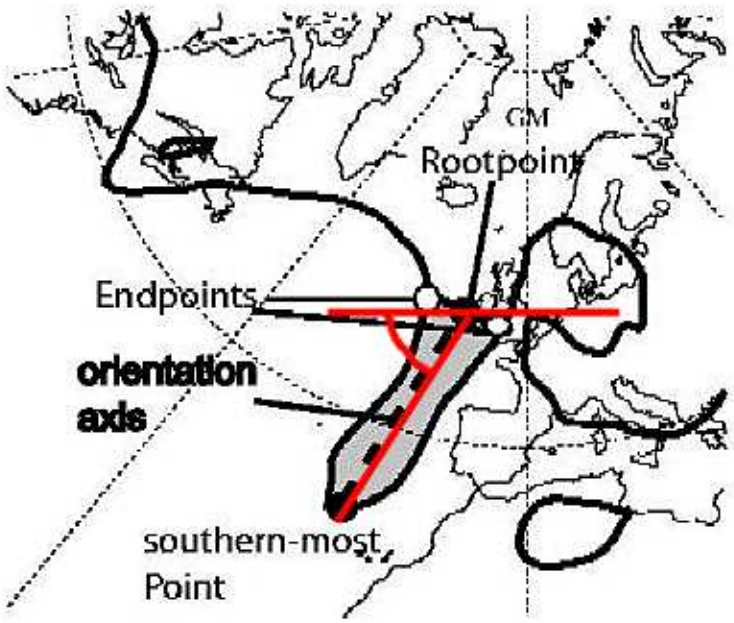

FIGURE 3.1: Identification of a PV-streamer between the root point, endpoints, southern-most point, orientation axis and streamer angle (in red), adapted from Martius et al. (2007).

between the root point and southernmost point. The width is calculated as an average of each set of outermost points perpendicular to the line of elongation going up the streamer. The quantified streamer and its features are used to investigate position, frequency and prediction capabilities in relation to heavy precipitation events in the following chapters.

3.2 Tracking PV streamers

Most of the movement between the stratosphere and troposphere due to wave breaking occurs at 330K and lower in winter, spring and autumn months. In the summer months the wave breaking occurs at higher isentropic levels of around 340K (Martius et al., 2006a). For this reason, streamers are examined at the 320K level for autumn, winter and spring, and on the 340K level for summer. In order to pinpoint the exact location of individual streamers at the time step in which they occur and at a specific θ level, a streamer location routine has been developed. This routine cycles through all the streamer data points at each time step and locates longitude by latitude gridpoints which are adjacent. The adjacent points are then classified as the same streamer, but non-adjacent points in the same time step are considered

a different streamer. Several streamers may occur at the same time step but in different longitudes or latitudes.

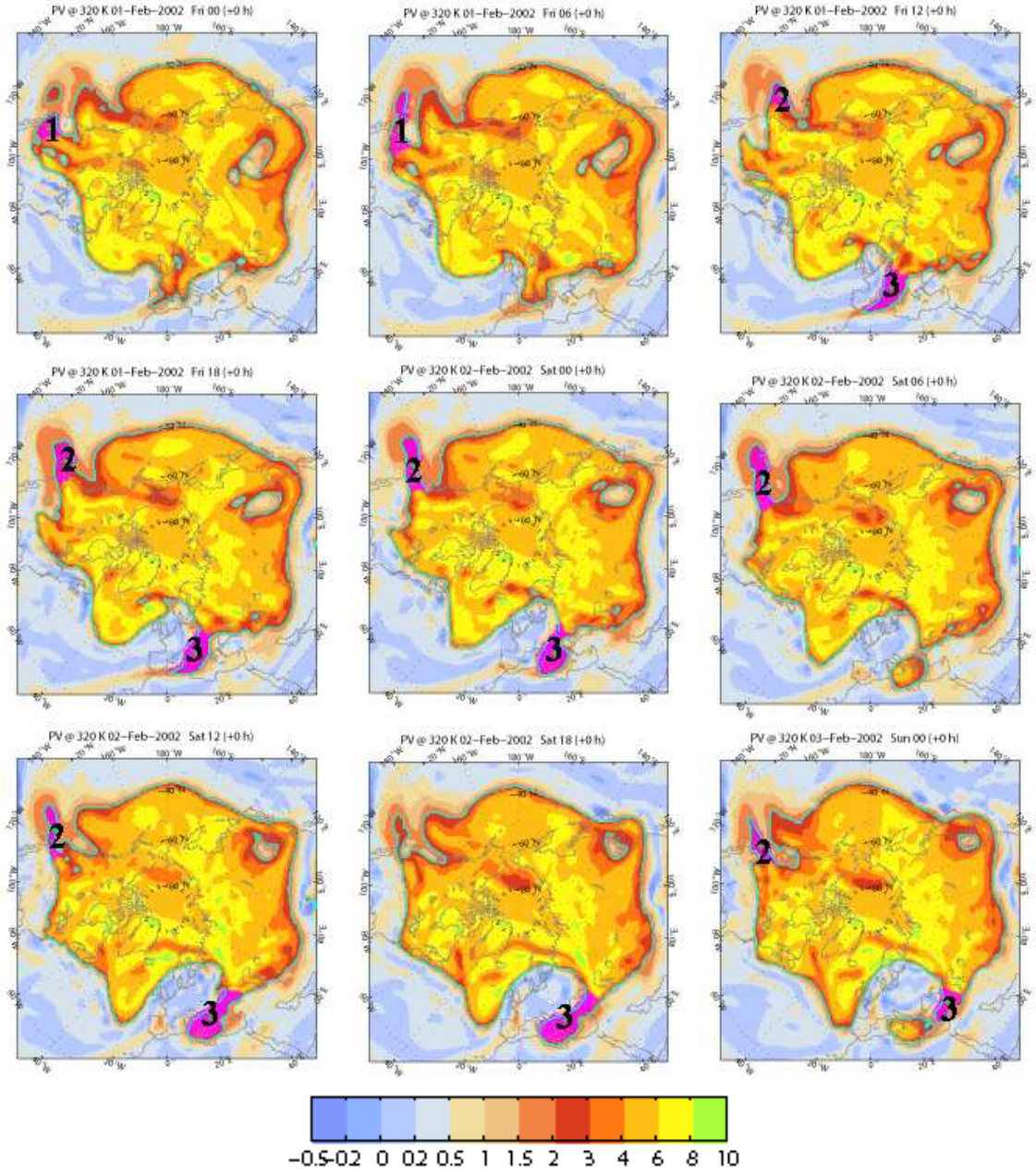

FIGURE 3.2: Isentropic plots of potential vorticity at 320K level with streamer grid-points (highlighted pink) and tracked streamer numbers plotted. The blue line indicates the tropopause occurring at PVU = 2.

The data is then analysed for the persistence of streamers over several time steps with a novel tracking routine which has been created to identify vertically coherent structures. The grid-points of each streamer (as identified in the location routine) are checked against the grid-points of streamers occurring in previous and subsequent time steps. If these overlap,

the two streamers are classified as the same streamer and are issued a tracking number. If the base points (the points where the streamer connects to the stratospheric air) of the two streamers move more than 2000km then the streamers are not considered the same feature. Streamers at 315K to 325K (for autumn, winter and spring) and 335K to 345K (for summer) are also indexed and checked against streamer grid-point positions on 320K (and 340K for summer). In this way, streamers which appear as cut-offs on the 320K surface, but in effect are still attached to the main body of stratospheric air, are still regarded as the same streamer feature. Each streamer is allocated a tracking number to illustrate streamers corresponding to each other (see below Figure 3.2), and the lifespan of each streamer is determined.

3.3 Hovmöller diagrams

The Hovmöller diagram was designed to display the propagation of mid-tropospheric ridges and troughs of a Rossby wave. It is used to examine the pattern of meridional velocity and geopotential height anomalies by plotting time against zonal variation (Hovmöller, 1949). Rossby wave trains are a series of wave packets centred about a dominant wave. Waves and wave trains which propagate along the tropopause and jet stream can be identified with the use of this diagram.

Martius et al. (2006a) constructed a refined Hovmöller diagram. By using the PV-gradients along the 2PVU contour line, the evolving wave guide is followed rather than just a pre-assigned latitudinal band. The diagrams are composed of the velocity of the north/south winds over longitude and time. Rossby waves consist of consecutive maximum and minimum velocity peaks (alternating signs) over time. Figure 3.3 illustrates the meridional wind velocities associated with Rossby wave peaks and troughs (represented by the black 2PVU contour) that would be found on a Hovmöller diagram. The new diagram effectively shows the initial propagation, the amplification, the culmination and final disappearance of the wave on the tropopause wave guide. The amplitude of the peaks and troughs of the wave are depicted to a greater extent than in the original diagram. Problems with the diagrams are due to wave breaking and cut offs which can disappear and then reappear. Also as the waves undulate up and down they may pass onto other jet streams (Martius et al., 2010). As only one meridional band is used some information about wave propagation is lost. This can be overcome by constructing several

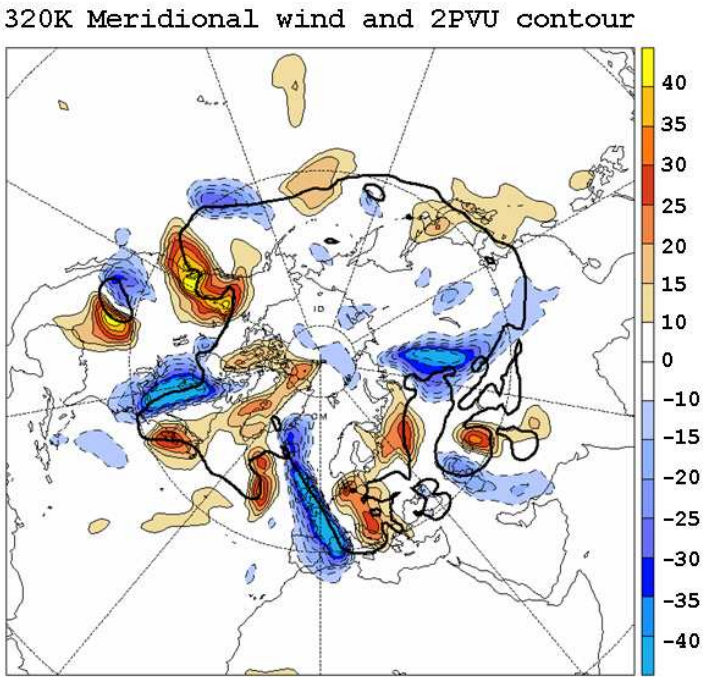

FIGURE 3.3: Meridional wind velocity in m s^{-1} (red and blue contours) of Rossby wave peaks and troughs (black contour)

Hovmöller diagrams at different meridional widths and longitudinal bands, or investigating potential temperature on 2PVU in order to construct a complete picture of the dynamics of waves and their movement. The refined Hovmöller diagram and 2PVU contour lines are employed throughout the thesis to illustrate Rossby wave progression.

Chapter 4

UK heavy precipitation linked to upper-level features

4.1 Introduction

Heavy precipitation and the resultant flood damage costs around £1 billion a year in the UK and nearly five million people live in flood risk areas in England and Wales (Hall et al., 2005). The day-to-day weather of the United Kingdom is influenced by the large-scale atmospheric circulation and synoptic-scale systems combined with local influences (meso-scale features, topography and local circulations). The synoptic-scale influences on the UK have been categorised into seven different regional airflow patterns (or circulation types) by Lamb (1950). The role of these regional patterns with regard to rainfall fluctuations was investigated by Mayes (1991). Mayes found that precipitation predominantly occurred during periods of Westerly circulation (high pressure located south of the UK with a low north of the UK promoting ridge/trough systems to travel from the Atlantic). Similarly Hand et al. (2005) found that most showers occur with a westerly wind component. An earlier study by Hand (2004) analysed 50 extreme rainfall events as identified by the flood studies report (1975) and categorised these rainfall events into three types: a) orographic, b) frontal, and c) convective. Only five cases were found to be orographically induced and occurred in November, December and January. Fifteen cases were considered frontal and these occurred in July, August, September and October, and the remaining 30 cases were classified as convective and mainly took place in June, July and August.

Studies have investigated the presence of upper-level PV-anomalies as an influencing feature for both frontal and convective heavy precipitation. Roberts (2000) analysed the importance of these upper-level anomalies in enhancing convection due to descent behind and ascent in front of the feature. Juckes and Smith (2000) also investigated the impact of PV anomalies on the enhancement of CAPE. Krishnamurti et al. (2003) diagnosed the heavy rains and floods in the UK in October 2000 and found a trough axis to the West of the British Isles during the period of the heavy rain. Similarly, Blackburn et al. (2008) identified a cyclonically wrapping trough was present in three cases during the summer of 2007 which led to flooding in the UK. In each case the troughs led to ascent and convectively unstable conditions. Several studies in the Alps (Massacand et al., 1998; Fehlmann et al., 1999; Martius et al., 2006b; Hoinka and Davies, 2007) and in the United States (Caracena et al., 2001) have found that the existence of a potential vorticity (PV) streamer were also present during heavy precipitation events.

Although PV streamers have been linked to heavy precipitation across the globe a systematic analysis of their role in UK weather has not been undertaken. This study presents a quantitative climatological assessment of the dynamical precursors leading to heavy precipitation days in the UK. The aim of this study is to determine the large-scale setting and understand the features' co-development during heavy precipitation events in order to aide in the prediction of high-impact weather.

4.2 Data and Methodology

4.2.1 Data sets

Three main data sets are used in the analysis of synoptic-scale features on the heavy precipitation days. The United Kingdom heavy precipitation data used in this analysis is taken from the MIDAS observational data set using 700 stations from Maraun et al. (2008) and the Met Office Hadley Centre HadUKP data set (Alexander and Jones, 2001). The station data is split into nine regions including: SEE (south-east England), SWE (south-west England and south Wales), CE (central and eastern England), NWE (north-west England and north Wales), NEE (north-east England), SS (south-west and southern Scotland), NS (north-west and northern Scotland), ES (eastern Scotland), and NI (Northern Ireland).

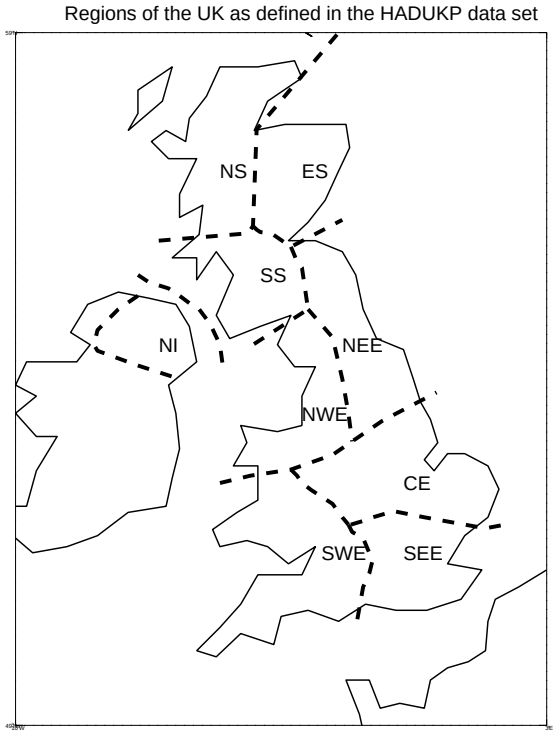

FIGURE 4.1: The 9 regions of the UK in the HADUKP heavy precipitation data set, Northern Scotland (NS), Eastern Scotland (ES), Southern Scotland (SS), Northern Ireland (NI), North Western England (NWE), North Eastern England (NEE), Central England (CE), South West England (SWE), and South East England (SEE).

The England and Wales regions were identified by Wigley et al. (1984) as areas of spatial coherence when they conducted a principle component analysis of 55 rain gauge stations across the UK. The study was extended to Scotland and Northern Ireland by Gregory et al. (1991). The precipitation amounts for each day are taken at 9:00 and 21:00 and the sum of these two readings comprise the daily precipitation amount (MIDAS, 2007). For this analysis, the daily measurements from the period from 1957 to 2002 (coinciding with the ECMWF ERA-40 reanalysis data set) are used to calculate the top 99% quantile (41 out of 4100 days), 95% quantile (205 days) and 90% quantile (410 days) for each region and season. Seasons are defined as September, October and November for autumn, December, January and February for winter, March, April and May for spring and June, July and August for summer.

The same number of days for each region and season are used so the minimum precipitation per day in the quantiles varies as shown in Table 4.1. The highest amounts of precipitation are consistently found in NS while the lowest precipitation is found in CE for all the regions, seasons and quantiles. There is also an east-west split across the UK with higher amounts located in western areas (NWE, SWE and SS) and lower levels in eastern regions (NEE, CE

and SEE). The mean precipitation across all the regions is highest in autumn, followed by winter and summer with the lowest totals in spring.

TABLE 4.1: Minimum and mean daily precipitation (mm) for each quantile, region and season

99% Quantile								
	Autumn		Winter		Spring		Summer	
Region	Min	Mean	Min	Mean	Min	Mean	Min	Mean
NS	28.71	38.27	28.74	39.68	21.27	27.04	20.77	26.41
ES	20.62	26.19	17.75	21.97	16.06	21.03	17.08	23.39
SS	26.13	31.59	24.38	29.92	18.36	23.02	19.78	25.72
NI	22.92	28.92	19.55	22.79	15.73	19.03	18.39	23.79
NWE	23.26	27.85	22.58	26.36	17.37	21.74	18.97	24.53
NEE	18.31	23.35	15.73	19.34	15.04	19.40	17.51	21.99
CE	15.65	21.13	12.30	16.28	12.12	17.35	14.36	20.99
SWE	23.54	27.34	21.48	25.42	16.43	20.03	17.83	23.87
SEE	21.53	26.93	15.86	19.69	14.07	17.16	18.03	23.73
95% Quantile								
	Autumn		Winter		Spring		Summer	
Region	Min	Mean	Min	Mean	Min	Mean	Min	Mean
NS	19.05	25.78	18.11	25.76	12.76	18.24	12.29	17.36
ES	11.43	16.95	10.15	14.74	7.78	12.74	8.72	13.92
SS	17.32	22.69	15.96	21.40	11.71	16.19	11.67	16.99
NI	13.13	19.01	12.17	16.54	9.4	13.04	9.99	15.31
NWE	14.87	20.08	13.62	18.83	10.67	14.85	11.72	16.49
NEE	9.92	15.06	9.68	13.49	8.14	12.23	8.53	13.74
CE	8.44	12.93	7.33	10.60	6.45	10.33	7.87	12.62
SWE	14.32	19.62	14.44	18.87	10.14	14.09	10.12	12.62
SEE	11.34	17.34	10.00	13.67	7.71	11.36	8.11	13.91
90% Quantile								
	Autumn		Winter		Spring		Summer	
Region	Min	Mean	Min	Mean	Min	Mean	Min	Mean
NS	14.49	21.16	14.09	20.86	9.36	14.58	9.43	14.03
ES	7.73	13.10	7.10	11.62	5.14	9.50	5.94	10.50
SS	12.83	18.77	11.96	17.58	8.27	12.96	8.41	13.41
NI	9.29	15.02	8.97	13.54	6.93	10.53	6.90	11.81
NWE	11.02	16.39	10.42	15.37	7.77	11.96	8.31	13.14
NEE	7.01	11.68	6.67	10.74	5.45	9.44	5.89	10.38
CE	5.78	9.96	5.15	8.38	4.50	7.80	5.26	9.50
SWE	10.30	15.78	10.86	15.64	7.32	11.36	6.81	11.86
SEE	7.71	13.32	7.04	11.02	5.34	8.90	5.32	10.19

The PV streamer data used in this analysis comes from the streamer climatology developed by Martius et al. (2006b) extracted from the ECMWF ERA-40 reanalysis data set at 1x1° resolution using the identification routine from Wernli and Sprenger (2007) described in Section 3.1. Streamers are identified every 6 hours on the Northern Hemisphere along the isentropic

2PVU contour line. The streamers are assessed over four time steps to synchronize with the entire heavy precipitation day. At each time step, streamer features are extracted as 0/1-fields (with a 1 at each grid point within a streamer feature and a 0 outside).

Three isentropic levels are chosen for stratospheric streamers; 310K to 320K in autumn, winter and spring and 320K to 330K in summer. These levels are selected based on the climatological distribution of stratospheric streamers near the UK for each season shown in Figure 4.2 where the distribution of streamers over the entire northern hemisphere is illustrated. The reduced frequency of streamers centred at 0° longitude is partly due to the use of only three isentropic levels as well as the natural distribution of PV streamers falling to the north-west of the UK over the Atlantic Ocean and to the east of the UK over Europe. Highest frequencies of 45-50% occur in the winter season over Europe while in autumn streamers are predominantly found west of the UK.

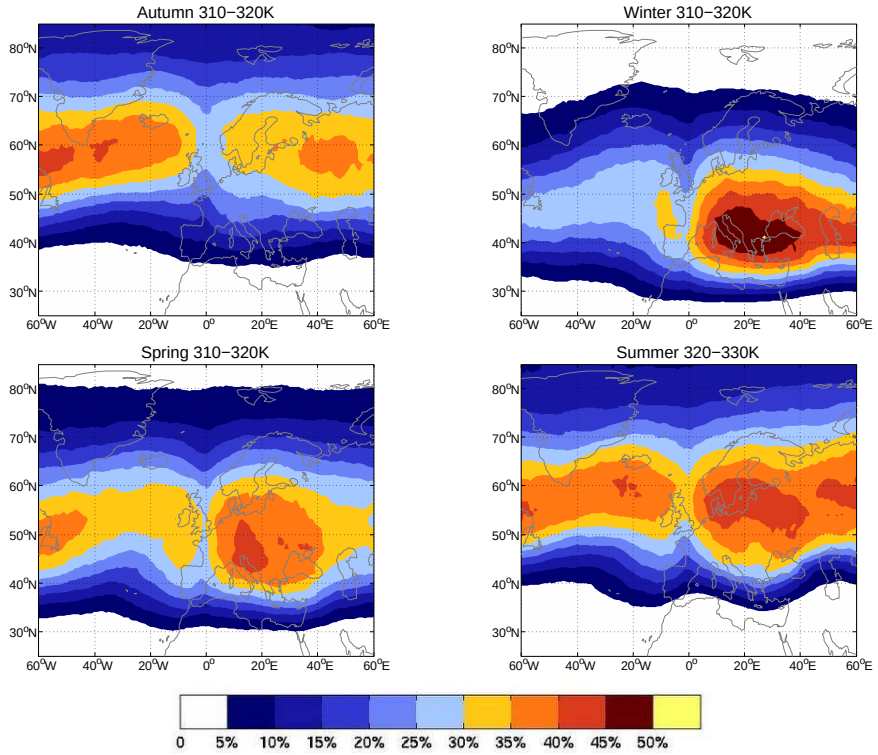

FIGURE 4.2: Climatology of stratospheric streamers located near the UK over 3 isentropic levels. Colour contours represent the percentage of daily occurrence in each season.

Tropospheric streamers are also identified on three isentropic levels 320K to 330K in autumn, 315K to 325K in winter and spring and 325K to 335K in summer coinciding with their climatological distribution near the UK for these seasons illustrated in Figure 4.3. The locations of tropospheric streamers are similar to the stratospheric streamers with two groupings to the

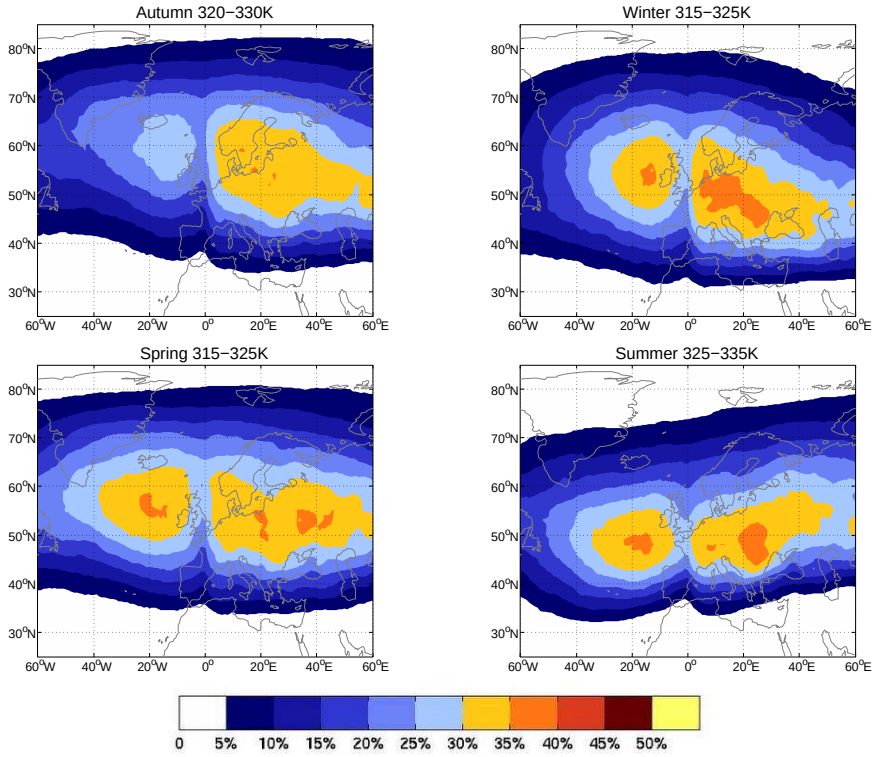

FIGURE 4.3: Climatology of tropospheric streamers located near the UK over 3 isentropic levels. Colour contours represent the percentage of daily occurrence in each season.

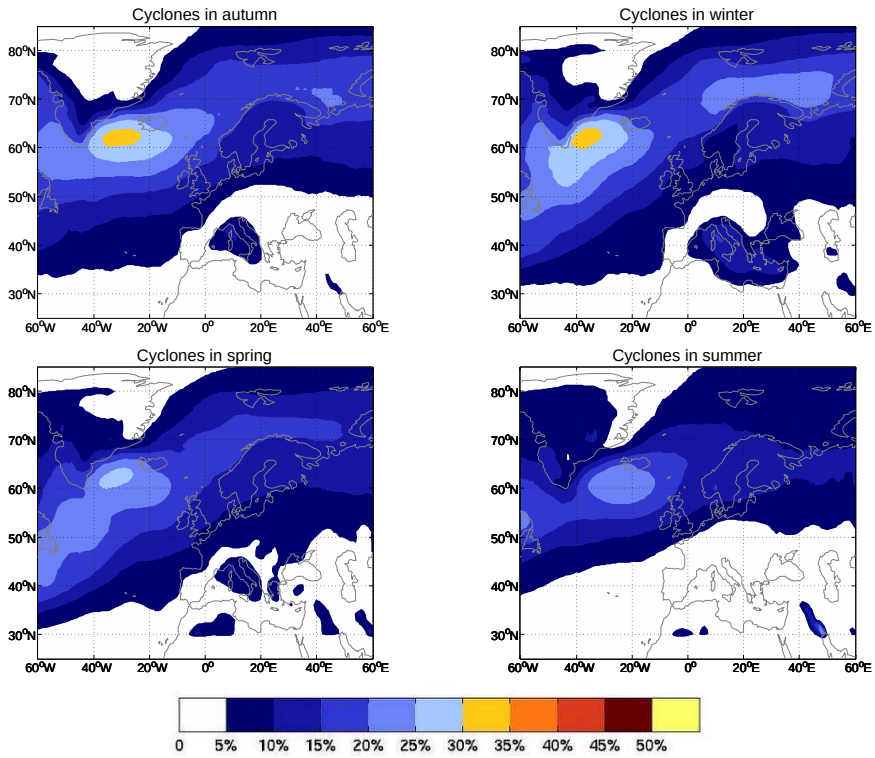

FIGURE 4.4: Climatology of cyclones located near the UK. Colour contours represent the percentage of daily occurrence for each season.

west and east of the UK. The frequencies for this streamer type are much smaller however, and in autumn they are predominantly located over Europe.

The third main data set used is the cyclone climatology from Wernli and Schwierz (2006) which is also extracted from the ECMWF ERA-40 data set. Cyclones (and anticyclones) are derived from sea level pressure (SLP) fields and are identified as the area that surrounds an SLP minimum (or maximum) extended to the outermost closed SLP contour. The data is also extracted on a Northern Hemisphere grid at each timestep as a 0/1-field for cyclone or anticyclone occurrence. The climatological distribution for cyclones in each season is illustrated in Figure 4.4 and anticyclones in Figure 4.5. Cyclones are most frequently found to the north west of the UK in the Atlantic Ocean between Greenland and Iceland with the highest quantity in winter and autumn. Anticyclones have a much higher frequency (especially in the summer season) and are located to the south west of the UK in the Atlantic Ocean off the coast of Portugal and Morocco.

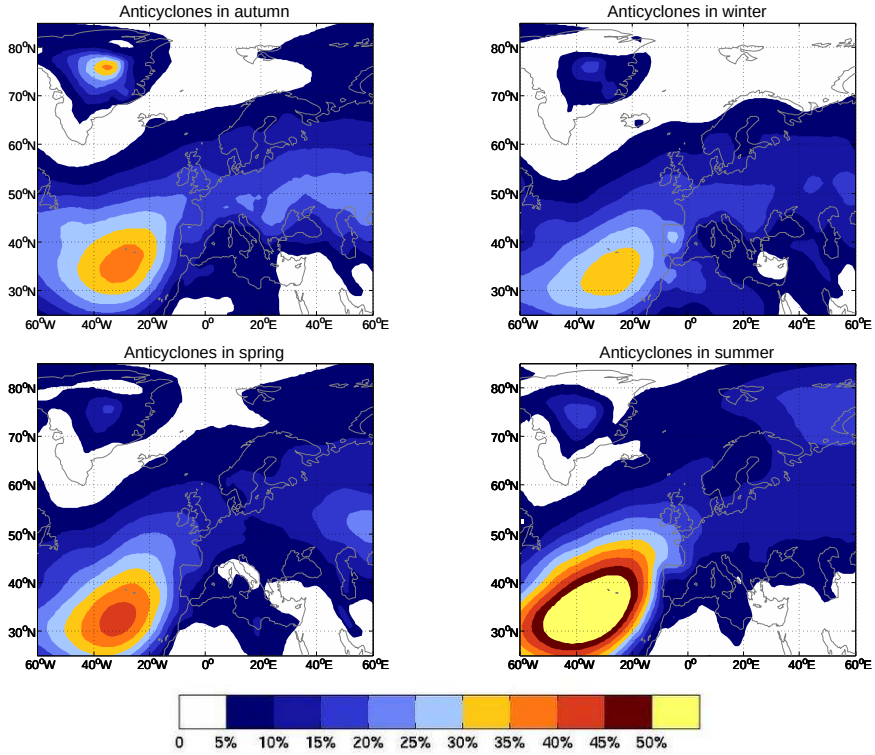

FIGURE 4.5: Climatology of anticyclones located near the UK. Colour contours represent the percentage of daily occurrence for each season.

4.2.2 Methodology

To develop a representation of typical conditions leading up to and during heavy precipitation events the frequency and distribution of stratospheric and tropospheric streamers, cyclones and anticyclones are investigated. In order to calculate the frequency of stratospheric and tropospheric streamers the 0/1 grids for each day are added together for each individual region and season and divided by the number of days. As the data occurs on several isentropic levels (from 310 to 350K) the analysis is carried out for each individual isentropic level as well as for the three specified levels together. If streamers on various levels overlap, each grid point is still only counted once so the maximum value at each point is one for each day. In this way, temporal means can directly be interpreted as local frequencies of occurrence.

A Monte-Carlo test is employed in order to determine the significance of the frequency distributions for features occurring on heavy precipitation days. Days are randomly selected from within each individual season across the whole data set and are used to create a frequency distribution composite. The number of random days selected coincides with the number of days in the top 99%, 95% and 90% quantiles. The stratospheric or tropospheric streamers on three isentropic levels are identified for each day and added to 0/1 grids in the same manner as the heavy precipitation cases. The process is repeated 1000 times in order to construct a suitable base for a climatological comparison. Each grid point of frequency data is checked against each of the 1000 Monte-Carlo frequency distributions. Numbers falling within the top 5% or the bottom 5% are considered significantly different to the Monte-Carlo sample and are thus distinctive for the heavy precipitation days. The same approach is applied to the cyclone and anticyclone data. Grids identifying each day where a cyclone or anticyclone occurs are added together for the heavy precipitation days and the Monte Carlo test is applied for significance.

The second step in the analysis of heavy precipitation days is to investigate how the upper-level features interact with one another and how conditions at the surface are impacted. Preceding Rossby waves along with lagged frequency composites are investigated for timesteps up to seven days prior to the events. This enables an assessment of the development of the upper-level streamer features. The position and occurrence of cyclones and anticyclones are also studied in order to identify the co-evolution of the features. Surface-level conditions such as relative humidity as well as u and v components of wind at 850hPa are analysed to examine the link and

influence of the presence of upper-level features on the heavy precipitation events. Selected case studies are employed allowing for a more detailed examination of typical conditions during extreme events.

Finally, the impact of streamers on the precipitation type, amount and location is investigated further. The main characteristics of the streamers are described including their occurrence, orientation and persistence. An assessment of the structure and PV amplitude of the streamer in relation to the heavy precipitation is then investigated.

4.3 Synoptic features occurring on heavy precipitation days

The seasonal and regional differences in the synoptic situation occurring on the heavy precipitation days will now be discussed. The figures depicted are for the top 99% days with the 95% and 90% cases shown in Appendix A.1. The analysis will be split into seasonal distributions and highlight the similarities and differences for each individual region. The following figures show the statistically significant frequency distribution (to the 95% confidence level) of each feature that occurs more often than in the climatology. Regions are displayed in their closest geographical position (from upper left to lower right: NS, ES, NI, SS, NEE, NWE, CE, SWE, and SEE) as illustrated in Figure 4.1.

4.3.1 Autumn

In the Autumn, for the 99% cases (Figure 4.6), stratospheric streamers are found to the north-west and over the main body of the UK with frequencies up to 80% for all of the regions except NS. For this region, they fall predominantly over northern Europe and Scandinavia. Tropospheric streamers are less frequent with the highest level occurring for NS to the south-east of the UK, over Europe. In many areas where there are significant tropospheric streamers there are also significant anticyclones. For NS, anticyclones occur over southern Europe while for NEE and CE anticyclones and tropospheric streamers are situated over Greenland. Similarly, cyclones are located to the north-west and over the main body of the UK coinciding with the stratospheric streamers. Winds at 850hPa (not shown) are cyclonic over the UK for ES, NI, and NEE, over Scotland for CE, SWE and SEE, and north of Scotland for SS and NWE. Strong westerlies are found over the UK for NS, SS and NWE with westerlies located south of the

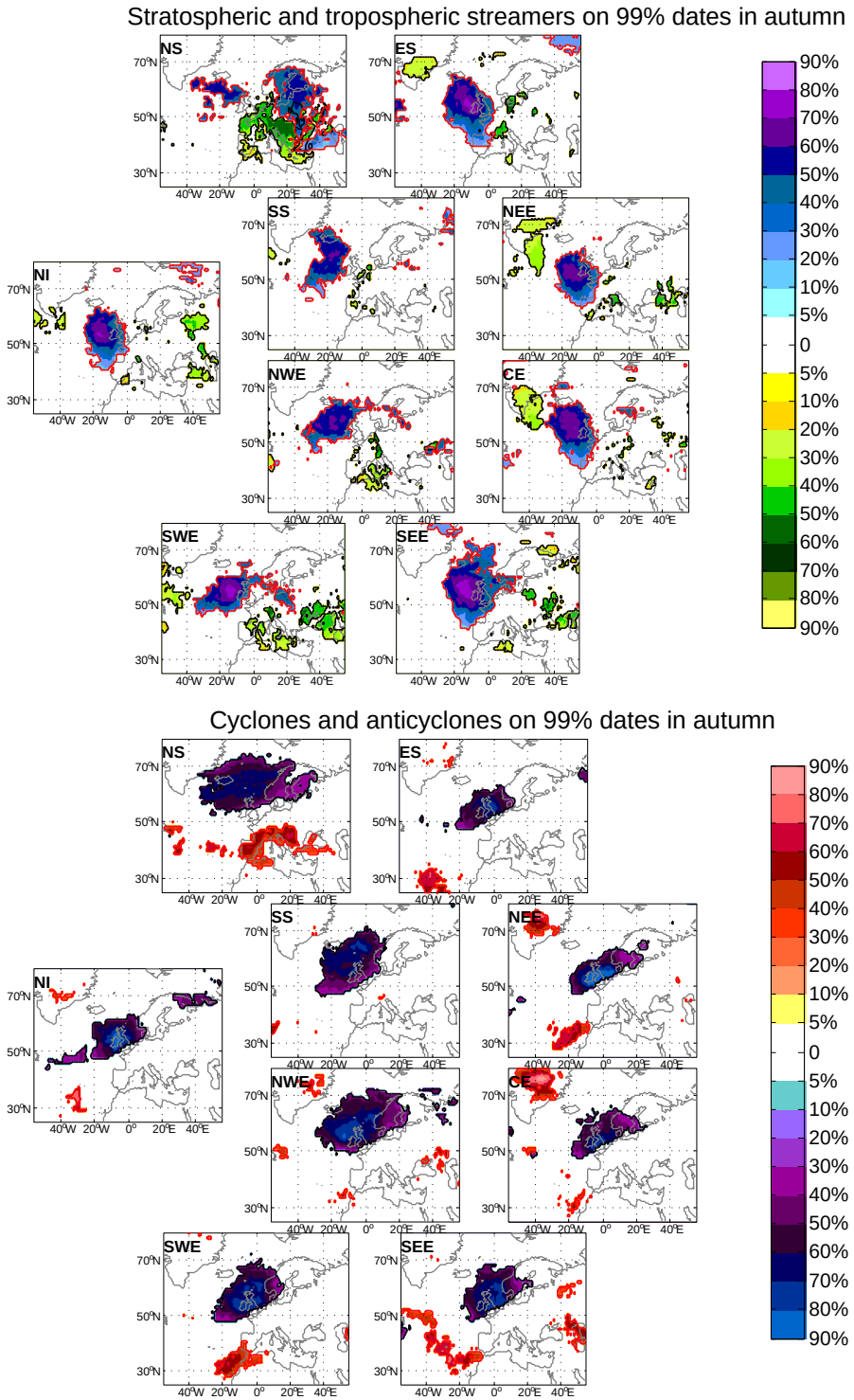

FIGURE 4.6: Frequency of significantly more features than the climatological comparison (to the 95% confidence level) for the 99^{th} percentile cases. Top: stratospheric streamers (blue scale) and tropospheric streamers (green scale) in autumn, bottom: cyclones (blue scale) and anticyclones (red scale) in autumn.

UK for CE, SWE and SEE. The frequency distributions indicate that the heavy precipitation is produced in periods of westerly flow (similar to the study by Hand et al. (2005)) by upper-level stratospheric PV streamers coupled with an associated cyclone. These two features occur together for all regions except NS where a pattern of low pressure to the north and high pressure to the south, as well as increased wind velocities, indicate that fronts pass over Scotland.

For the 95% and 90% cases the patterns for all the regions are very similar to each other with stratospheric streamers occurring to the north-west of the UK and tropospheric streamers over the Baltic Sea. Daily occurrences are lower than the 99% cases with 50-60% for stratospheric and 30-40% for tropospheric streamers. Cyclones are again found just to the north of the UK with anticyclones predominantly to the west of Morocco in the Atlantic Ocean. This pattern coincides closely with the climatologies of these features. In all of the seasons the frequency maxima decreases with increasing sample size. This is observed by an outward spread of the frequency distribution and reduced maximum values in the 95% and 90% figures.

4.3.2 Winter

Stratospheric streamers, for the 99% heaviest precipitation days in the winter season (Figure 4.7), are less frequent than other seasons coinciding with the reduced frequency in the climatological distribution (Figure 4.2). The highest number of occurrences are found for the ES, NI and CE regions where they are located to the west of the UK (Figure 4.7). In the southern regions (SWE and SEE) significantly more stratospheric streamers are found over Europe with tropospheric streamers closely following them over north-eastern Europe. Significantly fewer tropospheric streamers (not shown) are located in the Atlantic. As a result, there is a reduction in the number of preceding ridges, and hence fewer stratospheric streamers are positioned to the west of the UK. Anticyclones are generally found over Morocco and Spain for most regions with a northward placement in NS over central Europe. For southern regions (NWE, CE, SWE and SEE) the anticyclones are found to the south-west of tropospheric streamers.

Cyclones are located to the north-west of the UK in the winter time for all of the regions (Figure 4.7), with the greatest frequency in ES, SS, NWE, and SWE and least in NEE and CE (not shown). Winds at 850hPa are weakly cyclonic over the UK for ES, NEE and CE. Strong westerly winds are found over the UK for NS, SS and NWE while in SWE and SEE

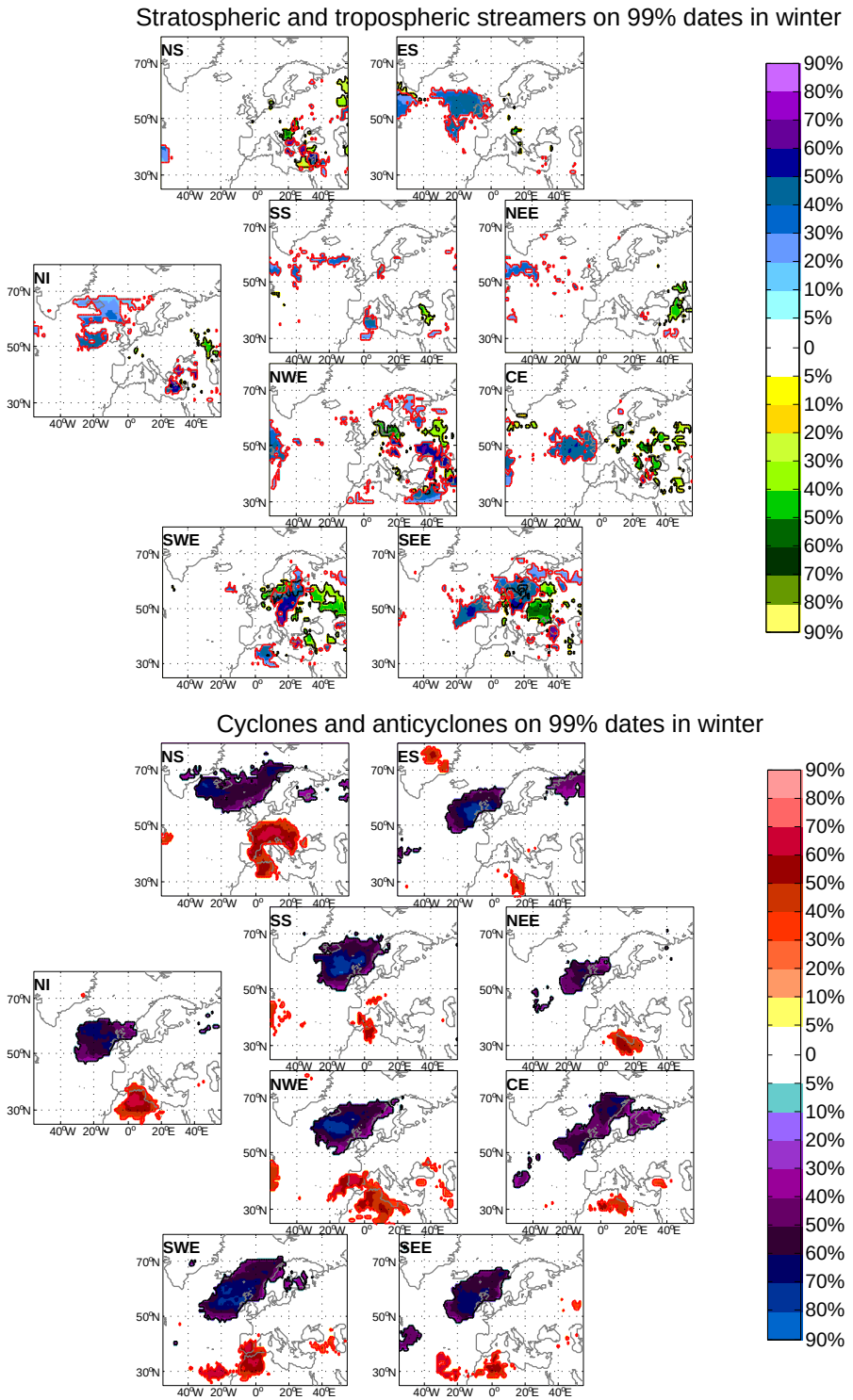

FIGURE 4.7: Frequency of significantly more features than the climatological comparison (to the 95% confidence level) for the 99^{th} percentile cases. Top: stratospheric streamers (blue scale) and tropospheric streamers (green scale) in winter, bottom: cyclones (blue scale) and anticyclones (red scale) in winter.

these are positioned further south, with a cyclonic component over the UK. The frequency distributions illustrate that low pressure systems are the dominant feature in this season, in combination with high pressure to the south of the UK, creating a frontal situation. Reduced wave amplification and breaking to the west of the UK could be a result of increased zonal winds (and jet) which decrease the potential for PV streamer formation (Postel and Hitchman, 1999).

The pattern in the 95% and 90% cases show cyclones north west of the UK and anticyclones over the Atlantic off of Portugal for all of the regions (with a slightly eastward placement over Algeria in the 95% cases). The streamers once again coincide with the climatologies with stratospheric and tropospheric streamers occurring predominantly over Europe. Stratospheric streamers to the west of the UK are still observed in ES, NI and CE regions.

4.3.3 Spring

In spring the distribution of significantly more stratospheric streamers for the 99% cases is more varied (Figure 4.8). There is an east-west split across the regions of the UK with western areas (NWE and SWE) displaying few stratospheric streamers and eastern areas (NEE, CE and SEE) characterised by frequencies up to 80% to the west of the UK. The opposite is found for cyclones with few occurring in SEE, CE and NEE and daily occurrences up to 70% in western regions (with the highest in SS of 80%). Tropospheric streamers are most prevalent in northern regions with a ridge/trough pattern found for ES, NI and NEE. For all of the regions tropospheric streamers occur to the east of the UK, with highest frequencies for NS. There is an eastward shift in tropospheric streamers in western regions with significantly fewer found to the west of the UK (not shown). Eastern regions meanwhile have a westward shift of stratospheric streamers with significantly less found over Europe. The highest frequencies of anticyclones are found over the Atlantic Ocean off the coast of Morocco and Portugal with a slightly northward placement for NS (Figure 4.8). Winds at 850hPa have a cyclonic circulation for most of the regions with weaker values for NEE, SWE and SEE and stronger winds for ES (not shown). Westerly winds are found over the UK for NS while in SS and NWE these are found to the south of the UK with a cyclonic component to the north.

The heavy precipitation daily values are lowest in the spring for all regions (Table 4.1) and especially for eastern regions (CE and SEE). Western areas have little influence from PV

streamers and are dominated by high pressure to the south-west combined with cyclones to the north-west of the UK. These features, combined with the orography of the western UK, combine to form higher rainfall amounts. In the east, very few cyclones are found and anticyclones are either near to their climatological position or found over eastern Europe. In these regions, stratospheric streamers have the largest influence with convective precipitation events more likely.

In the 95% and 90% cases SS resembles NS with higher frequencies of stratospheric streamers over eastern Europe. Anticyclones are found in the Atlantic off the coast of Morocco with a more northward position off Portugal for SS and NS. The highest maxima of cyclones (up to 70%) are also found in these two regions. The rest of the regions (ES, NI, NWE, NEE, CE, SWE and SEE) all have similar distributions with stratospheric streamers to the west of the UK and tropospheric to the east. NWE bears some resemblance to SS and NS with fewer numbers of stratospheric streamers to the west. Cyclones occur to the north-west of the UK and out into the Atlantic Ocean south of Greenland, with reduced frequency for eastern regions.

4.3.4 Summer

The highest maxima of stratospheric streamers (up to 90%) and tropospheric streamers (up to 60%) are both found in the summer season (Figure 4.9). Stratospheric streamers are mainly located west and over the UK for ES, NI, SS, NEE, CE, SWE and SEE. For NWE these streamers are predominantly situated north of the UK and over Scandinavia while for NS very few significant stratospheric streamers occur. Tropospheric streamers occur to the east of the UK, especially for north-eastern regions such as NS, ES, SS, NWE, NEE and CE.

The frequency of cyclones is reduced in summer primarily in southern regions (NEE, CE, SWE, and SEE) where convective precipitation is likely to be the predominant precipitation type. The winds at 850hPa are also reduced in summer with much smaller values for all regions. There is a weak cyclonic circulation for ES, NI, NEE, CE, SWE and SEE. Westerly winds are found over the UK for NS while for SS and NWE these are found to the south of the UK with a cyclonic component to the north, similar to spring. For the NS and SS regions, where cyclones have the highest maxima, very few anticyclones are found. In the other regions, anticyclones are more prevalent in the summer with occurrence up to 90% over the Atlantic Ocean (off the coast of northern Africa and Portugal). Patches of anticyclones also occur

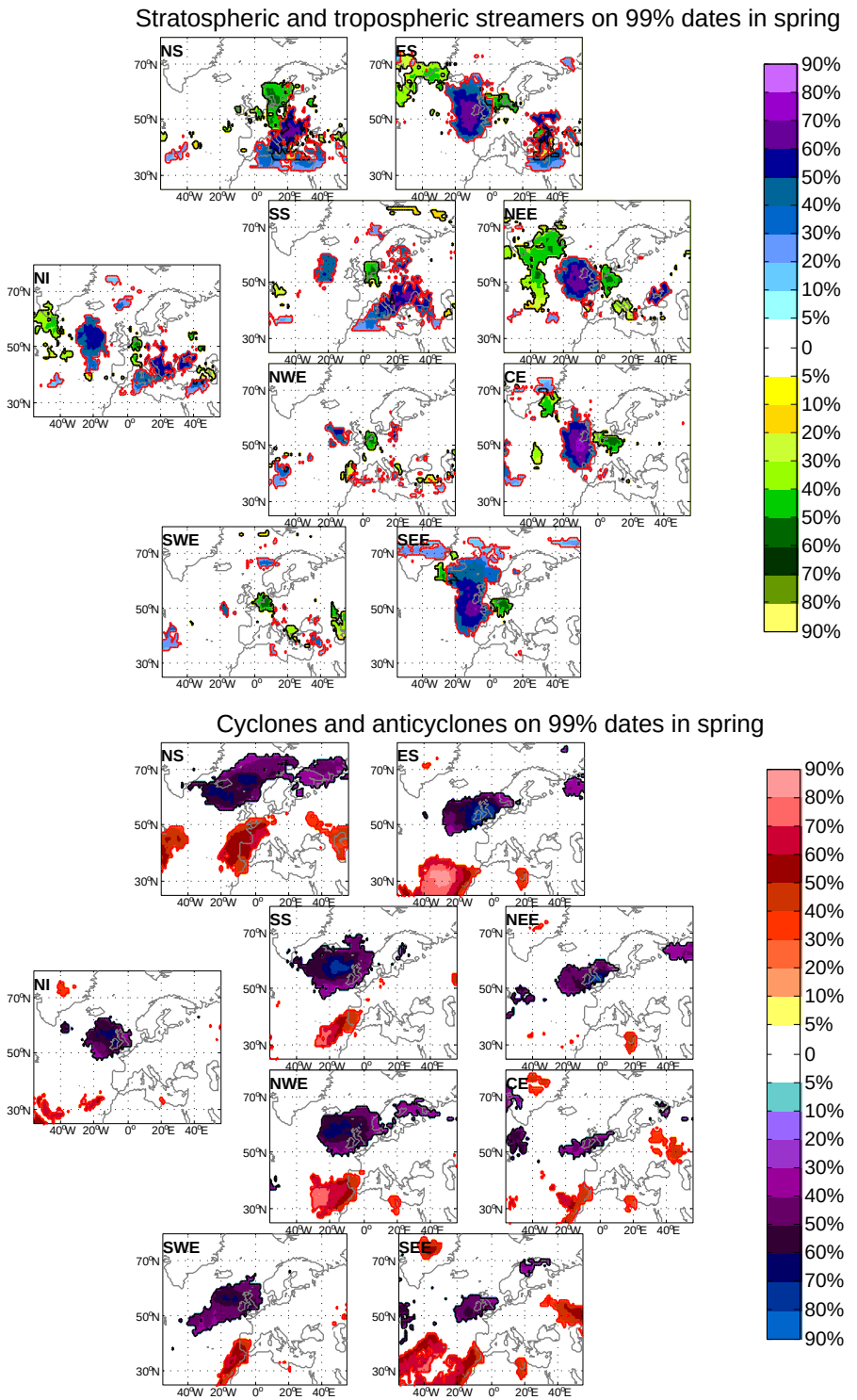

FIGURE 4.8: Frequency of significantly more features than the climatological comparison (to the 95% confidence level) for the 99^{th} percentile cases. Top: stratospheric streamers (blue scale) and tropospheric streamers (green scale) in spring, bottom: cyclones (blue scale) and anticyclones (red scale) in spring.

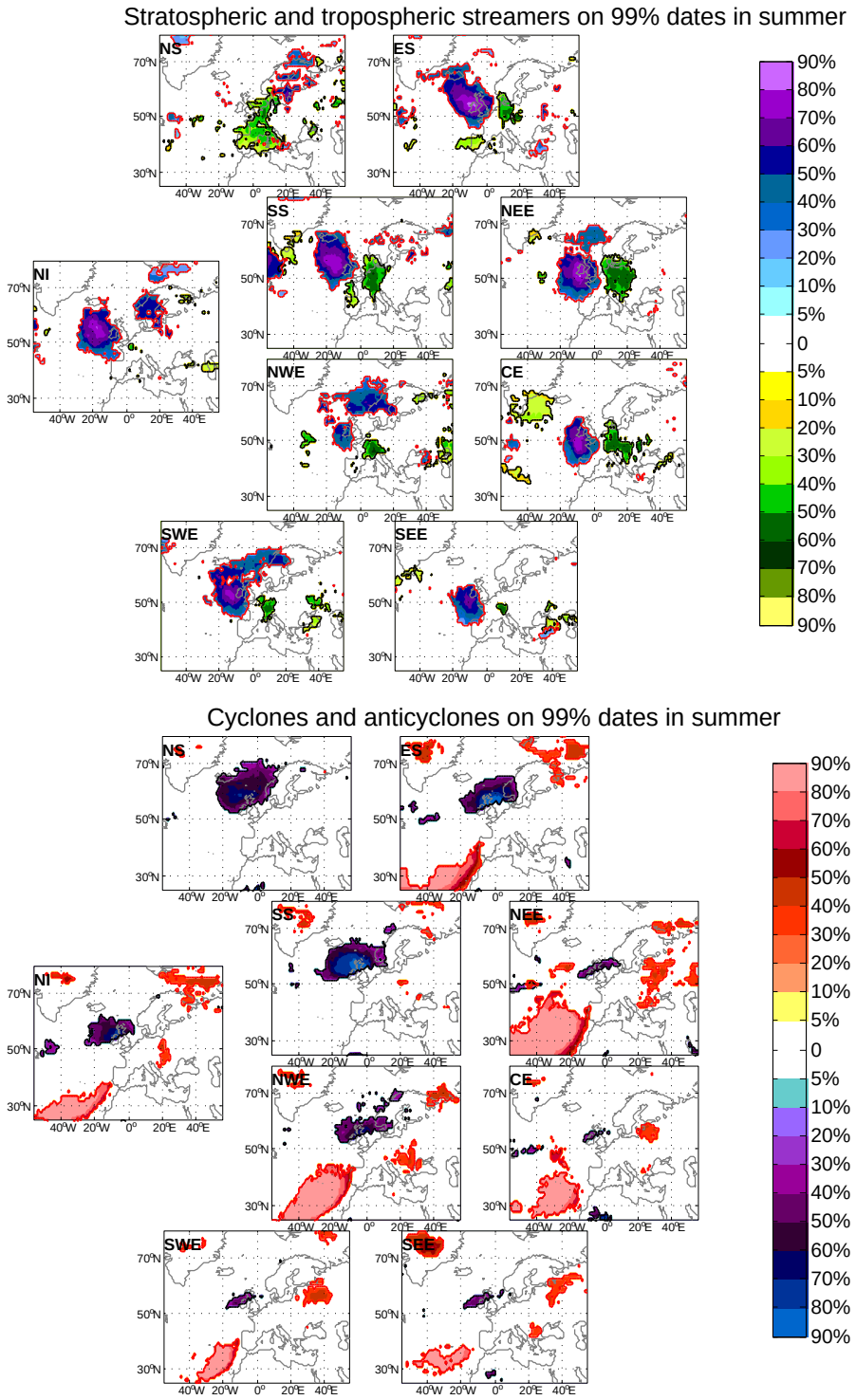

FIGURE 4.9: Frequency of significantly more features than the climatological comparison (to the 95% confidence level) for the 99^{th} percentile cases. Top: stratospheric streamers (blue scale) and tropospheric streamers (green scale) in summer, bottom: cyclones (blue scale) and anticyclones (red scale) in summer.

over Greenland and in eastern Europe. The statistically significant frequency distributions indicate that stratospheric streamers play a large role in heavy precipitation events. For north-western regions they coincide with cyclones, resulting in frontal precipitation while south and eastern regions resemble spring with stratospheric streamers mainly associated with convective precipitation. Evidence of upstream blocking for some of the cases is observed by anticyclones situated over eastern Europe, indicating the possibility of stationary troughs being present over or to the west of the UK (similar to Blackburn et al. (2008) in the summer of 2007).

The 95% and 90% cases all have a very similar distribution with stratospheric streamers west of the UK and tropopsheric streamers to the east. Cyclones are located to the north-west of the UK with few occurrences for NEE, CE, SWE and SEE. Anticyclones are grouped in their climatological position in the Atlantic off the coast of northern Africa and Portugal with the only exception to this in the 95% cases where NS, SS and NI have reduced frequencies. There are also anticyclones found over Greenland for all the regions on the 95% days.

4.3.5 Summary

The highest occurrence of significantly increased stratospheric streamers are observed to the west of the UK in autumn and summer. In autumn these combine with cyclones creating a more intense system and frontal precipitation. In the summer this situation occurs in north-western regions, while convective precipitation is prompted by an overlying PV streamer (that provides the mechanism for ascent) for eastern and southern regions. Summer also contains the maxima for significantly higher tropospheric streamers which are coupled with the stratospheric streamers. Winter is categorised by a stronger waveguide, leading to less wave breaking and thus few streamers but more cyclones, such that frontal systems are the main cause of the heavy precipitation in this season. In the spring, there is much more variation in the placement of synoptic features with a distinct east-west split across the UK. Cyclones are the dominant feature in western regions and interact with topography to create higher rainfall amounts. Stratospheric streamers have the most significance in eastern areas with a similar pattern to summer time conditions.

Winds at 850hpa are westerly to the south and cyclonic over the UK for southern regions CE, SWE and SEE in autumn and winter. In spring and summer this pattern is found for NS, SS and NWE, while in autumn and winter it is pushed further north, so that westerlies occur over

and cyclonic winds are north of the UK. For precipitation in other regions cyclonic winds are found over the UK with strongest amplitudes in autumn and winter.

In all of the seasons, NS and ES stand out from the rest of the UK in the 99% cases. ES is characterised by the most consistent distribution of stratospheric streamers, combined with cyclones. The orography in this region, along with the upper-level PV streamers and surface lows, produces a similar situation to that in the Alps with uplift and precipitation south-east of the Highlands. The systems associated with the highest precipitation in the UK over NS are less frequently supported by stratospheric streamers to the west. Instead, the westerly winds are stronger on heavy precipitation days in NS associated with a low to the north and a high to the south of the UK and probably fronts passing over Scotland. Stratospheric and tropospheric streamers are shifted to the east over Europe and may have an influence on the position of the southerly placed anticyclones.

4.4 Preceding Rossby waves and synoptic features leading up to heavy precipitation days

Refined Hovmöller plots are used in order to investigate the Rossby waves leading up to the heavy precipitation events. The waves are analysed on one isentropic level, 320K for autumn, winter and spring and on 330K for summer. Figure 4.10 displays all the Hovmöller plots for the 99% heavy precipitation cases from northern regions (top) to southern regions (bottom) for all the seasons. Individual plots are centered at 0° longitude and show the heavy precipitation day (top) to 7 days prior to the event (bottom). Each plot represents the combined waves from all the cases within the region and season. A Monte Carlo test for significance is applied by creating 200 composites of velocity values for the same number of days in each season and region. Data points exceeding the top 98% quantile within the composites are then considered significant and are displayed in the diagrams.

The plots represent the statistically significant consistent wave signal leading up to the heavy precipitation days as described in Section 3.3. Positive and negative peaks are apparent in most of the regions on the heavy precipitation days indicating the presence of a ridge and trough near the UK. The most homogeneous Rossby wave signals are found in autumn and summer with less coherent wave development in winter and spring. In the autumn, the highest

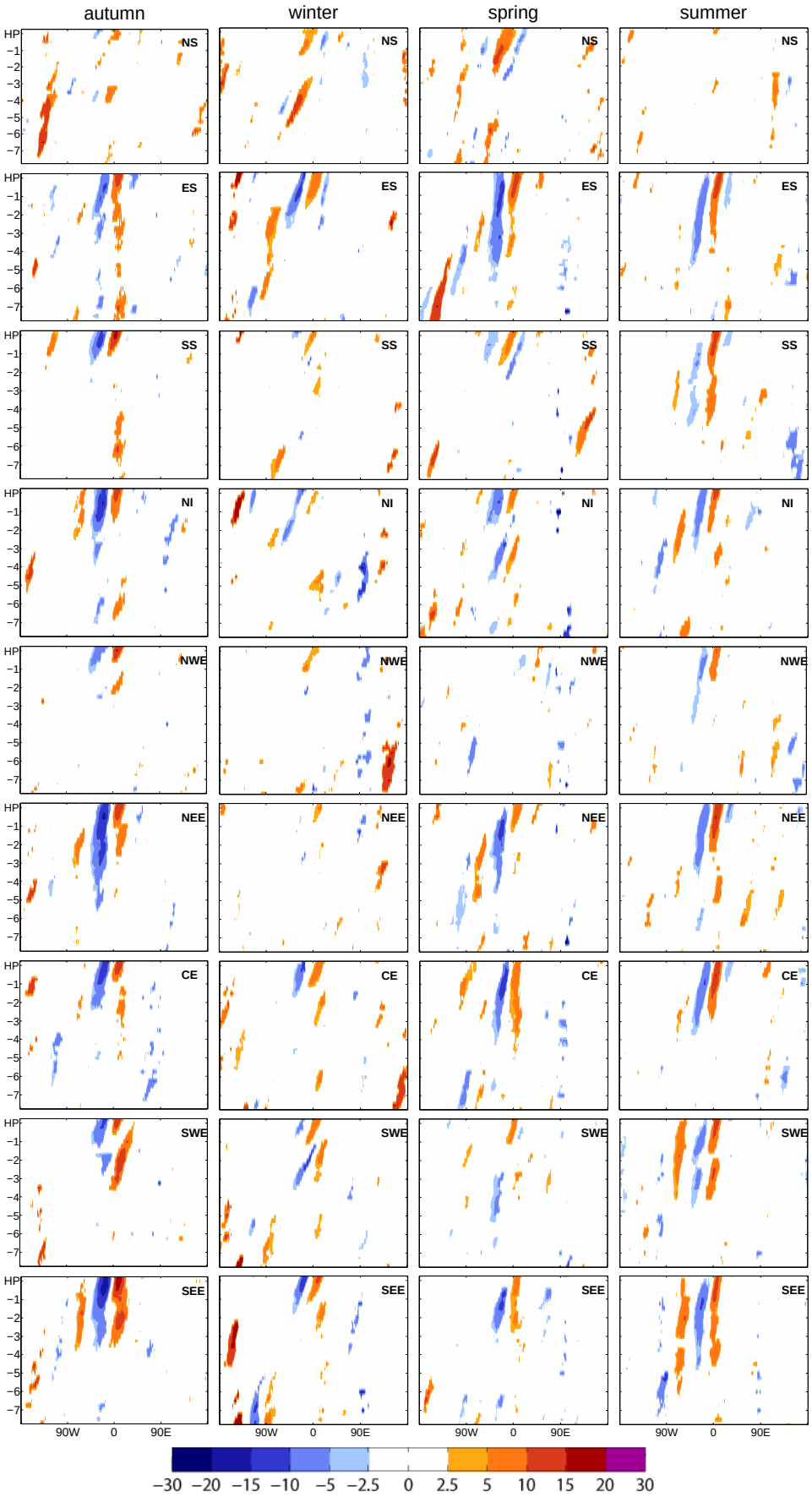

FIGURE 4.10: Hovmöller plots of the meridional wind speed (m s^{-1}) for the preceding Rossby waves (precipitation day to 7 days prior) for 99% heavy precipitation days in all regions (northern: top to southern: bottom) and seasons. One isentropic level is used for each season: 320K for autumn, winter and spring and 330K for summer.

.

velocities occur, and wave trains extend back to around $90°$W (near the eastern Atlantic) 2-3 days prior to the event in ES and NI. NEE and SEE show evidence of a more stationary trough positioned over the UK. The wave signal is reduced in SWE and CE while in NS, SS and NWE the presence of a trough or streamer only occurs on the heavy precipitation day, with no preceding signal. In the summer season almost all of the regions have a wave signal extending back 3-4 days to $90°$W. SEE is characterised by a persistent wave pattern, a feature that is unusual in summer seasons (Martius et al., 2008). In NWE there is a reduced wave signal while in NS no signal is apparent. ES, NEE and CE have 2 velocity peaks which indicate a slow moving trough beginning in the Atlantic and progressing towards the UK.

Winter has very little evidence of a precursor signal in the 99% cases, with most regions only having a ridge/trough system appearing on the heavy precipitation day. SS, NWE, and NEE have virtually no signal even during the precipitation event. The longest wave train is found in ES extending back 3 days prior to the heavy precipitation. In the spring, many of the regions are similar to winter and have little or no precursor signal (SS, NWE and SWE). In contrast, the longest wave trains are also found in this season extending back nearly 7 days to the Pacific in ES and NEE. There is an east-west split with longer wave trains in eastern regions and shorter wave trains in the west corresponding to the stratospheric and tropospheric streamer patterns on the heavy precipitation days.

The 95% heavy precipitation days (shown in Appendix A.9) have similar patterns but with slightly longer wave trains in autumn and for some regions in the spring (NWE, CE and SEE), as well as in NS in the winter season. The pattern in NS coincides with the altered frequency distribution between the 99% and 95% events signaling a change in upper-level patterns impacting the heaviest compared to high precipitation events. The summer season was unexpectedly dominated by a stationary velocity peak at $0°$ longitude. This could highlight the position of a persistent anticyclone, a prominent feature in this season.

After analysing the preceding Rossby wave signal, lagged composites of potential temperature on PV2 are also investigated for the seven days preceding the 99% quantile precipitation events. The statistically significant lagged frequency distributions (to the 95% confidence level) of stratospheric streamers, tropospheric streamers, cyclones and anticyclones for each region are used to identify the development of the synoptic-scale features prior to the heavy precipitation event. The consistent signal from over 50% (unless otherwise stated) of the cases is used to determine the position and commencement of each feature. Although each case

in the 41 days evolves slightly differently, an average picture of the co-initiation of the main synoptic features is constructed and the seasonal and regional conclusions are described.

Northern Scotland (NS):
Cyclones are the dominant feature and are present several days in advance coming from the north west and moving towards the UK. In winter they can be tracked back 5 days from the coast of Canada and southern Greenland. Anticyclones are a coherent feature in all seasons coinciding with tropospheric streamers to their east. In autumn, winter and summer they are present to the south of the UK 2 days (5 days in spring) before the heavy precipitation event pushing the cyclones further north over Scotland. In autumn, stratospheric streamers in eastern Europe are paired with the tropospheric streamers intensifying them.

Eastern Scotland (ES):
In all the seasons, stratospheric streamers co-evolve with cyclones travelling from a western direction. The preceding signal is longer in spring (6 days) and summer (4 days) and shorter in autumn (2 days) and winter (3 days). Anticyclones are an important feature for this region as they appear 3 days in advance for winter, spring and summer. Their position to the south of the UK helps to steer the cyclones north and west. In spring and summer, anticyclones are accompanied by tropospheric streamers, which aide in their intensification.

Southern Scotland (SS):
This region has synoptic elements similar to NS in winter and spring and ES in summer and autumn.

Northern Ireland (NI):
Preceding Rossby waves are present in most seasons 1 to 2 days before the precipitation event. Cyclones are the dominant feature for this region with co-evolution occurring with stratospheric streamers to the west of the UK in summer only. In autumn and winter cyclones are detected 4/3 days prior in the Atlantic Ocean to the west of the UK and stratospheric streamers evolve to the west of these features 1/2 days prior to the heavy precipitation event. In the spring time a cyclone signal emanates from the southern US 5 days before the event. Anticyclones are only present before the heavy precipitation day in winter (accompanied by a tropospheric streamer) and in summer.

North West England (NWE):
Although a preceding trough/streamer is only present 1 day ahead in autumn and summer

for the 99% cases, initial synoptic signals begin earlier than in many regions with cyclones travelling from a south-westerly direction toward the UK. In autumn and spring a stratospheric streamer and cyclone pairing occur in the Atlantic off the southern coast of the US 6 days ahead. Anticyclones are also coupled with tropospheric streamers over Europe and Scandinavia creating a blocking feature (however this feature diminishes 1 day prior to the precipitation event). A cyclone evolves 3 days before the precipitation in winter (with a stratospheric streamer in summer) to the south west, off the coast of the US, and moves toward the UK. An anticyclone again sits over Europe 2 days ahead (in 45% of the cases) and then moves to the south of the UK.

North East England (NEE):
There is more variability in the synoptic features leading up to the heavy precipitation day in the north east region with anticyclones only occurring in summer to the south west of the UK and over Greenland. In autumn and summer a ridge trough pattern can be detected from Canada to the UK 1 to 2 days prior and in spring 3 days before. Cyclones occur to the north west of the UK (3 days ahead) before the stratospheric streamers appear (2 days ahead) in autumn. In summer, stratospheric streamers are located to the west of the UK 3 days ahead (co-evolving with a cyclone in 35% of the cases). In spring, cyclones develop after the stratospheric streamer to the south west of the UK in 30% of cases and in winter a cyclone is present over the UK 4 days prior.

Central England (CE):
In this region co-evolution of stratospheric streamers and cyclones occur in autumn and spring (30% of the time) 4 days prior to the event to the west of the UK. Stratospheric and tropospheric streamers are also present to the west and east when the cyclone first develops off the eastern US coast 5 days ahead in winter. The cyclone then moves towards the UK but the streamers diminish. In the summer, the stratospheric signal appears first (3 days prior), to the west of the UK, followed by a cyclone (2 days prior in 35% of cases) under the body of the streamer.

South West England (SWE):
In the south west region cyclones develop to the east of stratospheric streamers in autumn, winter and summer off the US coast 4 days before the heavy precipitation events. In spring a cyclone develops in the Atlantic 3 days before and strengthens as time progresses. Anticyclones

form 4 days ahead in autumn and winter and 3 days ahead in spring and summer in the Atlantic off Portugal and Morocco.

South East England (SEE):
Cyclones develop further north in autumn (6 days ahead with stratospheric streamers) and winter (5 days ahead) off the coast of Iceland and Canada. They develop further south in spring and summer, south west of the UK (3 days ahead) and off the coast of the US (2 days ahead) respectively. Stratospheric streamers are sporadic in winter and spring developing 1-2 days before the heavy precipitation event. Tropospheric streamers are only present in the summer, corresponding to an anticyclone over Iceland 1 day prior. Anticyclones are also situated in the Atlantic Ocean, south west of Portugal. In autumn and spring anticyclones are further south off the coast of Morocco 6 days and 3 days ahead respectively.

4.5 Case studies

Now that a general picture of each region has been constructed, a detailed analysis of 2 heavy precipitation events will be described. As the summer was highlighted as a season with high correspondence to PV streamers, the first case investigates a summer case of heavy precipitation that occurred in several regions over a few days. Northern Scotland has an unusual upper-level pattern in comparison to the other regions, so a winter heavy precipitation event in this region will be explored in more detail.

4.5.1 Case study 1: 24-26 June 1997

From the 24th to the 26th of June heavy precipitation affected several regions of the UK. Three regions in particular (NI, NEE and CE) each had rainfall within the top 99% quantile. Heavy precipitation initially fell over northern Ireland (NI) on the 24th of June (Figure 4.11) in combination with a low pressure system. Over the next two days the precipitation moved further east and fell over central and north-east England (CE and NEE).

The upper-level situation preceding and on the heavy precipitation days is shown in Figure 4.12. On the 23 of June 1997, a PV streamer co-evolved with a low pressure system in the Atlantic, south of Greenland. The two synoptic features travelled eastward together and the low began

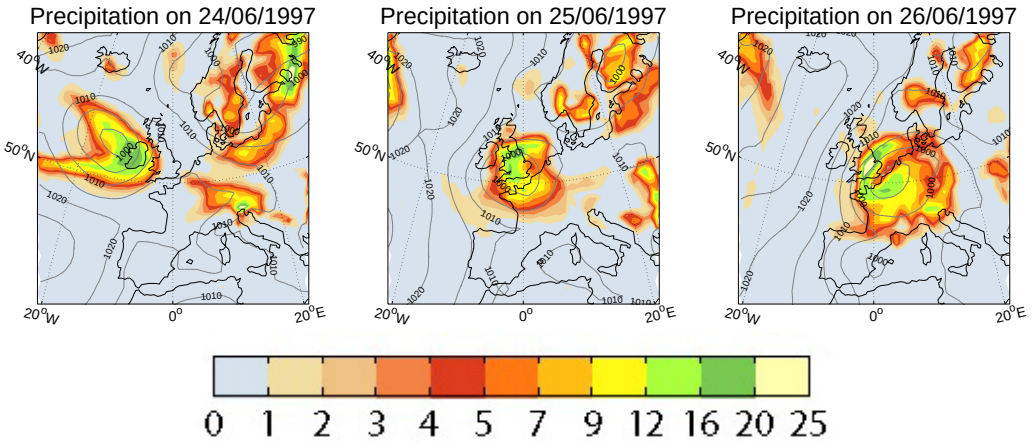

FIGURE 4.11: 24 hour precipitation in mm from 24/06/97 to 26/06/97. Grey contours show sea level pressure on 850hPa.

to intensify but remained relatively small in size. By the 25th, the streamer feature caught up with a larger stationary trough situated over Europe and began to re-intensify. The feature then wrapped up cyclonically and eventually joined the larger stationary trough.

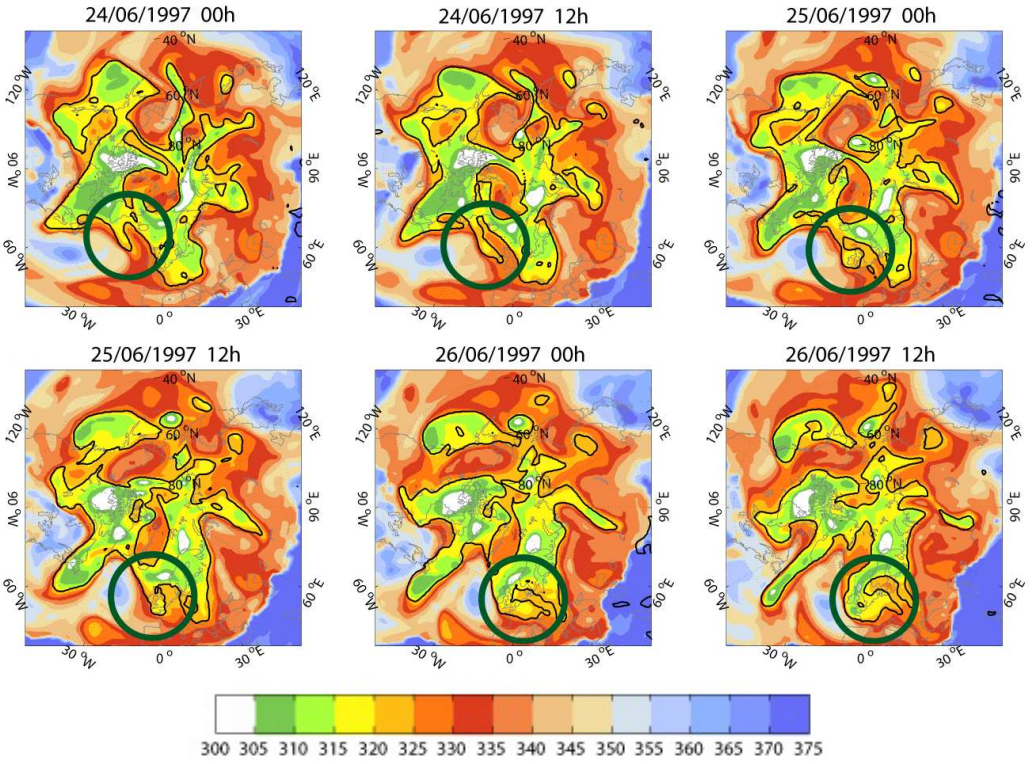

FIGURE 4.12: Development of a stratospheric streamer over the UK from 24/06/97 to 26/06/97 (highlighted by a green circle). Potential temperature on PV2 is shown as the colour contours and the black line represents the 320K PV2 line.

On the 24th of June, the low pressure system was situated directly beneath the PV streamer to the west of the UK and Northern Ireland (Figure 4.13a). Cyclonic circulation drew moist air

in from the south west of the UK (Figure 4.13b). The PV streamer penetrated equatorward as well as southward towards the surface as shown in the cross section in Figure 4.13d. Vertical ascent beneath this anomaly led to moist air being lifted and precipitation falling over Northern Ireland. A sting jet feature is also present at this time with the warm conveyor belt located beneath the PV intrusion and cold conveyor belt located at the surface to the west (not shown). The descending air on the western side of the PV streamer (Figure 4.13d) shows the position of the sting jet (as described by Browning (2004) and Browning and Field (2004)) and thus strongest winds.

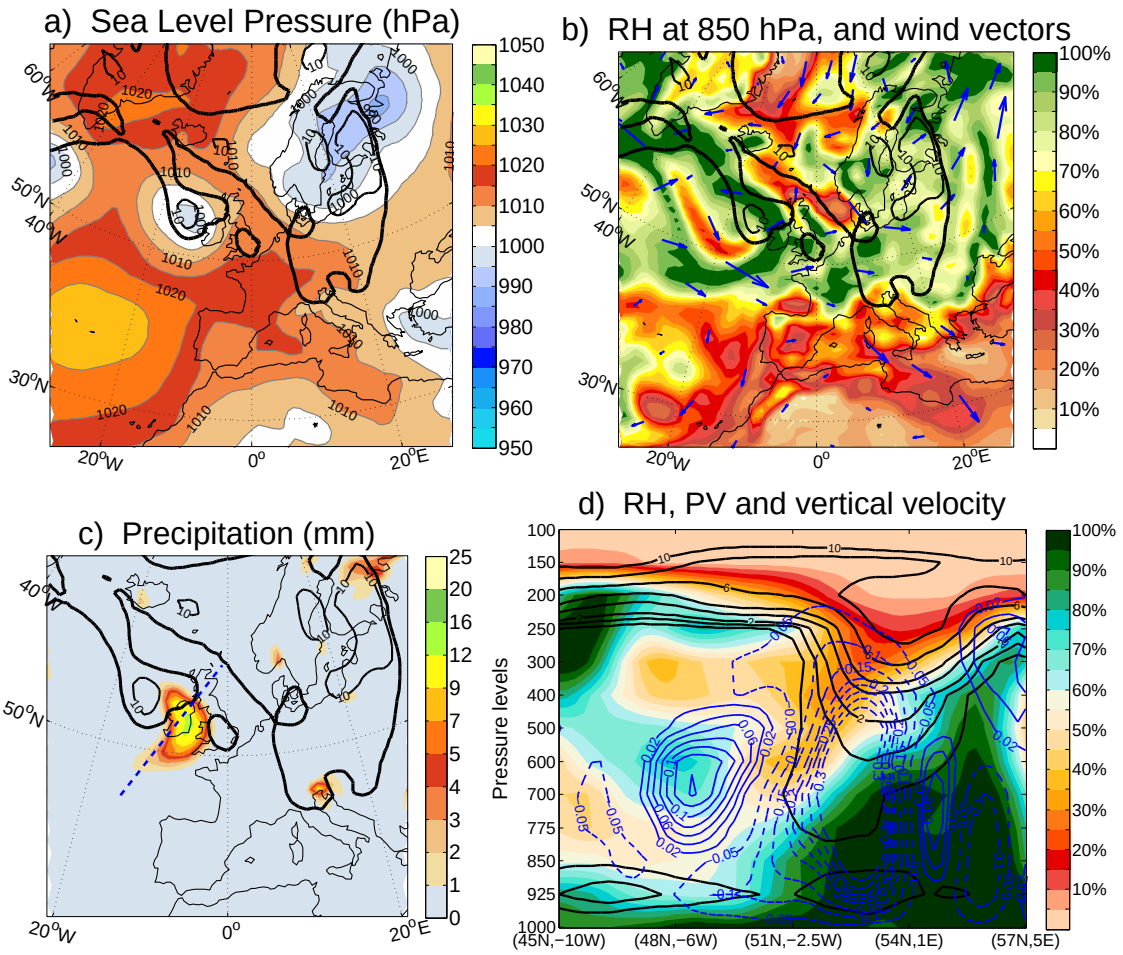

FIGURE 4.13: The situation on the 24th of June 1997 at 18UTC. Sea level pressure in hPa (a), relative humidity with wind vectors as blue arrows (b) and 6-hourly precipitation (c). Plots a-c also show the 320K PV2 line in black. The blue dashed line in c indicates the position of the cross section. Cross section (d) with relative humidity as the colour contours, PV is shown by solid black lines and vertical velocity (ms^{-1}) is represented as blue lines. Areas of ascent are dashed and descent are solid.

As the days progressed, the low stalled over the UK as the PV streamer caught up with a downstream trough over Europe (Figure4.14a). Warm moist air was still pulled in front of the

streamer through cyclonic circulation (Figure 4.14b). Vertical ascent continued to the east of the positive PV anomaly lifting the moist air up. Saturation transected the entire troposphere reaching into the tropopause. Precipitation fell over south and eastern England as a result of these combined elements (moisture influx, upper-level PV anomaly and cyclone).

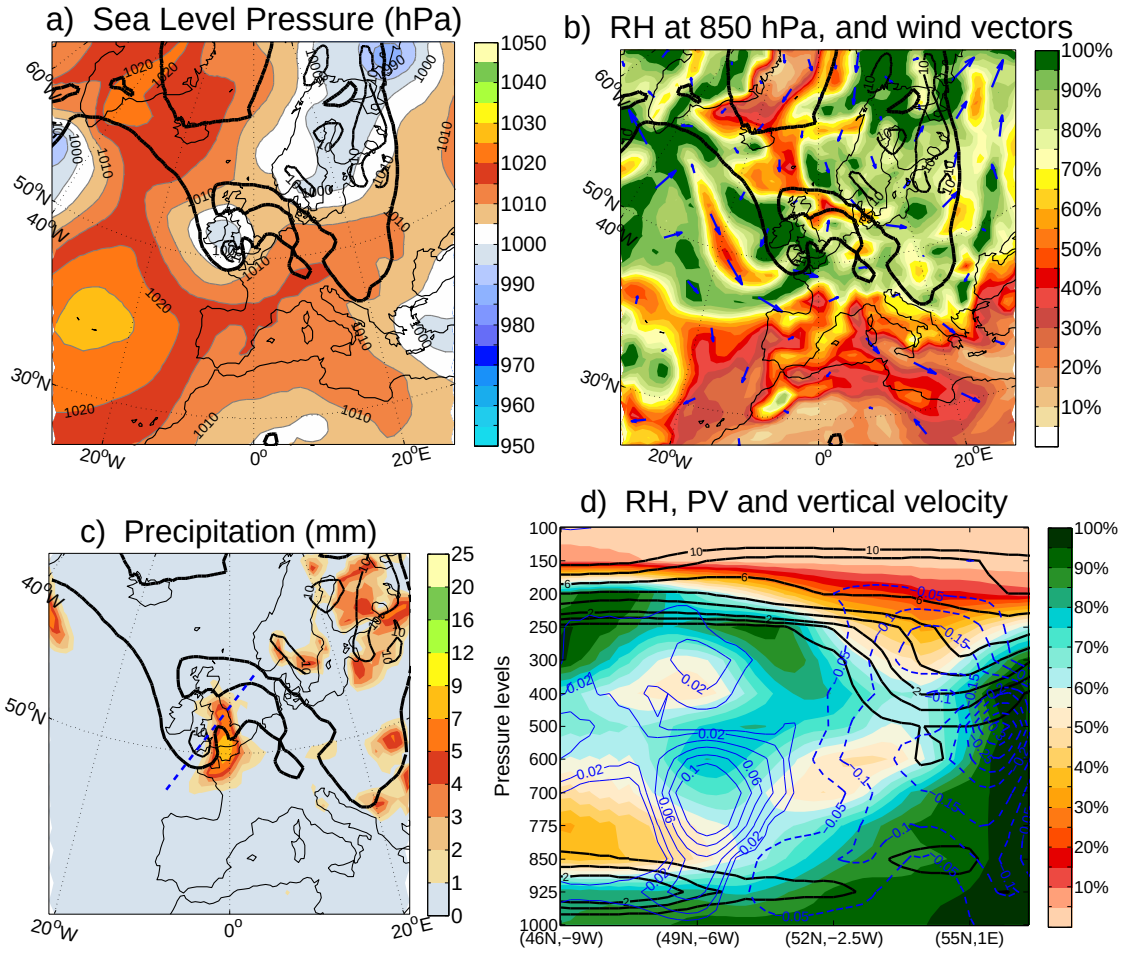

FIGURE 4.14: Same as Figure 4.13 except for the 25th of June 1997 at 06UTC.

As the PV streamer continued to wrap up cyclonically, the low pressure stayed directly underneath the central portion of the streamer, allowing further precipitation to fall. The southward extent towards the surface was reduced in the final stages (probably caused by diabatic reduction of PV) and the vertical ascent also lessened as the streamer joined the main trough. Precipitation only continued until the streamer was absorbed completely by the trough and then the whole system moved further east. The length of time that the low pressure and PV streamer were present over the UK contributed to the increase in precipitation. Other factors, such as the intense air saturation and thus moisture within the area also led to this anomalously high precipitation event.

4.5.2 Case study 2: 05 December 1997

In the winter of 1997, a heavy precipitation event took place over Northern Scotland. There was no evidence of a stratospheric PV streamer associated with this event, but instead a steep pressure gradient was positioned over the UK between a high and low pressure system. The precipitation fell mostly on the 5th of December and continued until the 6th. Figure 4.15 shows the sea level pressure contours and the associated precipitation. These combined features act as an atmospheric river transporting large quantities of moisture-laden air at high speeds towards Northern Scotland.

The situation at the upper-levels is shown in Figure 4.16. On the 4th of December, a cyclonically wrapping streamer was evident upstream in the Atlantic. A trough was also present, initially located over England. As the days progressed, an enhanced tropospheric ridge formed over the UK and a stratospheric streamer developed to the east over Europe, with a southward extension reaching as far as northern Africa. The stratospheric air from the cyclonic streamer over the North Atlantic re-attached to the main body of stratospheric air forming a trough. The UK was positioned directly beneath the enhanced ridge, and yet a heavy precipitation event occurred in Northern Scotland.

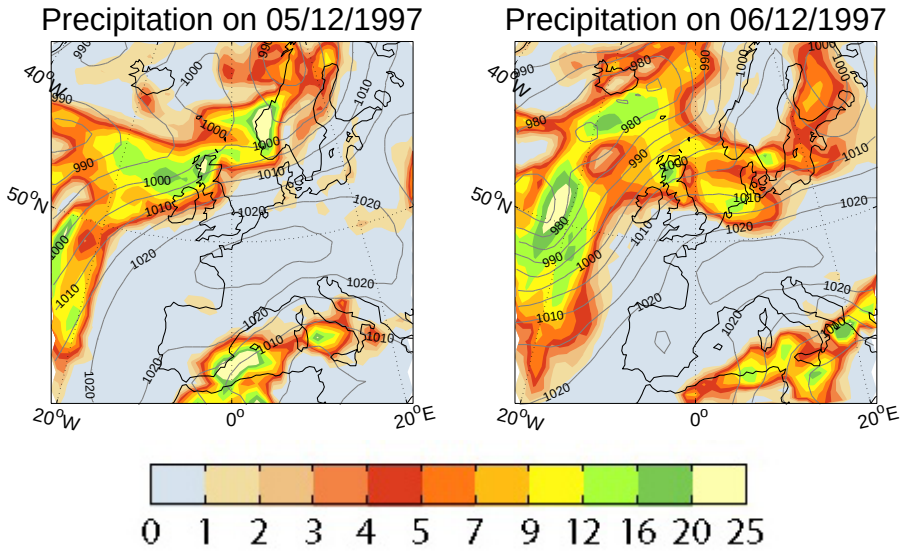

FIGURE 4.15: 24 hour precipitation on 05/12/1997 and 06/12/1997. Grey contours show sea level pressure on 850hPa.

Figure 4.17 illustrates the development of a low pressure system under the stratospheric streamer in the Atlantic on the 3rd of December (highlighted by a green circle). On the 4th, high pressure developed under the tropospheric ridge over the UK (Figure 4.17 - purple

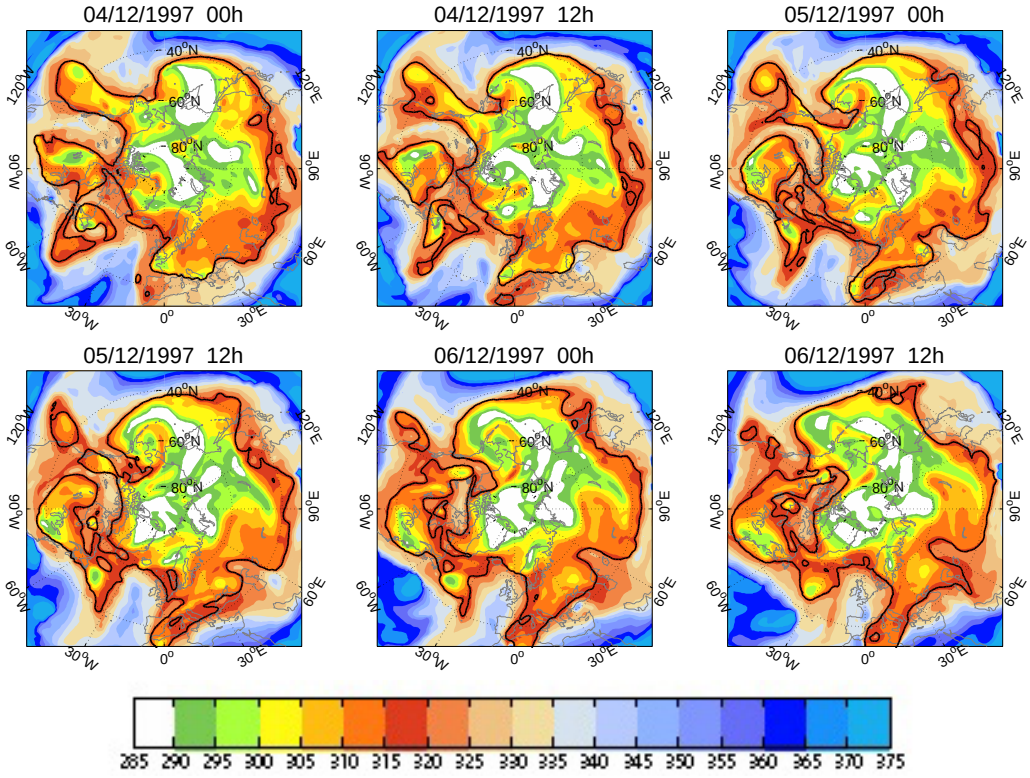

FIGURE 4.16: Development of tropospheric ridge over the UK from 04/12/97 to 06/12/97. Potential temperature on PV2 is represented by the colour contours and 315K is shown as a black line.

circle). As the cyclone moved towards the UK, the streamer to the east in Europe was associated with a low on its eastern and a high on its western flank. This high pressure (anticyclone) forced the low pressure system further northward, creating a strong pressure gradient directly over Scotland.

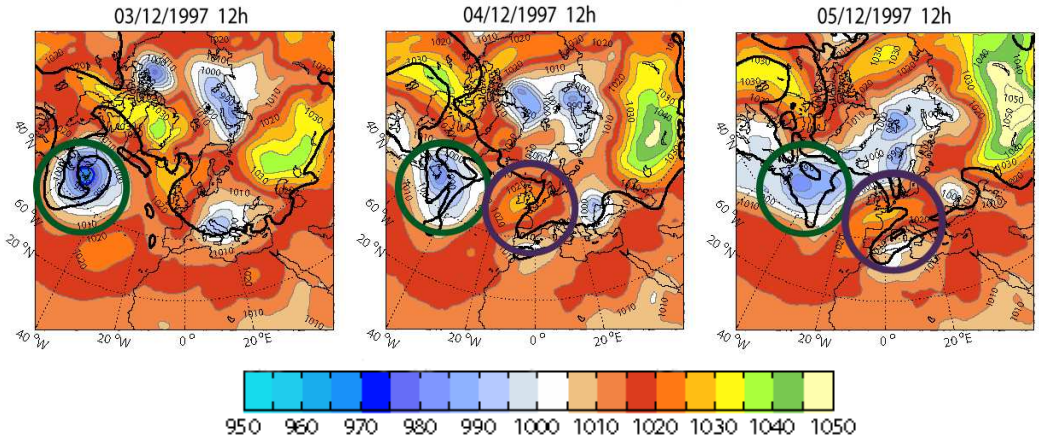

FIGURE 4.17: Sea level pressure (in hPa) on 3-5 December. PV2 on 315K is displayed as a black line. The cyclone system is highlighted by a green circle while the anticyclone is shown with a purple circle.

The situation occurring on the 5th of December is shown with more detail in Figure 4.18. Again, the sea level pressure indicates the low to the north west and high to the south west creating a steep pressure gradient (Figure 4.18a). The strong south-westerly winds, experienced during the periods of high precipitation accumulation and associated with the pressure systems, enabled moisture transport from the south-west (an atmospheric river) to pass over the region (Figure 4.18b). Rainfall occurred over Scotland and northern England (Figure 4.18c) and the cross section indicates ascent over the Scottish Highlands (Figure 4.18d). There was no PV intrusion near the ascending moist air, however, the upper-level patterns still had an impact on this heavy precipitation event. The trough to the east and streamer to the west aided in the development of surface level features which combined to force moisture laden air over the Scottish topography resulting in a heavy rainfall event.

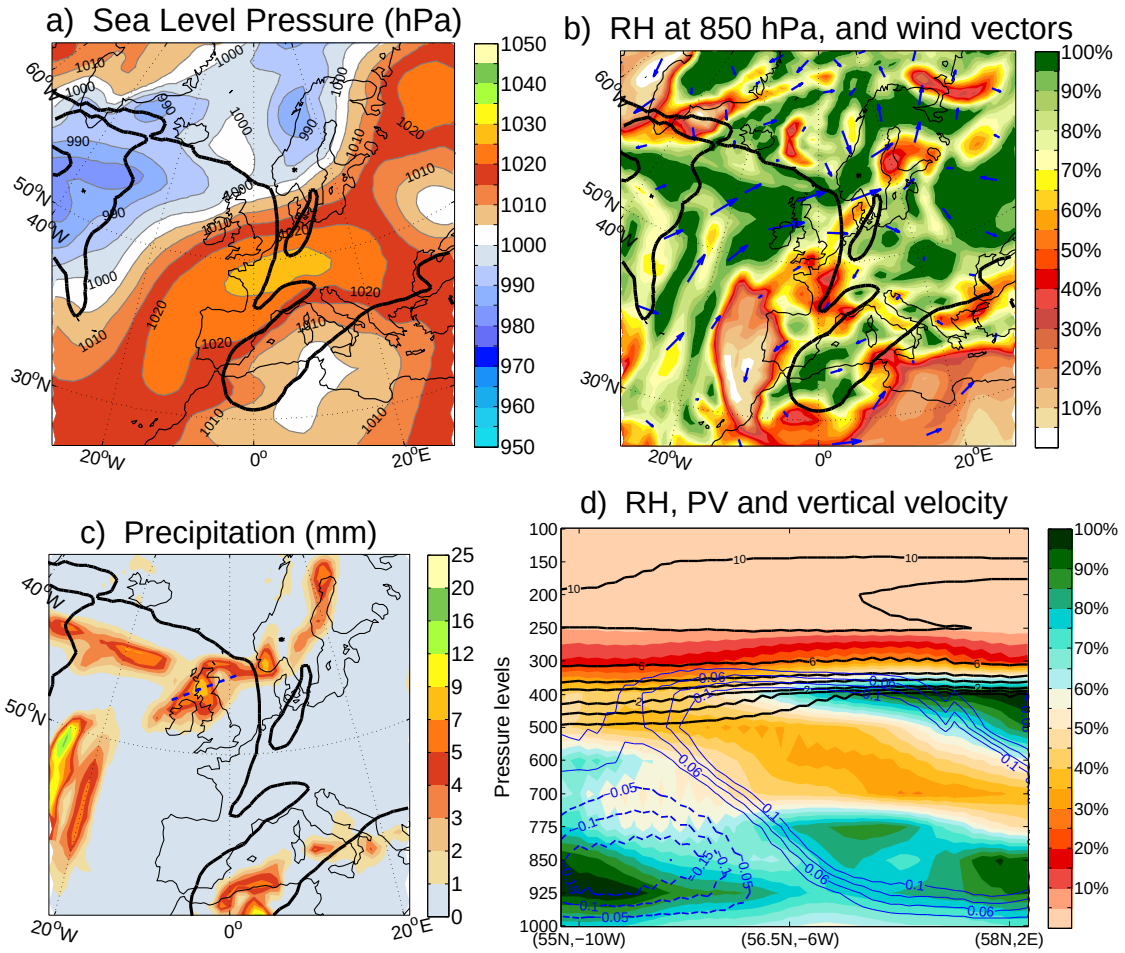

FIGURE 4.18: The situation on the 5th of December 1997 at 18UTC. Sea level pressure in hPa (a), relative humidity with wind vectors as blue arrows (b) and 6-hourly precipitation (c). Plots a-c also show the 320K PV2 line in black. The blue dashed line in c indicates the position of the cross section. Cross section (d) with relative humidity as the colour contours, PV is shown by solid black lines and vertical velocity (ms^{-1}) is represented as blue lines. Areas of ascent are dashed and descent are solid.

4.6 Streamer characteristics

The following sections describe the in-depth analysis of stratospheric streamers in the 99%, 95% and 90% heavy precipitation days. Firstly, the streamers are selected based on their location. Then the streamers are classified with regard to their orientation. Finally the persistence (i.e. length of time the streamer lasts) is calculated. When calculating the percentage of days with stratospheric streamer occurrence a spatial criterion is taken into account in order to identify streamers close enough to impact the precipitation in the UK (similar to the approach used in Martius et al. (2006b)). For this analysis a streamer day is defined as having at least one grid point of the stratospheric streamer falling within the box $50-60^{\circ}$N and $5-20^{\circ}$W over the 24 hour period. This box (illustrated in Figure 4.19) encompasses the frequency maximum derived for heavy precipitation days throughout the whole year for all of the regions and also identifies streamers with the ability to impact the weather of the UK. On each day, streamers are found over three isentropic levels and on four 6-hourly timesteps. This means that for each day several streamers may be detected. In order to get the best representation of characteristics the streamer with the largest area (and most dynamically significant) observed over the entire period and all isentropes is used.

4.6.1 Occurrence

The occurrence of stratospheric streamers in the box $50-60^{\circ}$N and $5-20^{\circ}$W during the 99% heavy precipitation days is illustrated in Table 4.2. The daily percentage rate is based on at least one streamer occurring in the specified box over the three isentropes and the four 6-hourly timesteps. For this reason, the percentages appear slightly higher than the 24 hour frequency distribution illustrated in Section 4.3.

The highest percentage of streamer occurrence is in the summer with an average of 88% over all 9 regions, followed closely by autumn with 85%. In spring the average is 72% and the lowest is in winter with 63% of days having a streamer. This pattern coincides with the climatological distribution of stratospheric streamers for each season and is also found in the 95% and 90% quantiles, but with reduced frequency. In the winter, the occurrence of streamers for most of the regions are close to the climatological mean (60%) with SS, NS and SWE values below this figure. The link between stratospheric streamers and heavy precipitation events is most pronounced in autumn and summer where the highest deviation from the climatology (68%

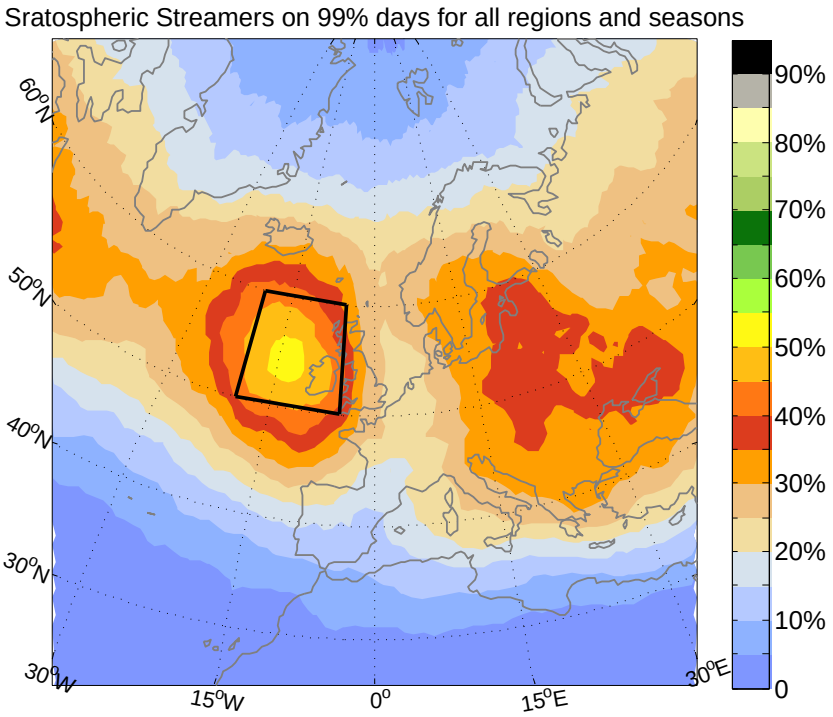

FIGURE 4.19: Occurrence of stratospheric streamers on 99% UK heavy precipitation days for every region and season. The black box is located over $50 - 60°$N and $5 - 20°$W and illustrates the spatial criterion used to identify streamer days.

TABLE 4.2: Number of streamer days for region and season

99% Quantile: 41 days								
Region	Autumn		Winter		Spring		Summer	
NS	32	78%	20	49%	19	46%	31	76%
ES	36	88%	29	71%	33	89%	37	90%
SS	37	90%	24	59%	26	63%	34	83%
NI	34	83%	29	71%	31	76%	38	93%
NWE	31	76%	23	56%	27	66%	33	89%
NEE	32	78%	26	63%	31	76%	39	95%
CE	37	90%	28	68%	34	83%	39	95%
SWE	36	88%	26	63%	27	66%	39	95%
SEE	38	93%	28	68%	37	90%	36	88%
Average	85%		63%		72%		88%	

and 73% respectively) is found. Several regions (NEE, CE and SWE) even have stratospheric streamers present on 95% of heavy precipitation days. Interestingly, CE and NEE have the lowest minimum and mean precipitation for the 99% quantile with the highest streamer occurrence. These regions of the UK are less prone to higher precipitation due to their location and topography, so when heavy precipitation occurs, a dynamic forcing seems to be necessary (leading to higher streamer frequency). Similarly, NS has the largest values of minimum and

mean precipitation, while the smallest frequency of streamers are found (i.e. other factors or dynamical settings can also produce heavy precipitation).

4.6.2 Orientation

There are three classifications into which streamers can fall based on their angle of orientation, LC1 or anticyclonic (with an angle $< 75°$), LC2 or cyclonic (with an angle $> 105°$) and meridional (an angle between $75-105°$). Figure 4.20 illustrates the percentage of stratospheric streamers which fall into each category for each season, region and quantile.

FIGURE 4.20: Percentage of streamers classified as LC1, LC2 or meridional for the 90%, 95% and 99% heavy precipitation cases.

The 90% and 95% quantile streamers have similar patterns for all seasons and regions with higher frequencies of LC2 streamers. This is most pronounced in autumn (60-65% of cases)

and lessened in winter (45-55% of cases). Meridional streamer types have the lowest frequency in all seasons with the most occurring in winter and spring.

Similarly, for the 99% quantile streamers in autumn, LC2 is the predominant streamer type. LC2 streamers are associated with stronger zonal winds and a southward shift of the jet which are present during the autumn season. NWE, NEE and CE have the most meridional streamers in autumn and coincide with anticyclones (and tropospheric streamers) over Greenland. This combination is also true of increased meridional cases in winter (ES) and spring (ES, NEE, CE and SEE) but is not present in the summer. In summer NWE, CE and SWE have equal or more LC1 type streamers. These regions are characterised by few cyclones while the opposite is true in spring with areas having the highest cyclone occurrence also having the most LC1 streamer types (NS, SS and NWE). The winter season has the largest percentage of LC1 cases (with the maximum of 55%) although zonal winds are strongest in this season, which would suggest LC2 streamers should be the dominant type. However, LC1 streamers usually occur on higher isentropic levels that pass over the UK in the winter season (Isotta et al., 2008), which explains the increased number of LC1 type streamers in this season. The northward shift of the jet in summer heavy precipitation cases can also explain the tendency towards the occurrence of LC1 type streamers in the summer season.

4.6.3 Persistence

The persistence of the stratospheric streamers is analysed by tracking the streamers using the method described in Section 3.2. The number of days on which the streamers occur before and after the heavy precipitation event are calculated as well as the entire lifetime from initiation to dissipation. The summary of total track lengths for each region and season in the 99% heavy precipitation cases are depicted in Figure 4.21. The box-and-whisker plots show the lower and upper quartiles (coloured portion) with a black line (as well as notch) indicating the median, and dashed lines for the minimum and maximum. Track lengths in the 90% and 95% quantile (not shown) are moderately smaller with less regional differences.

The average lifetime of the streamers related to the 99% cases is around 2 days for autumn, spring and summer and around 1.5 days in winter. However, the largest variance of lengths are found in winter with increased spread in many of the regions. Western regions including NWE and SWE have shorter tracks while eastern regions (NEE and CE) along with NI and ES

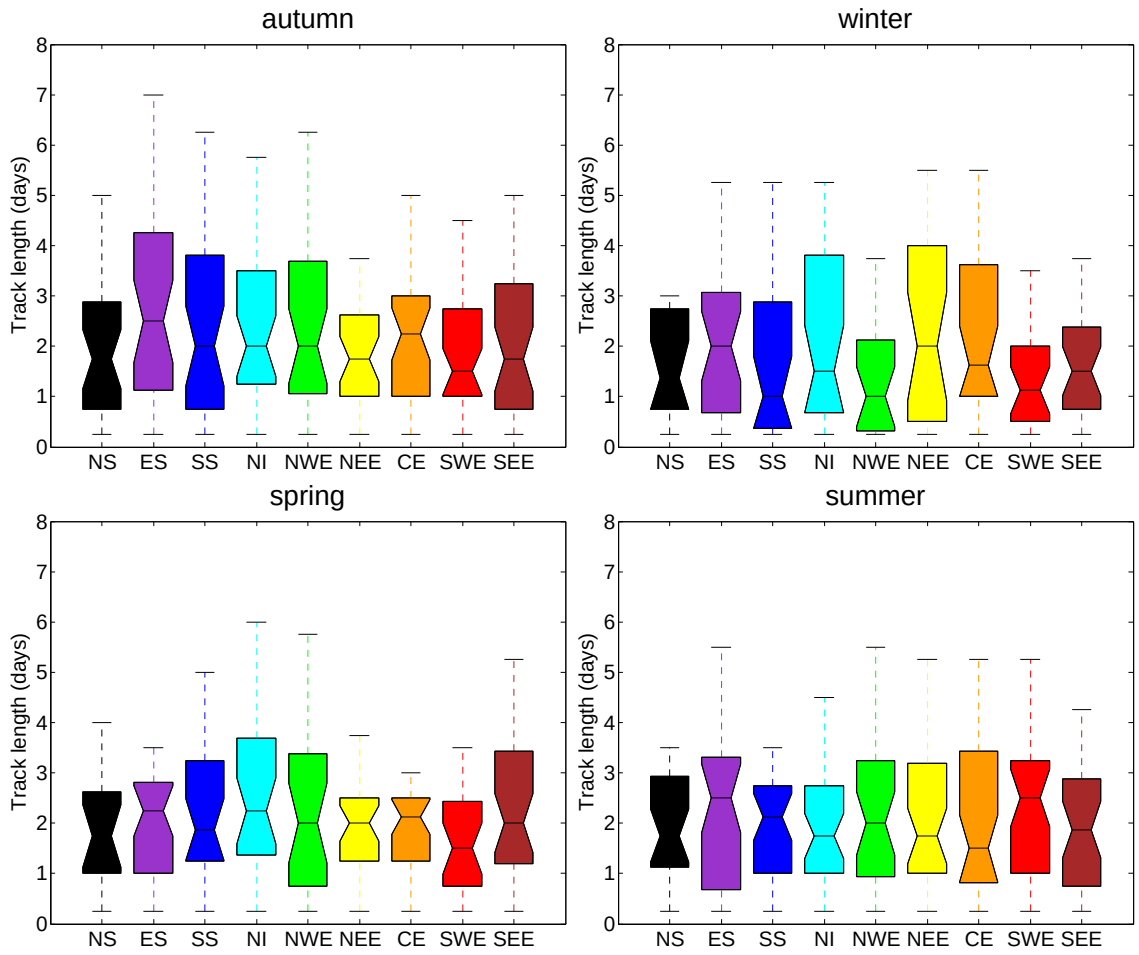

FIGURE 4.21: Stratospheric streamer track length in days for 99% quantile events.

have longer lasting streamers. There was a link between longer lasting streamers and higher precipitation amounts on the south side of the Alps (Martius et al., 2006b), and similarly ES has the longest average track length in all the seasons and regions. The enhanced streamer track length and orography in both of these locations leads to higher precipitation accumulation. ES also has longer tracks leading up to the precipitation in spring but these dissipate quickly after the precipitation has fallen (not shown). In autumn and summer the opposite occurs with longer tracks continuing after the precipitation event. For NS, streamers have longer tracks leading up to the event in autumn, winter and spring but tend to diminish quickly after the precipitation day. In the autumn, northern regions (especially ES, SS, NI and NWE) tend to have streamer tracks which last longer than those in the south, while the differences are less noticeable in spring and summer and less variation in medians is observed (Figure 4.21).

4.6.4 PV amplitude

The maximum (95% quantile), minimum (5% quantile) and mean values of PV (measured in PVU) within the identified streamers have also been investigated. As a streamer is defined by following the tropopause along 2PVU the minimum for each streamer is equivalent to this figure. The mean PV amplitude throughout the streamers have a homogenous spread for all the seasons and regions. This is centred around 4PVU with a range of $+/-1$ to 2PVU. The maximum PV amplitude (pictured in Figure 4.22) within the streamer has much more variance and spread.

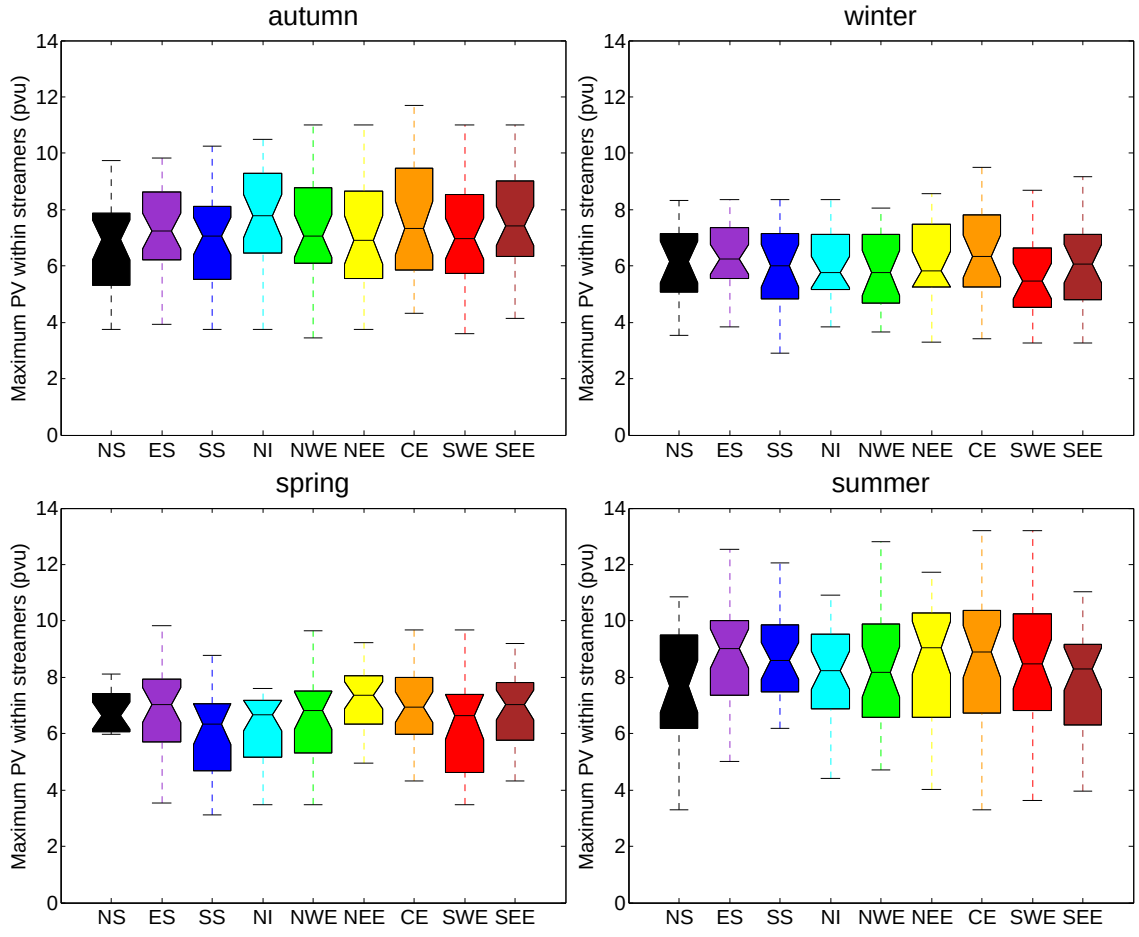

FIGURE 4.22: Maximum PV amplitude in streamers on 99% heavy precipitation days.

The highest PV values are found in the summer due to the fact that these streamers occur on higher isentropic levels. This season also has the largest spread within each individual region. The regions do not have much variance, however NS, NI and SEE have the lowest values. Autumn has the next widest spread ranging from 4-10PVU for most regions. Spring and winter have a reduced range and overall the values are slightly lower for these seasons as

well, again because the streamers in these seasons occur on lower isentropes. In the spring, the trend continues towards a slight east-west split. Eastern regions such as NEE, CE, and SEE have marginally higher maximum PV amplitudes in comparison to western regions (NWE and SWE).

4.7 Impact of stratospheric streamers on heavy precipitation

Stratospheric streamers regularly occur to the west of the UK on heavy precipitation days. The effect these streamers have on the precipitation will be analysed by examining the differences in the heavy precipitation days that have an overlying stratospheric intrusion and those that do not. The structure of the streamers will then be investigated and compared with streamers which fall within the identified box on all the days within the ERA40 data set.

4.7.1 Days with no streamer

As detailed in Section 4.6.1 a majority of the 99% quantile heavy precipitation cases have a stratospheric streamer lying to the west of the UK. Potential temperature on PV2 is investigated for each day where no streamer feature occurs in this region in order to determine the structure of the upper atmosphere for each event. Table 4.3 summarizes the situation for individual regions and seasons placing each day into four possible categories. These include a) the presence of a larger stratospheric trough which is not identified as a streamer (due to the restrictions in the streamer identification routine, see Section 3.1), b) a cut-off is present over or to the west of the UK, c) a streamer or trough in the wave occurs but not within the specified box, and d) no significant feature is present aloft or the isentropic surfaces show no wave or trough signal in the region.

The highest percentage of non-streamer cases on the heavy precipitation days take the form of a larger stratospheric trough situated over or to the east of the UK in autumn, winter and spring. The main exception to this is in NS where a deep stratospheric intrusion (streamer or trough) over Europe (represented as the 12 shifted features in winter and 15 in spring) extends into Africa prompting tropospheric streamers to fall just over or to the south-east of the UK. This situation also occurs in SS in the winter and spring. Days where no upper-level features occur often have strong isentropic gradients where several levels coincide and the jet stream

TABLE 4.3: Features present on non-streamer 99% days

Autumn				
Region	Larger trough	Cut-off	Shifted feature	No feature
NS	0	0	8	1
ES	3	0	1	1
SS	1	0	1	2
NI	2	1	2	2
NWE	4	0	3	3
NEE	5	1	2	1
CE	3	0	0	1
SWE	1	0	3	1
SEE	2	0	1	0
Winter				
Region	Larger trough	Cut-off	Shifted feature	No feature
NS	3	0	12	6
ES	7	1	1	3
SS	4	0	8	5
NI	5	1	3	3
NWE	8	0	5	5
NEE	7	0	3	5
CE	6	0	2	5
SWE	9	0	3	3
SEE	6	0	2	5
Spring				
Region	Large trough	Cut-off	Shifted feature	No feature
NS	3	0	15	4
ES	6	0	1	1
SS	6	0	6	3
NI	6	0	3	1
NWE	7	0	5	2
NEE	8	1	0	1
CE	4	0	1	2
SWE	7	0	3	4
SEE	3	0	1	0
Summer				
Region	Large trough	Cut-off	Shifted feature	No feature
NS	2	2	3	3
ES	2	1	0	1
SS	3	0	1	3
NI	1	0	1	1
NWE	1	0	1	6
NEE	1	0	0	1
CE	1	0	1	0
SWE	1	1	0	0
SEE	1	2	1	0

is located directly over the UK. The strongest of these gradients are experienced in the winter season where an increase in the zonal wind inhibits wave breaking (Postel and Hitchman, 1999) and the increased airflow brings an influx of moisture from the Atlantic creating precipitation (Maraun et al., 2011). In the summer, the most variance between the four categories is found as few cases have no streamer present. In most regions either a large trough is present or no feature occurs. Very few cut-offs are found in any of the seasons or regions.

The relative humidity and wind vectors (not shown) are also examined on 850hPa for days with and without a streamer present. On the day preceding the heavy precipitation event, the relative humidity tends to be higher on days with an overlying streamer. This is most pronounced in the winter where values are 6-10% higher on streamer days for NS, SS, NWE, SWE and SEE. In other seasons the values range from 1-6% higher. On the actual day of the precipitation event the relative humidity levels become lower on streamer days than on days with other features present. The range is from 3-9% lower and is again most noticeable in the winter season. The ascent associated with the PV streamer appears to lower the surface level moisture saturation, while this remains higher for longer on non-streamer days. The winds do not differ much for days with and without a streamer. In general wind speeds take on a more south-westerly component with slightly higher velocities on non-streamer days.

4.7.2 Structural differences in stratospheric streamers

In order to identify significant structural differences which may impact precipitation, stratospheric streamers occurring on heavy precipitation days are compared with "typical" stratospheric streamers. The comparison is undertaken by finding all the streamers which fall into the specified box throughout the entire ERA40 data set. For each day the largest streamer that is situated within the box is used to coincide with the same selection process utilised for streamers on heavy precipitation days. The elongation, width and southern extent of the streamers is then compared.

The elongation of a typical streamer near the UK is very similar for all the seasons (Figure 4.23). On average they are between 2000-3000km in length. Most streamers for the individual regions and seasons fall within the range of an "average" streamer. The summer season has the least deviation from the climatological average with only a few regions displaying slightly shorter streamer lengths (CE and NS). NS is the northernmost region so is affected by streamers with

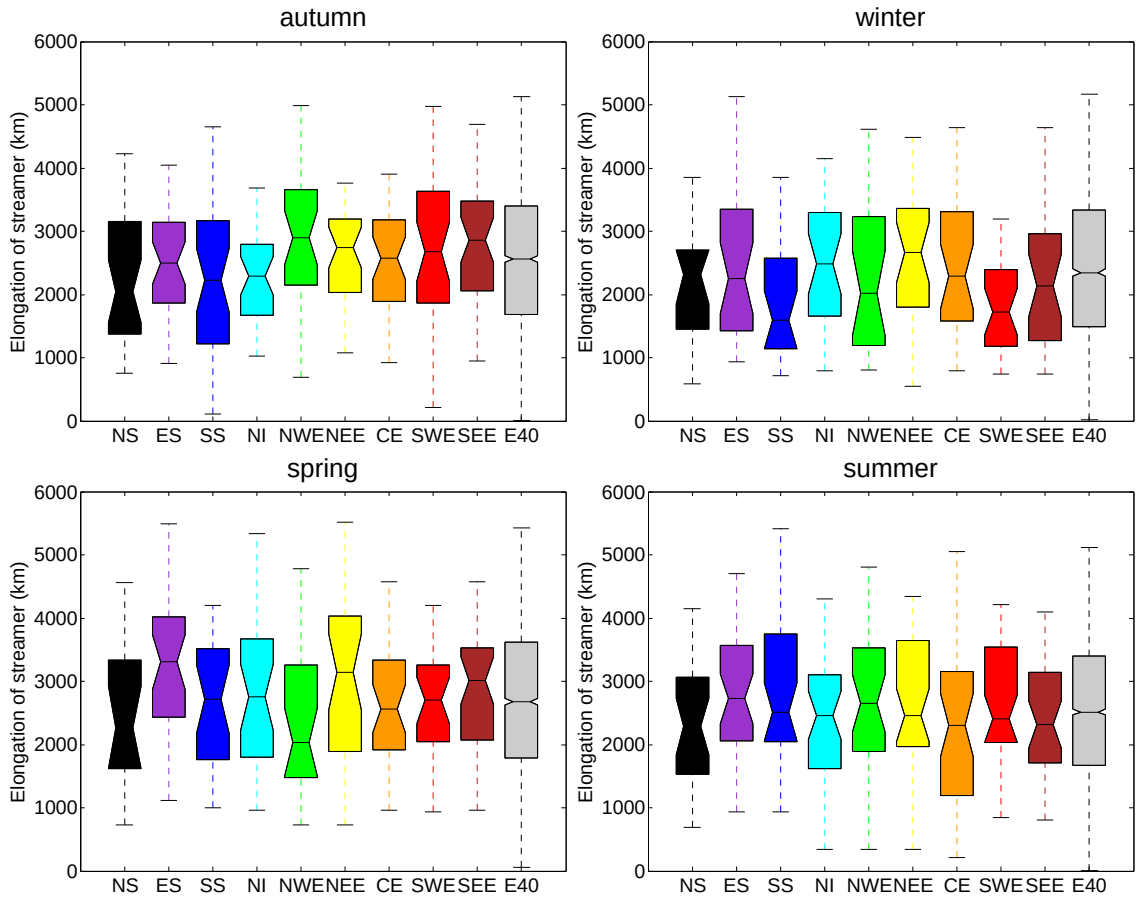

FIGURE 4.23: Elongation of streamers on 99% heavy precipitation days in each region and season compared with those occurring in the ERA40 data set (E40).

the shortest elongation of all the regions with below average lengths also found in autumn and spring. Autumn has a north south split, northern regions have streamers with below average lengths while in the south they are slightly above average. This is a reasonable outcome as longer streamers have the tendency to extend further equatorward, enabling the streamer to impact southern regions. There is more variance in the spring and winter seasons. In winter, many of the regions have shorter than average streamers (SEE, SWE, NWE, SS, and NS) while in the spring ES and NEE have the longest streamers.

The average width of the climatological streamers is around 750km with the lowest ERA40 streamers found in the winter season with an average of 650km. In winter, similar to the elongation streamers, the most variance occurs. An east-west split across the country is found for southern regions with wider streamers occurring to the east (SEE and CE) and narrower found in the west (NWE and SWE). Autumn has the widest and narrowest outliers although average streamer widths still mainly fall within the range of the typical streamer. Summer

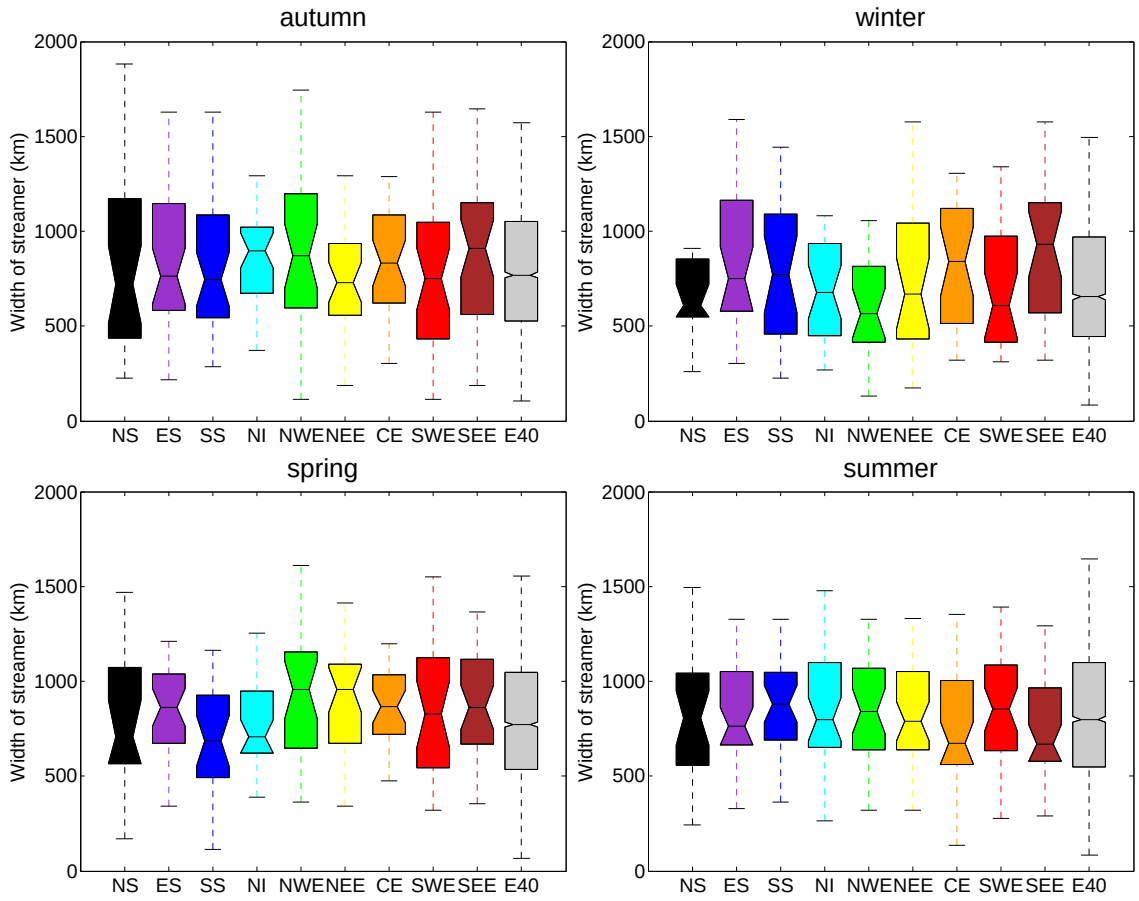

FIGURE 4.24: Width of streamers on 99% heavy precipitation days in each region and season compared with those occurring in the ERA40 data set (E40).

again has the lowest variation between regions with the most PV streamers which are similar to the climatological mean.

4.8 Conclusions

The main conclusions indicate that stratospheric streamers play a prominent role in the heaviest precipitation days (top 99^{th} percentile) in most regions, especially in the autumn (with an average of 85%) and summer (88%) but are close to the climatological mean in winter. Cyclones are also important on the heavy precipitation days in the UK especially in the winter, where they are the dominant influence on precipitation. In autumn, PV streamers combine with cyclones to initiate precipitation, while in summer the precipitation type is most frequently convective. The spring has a very prominent east/west split with frontal precipitation (cyclones and anticyclones) in the west, while long wave trains leading to stratospheric and tropospheric

streamers influence convection in the east. Similarly, a study by Maraun et al. (2009) found that extreme precipitation takes the form of frontal in western regions with convective events dominating in the south east.

Synoptic-scale influences on heavy precipitation vary regionally across the UK. Eastern Scotland has the most significant Rossby wave trains leading up to the heavy precipitation days and also has similarities to Alpine streamer cases described by Martius et al. (2006b). Stratospheric PV streamers are the most prominent feature in all seasons for this region and combine with cyclones and the orography to produce heavy precipitation. Northern Scotland is the most unusual region as it has the highest precipitation in each season but the lowest percentage of streamer occurrence. The winter case study (case study 2) illustrated in more detail how a PV streamer to the east over Europe impacted the precipitation by enhancing an anticyclone to the east of the UK. This anticyclone, that formed within the tropospheric ridge over the UK, steered a large cyclone just north of Scotland. The intense pressure gradient created strong south-westerly winds which transported moisture over the region. The 95% cases in northern Scotland take on a similar pattern to the other regions, so it appears that only the most extreme precipitation events require a more intense initiation.

The summer case study described an event where a stratospheric intrusion, combined with a cyclone, influenced a heavy precipitation event. The PV streamer extended southward toward the surface initiating ascent to the east of the streamer. Humid air was brought up to near tropopause level and then fell as precipitation. Differences in days with and without a streamer show a spike in relative humidity just prior to the precipitation event at the surface. During and after the event this drops, while higher values of relative humidity are found for longer at the surface on non-streamer days. Wind velocities also tend to be slightly higher on non-streamer days and often take on a more south-westerly component rather than westerly.

Stratospheric streamers influencing the heavy precipitation events have an average life time of 2-3 days with lowest level of persistence in the spring. The majority of the streamers are LC2 (especially in the autumn) or LC1 (in the winter and southern regions in the summer) with very few meridional streamers found in any season. Maximum PV amplitudes within the streamer are lowest in the winter and spring season and highest in the summer due to the variation in isentropes. The size and position of the streamers occurring on heavy precipitation days are similar to typical streamers (2000-3000km in length and 750km in width) especially in the summer season. The most variance of streamer elongation is found in spring and winter

(where shortest lengths are also experienced). The seasonal variation of elongation may also depend on the steepness of isentropes so the same southward elongation can have the effect of a deeper intrusion and more impact on the ground level.

Days where no streamer occurred were often categorised by a larger overlying trough or a feature outside the selected box either shifted further to the west or east over Europe. This indicates that upper-level influences may still be associated with the events even if they are not the main contributor. The evidence diagnosed within this chapter points to the main conclusion that PV streamers have a significant influence on heavy precipitation in the UK.

Chapter 5

Triggers of Rossby waves and PV streamer formation

5.1 Introduction

The life cycle of a Rossby wave begins when a column of air stretches or contracts (for instance when passing over a mountain) leading to changes in vorticity. This creates a ridge/trough pattern as the wave propagates downstream. As the wave matures, it may become nonlinear and break or irreversibly deform so that the wave train no longer propagates forward and a PV streamer may be generated. Rossby wave trains can propagate over long distances and the waves travel along the potential vorticity gradient at the tropopause (Schwierz et al., 2004). The wavelike structure is enhanced by the generation of positive and negative potential vorticity anomalies at upper and lower-levels (Sardeshmukh and Hoskins, 1988; Schwierz et al., 2004). These anomalies can be formed by the creation or destruction of PV which may be caused by diabatic heating from tropical cyclones experiencing transition (Jones et al., 2003), extratropical cyclones (Stoelinga, 1996) or friction from orographic features (Aebischer and Schär, 1998).

Grams et al. (2011) found that latent heating played a role in warm conveyor belts associated with cyclones by producing high PV at lower tropospheric levels and low PV in the upper troposphere. This injection of low-PV air perturbed the upper-level flow which enhanced ridges

preceding streamer formation. Diabatic processes have also been shown to shape the waveguide and amplification of the wave (Massacand et al., 2001; Riemer et al., 2008; Torn, 2010). This in turn plays a role in perturbing the PV band, causing wave breaking and subsequently streamer formation (Martius et al., 2008; Riemer and Jones, 2010). Although the presence of diabatic heating has been shown to precede wave initiation and streamer formation it is not always the main contributor as found by Meier and Knippertz (2009).

The western North Pacific has been implicated as an area of importance for downstream midlatitude circulation. Baroclinic energy conversion over the western and central North Pacific generates kinetic energy which facilitates the maintenance of downstream storm tracks (Chang and Yu, 1999; Danielson et al., 2004). Rossby waves initiated by tropical heating, convection and extratropical transition from the North Pacific can travel to North America, or beyond to the North Atlantic and Europe. The implications of Rossby wave initiation for Europe have been studied by Martius et al. (2008). Wave signals over Europe are traceable back to the Pacific up to one week in advance particularly in autumn and winter. In the spring and summer, wave signals emanate from the western Atlantic and are limited by the lack of coherence in the waveguide (i.e. there are fewer areas of strong PV gradients where parcel displacements lead to higher vorticity perturbations). The extent of the zonal propagation was consistent with other studies for the Alps (Grazzini, 2007) and the UK (Krishnamurti et al., 2003).

In Section 4.4 a composite of Rossby wave trains was performed for the 99% and 95% UK heavy precipitation cases. The Hovmöller plots revealed that there was large variability in the wave structure leading up to heavy precipitation events for the nine regions of the UK. The results indicated that wave signals were present in autumn and summer about 3-4 days ahead, mainly observed as slow moving troughs present from the western Atlantic. Little or no preceding wave trains were found in the winter and greater variability was observed in spring. These results differ from those found for Alpine streamer cases and will be explored in more detail in this chapter.

First, an Alpine heavy precipitation case study is examined to illustrate the genesis of a Rossby wave that leads to downstream streamer formation. Then, the initiation of Rossby waves preceding streamer formation in the 734 cases in the top 99% of UK heavy precipitation events for each season and region as described in Section 4.2 will be investigated. The geographical location and time scale of the trigger for the preceding Rossby wave as well as the streamer

initiation will be studied for each case. A final case study identifies the upstream influences on the formation of a PV streamer in the Pacific using an adjoint model.

5.2 Rossby wave triggers

Rossby waves which lead to PV streamer formation and subsequently heavy precipitation and severe weather are examined in this study. The location and time of Rossby wave initiation is studied by diagnosing the wave from the end of the life cycle, after wave breaking and PV streamer formation, beginning at the heavy precipitation event over the UK (or Alps in Section 5.2.1). The precursor waves to these events are then analysed by projecting the wave train back to the genesis of that wave and its initial trigger.

The 734 UK cases used in Section 5.2.2 are from the 99% quantile UK heavy precipitation cases as defined in Chapter 4. These are made up of the events for each region and season where a streamer was present on the precipitation day. The ECMWF ERA40 reanalysis dataset covering 1957 to 2002 is used to determine the position of the streamers occurring during the month of the heavy precipitation events. The streamers are identified and tracked using the method described in Sections 3.1 and 3.2.

After defining the streamers and their persistence, they are then related to the Rossby waves. This is accomplished by creating individual refined Hovmöller diagrams as outlined in Section 3.3. The isentropic level chosen for each season coincides with the level where the highest number of PV streamers occurred on the heavy precipitation days (315K for winter, 320K for autumn and spring and 325K for summer). Each diagram consists of the north/south winds over longitude and time (illustrating the Rossby wave) along with the time of the precipitation and position of the streamers and their lifespans. Rossby waves are identified by the consecutive peaks of maximum and minimum velocities along the diagram. By using this method the group velocity of the wave is captured visually. In this way, wave packet series are examined along with the relationship to previous streamer development and wave breaking. In comparison to the numerical method of ray tracing (a wave ray is defined as the path of group velocity showing propagation of wave activity) developed by (Hoskins and Karoly, 1981; Karoly, 1983; Hoskins and Ambrizzi, 1993), the Hovmöller diagram is more subjective. However, the trigger or initiation of the wave not only follows group velocity but is also traceable to previous streamer activity or wave breaking events, so in some cases, the possible trigger source is

observed within the diagram. The ridge-and-trough method has been compared with Hovmöller diagrams created using wave activity energy by Glatt et al. (2011). It was determined that the ridge-and-trough diagram (developed by Martius et al. (2006a)) was more straight-forward to interpret as well as beneficial for studying elements of Rossby wave propagation.

Starting from the precipitation event (the red circle in Figure 5.1), the trajectory of consecutive velocities is projected onto the diagram manually, until they disappear or a previous streamer/wave breaking event occurs (shown as the black line and green circle in Figure 5.1). This location (highlighted by the green circle) is then considered the trigger point of the Rossby wave. The slope of the line is determined between the precipitation event point to the trigger point with a best fit line going through each velocity peak. The longitude and latitude location of the trigger points as well as the time are checked by examining potential temperature on PV2 for each timestep of the entire wave lifespan. The plots are analysed for coherence in the wave movement and structure to determine where the wave begins. The "trigger" or trigger point is identified as the point where the first perturbation to the waveguide occurs that then leads to the propagation downstream of a full Rossby wave. By using both methods the most precise position and time of the trigger can be assessed. As the Rossby waves are examined on one isentropic surface as well as the dynamic tropopause (through the use of the Hovmöller diagram) trigger points are only identified within the mid-latitudes. Because of this, waves emanating from higher or lower isentropic surfaces (including the tropics) are only identified once they reach the mid-latitudes. The sources for the triggers could thus have both local and more distant influences.

5.2.1 Alpine case study: November 1996

In order to show more detail of the possible triggers to Rossby waves a case study examining the source of an upstream wave trigger has been investigated. This case occurred on the 13th of November, 1996 and was associated with an elongated PV streamer over Europe. It was selected based on the impact of the heavy precipitation in the Alps as well as the nature and alignment of the PV streamer which is "typical" during high-impact events in this region.

5.2.1.1 Discussion

Figure 5.1 shows the location of the heavy precipitation event (red circle) which took place on the 13th of November 1996 in the Alps. The pink line indicates the position and lifetime of the PV streamer associated with the Rossby wave. The wave has been projected back to the 5th of November at around $145°$E which is the location of the trigger point (green circle).

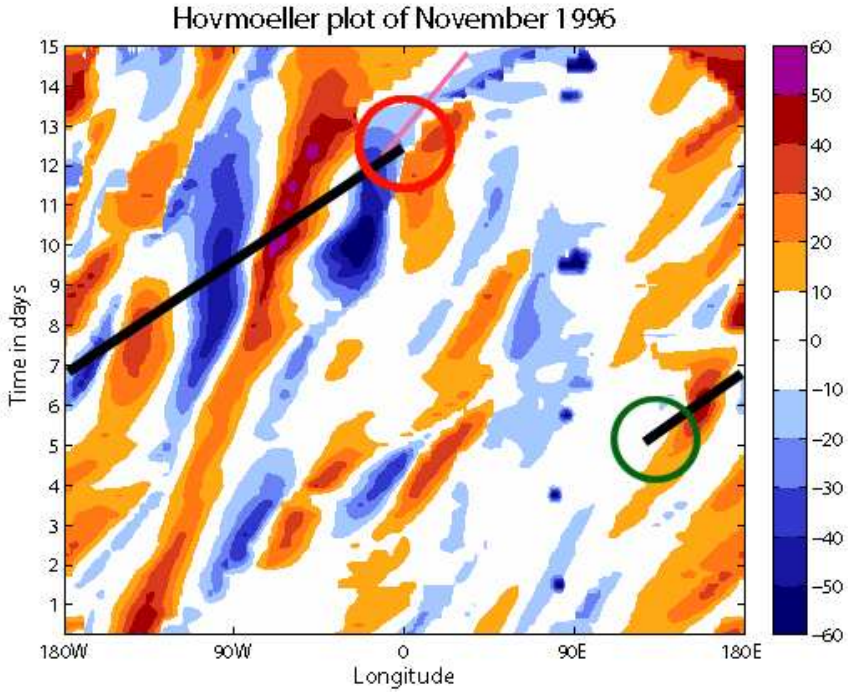

FIGURE 5.1: Hovmöller plot from the the 1st to 15th of November, 1996. The heavy precipitation event is highlighted by a red circle, and the associated streamer and its lifetime is shown by a pink line (the line extends from the starting to ending central point of the streamer). The thick black line denotes the projected Rossby wave train and green circle shows the trigger point.

The progression of the wave is then illustrated in Figure 5.2, from the date of the heavy precipitation and PV streamer highlighted in pink (a), to the trigger point (k). Looking back through time the progression of the wave can be seen (shown by the red circle). The wave energy travels back from the PV streamer through a trough situated over North America and into a deep ridge over the Pacific Ocean. The wave train culminates in a small perturbation on the 5th of November (the green circle highlights the trigger position). The sea level pressure charts (j and l) have been added to illustrate the situation at the surface during the time of the initiation of the wave. A low and high pressure boundary is present at the position of the initiation (green circle in l). This pressure gradient increases with time as the low and

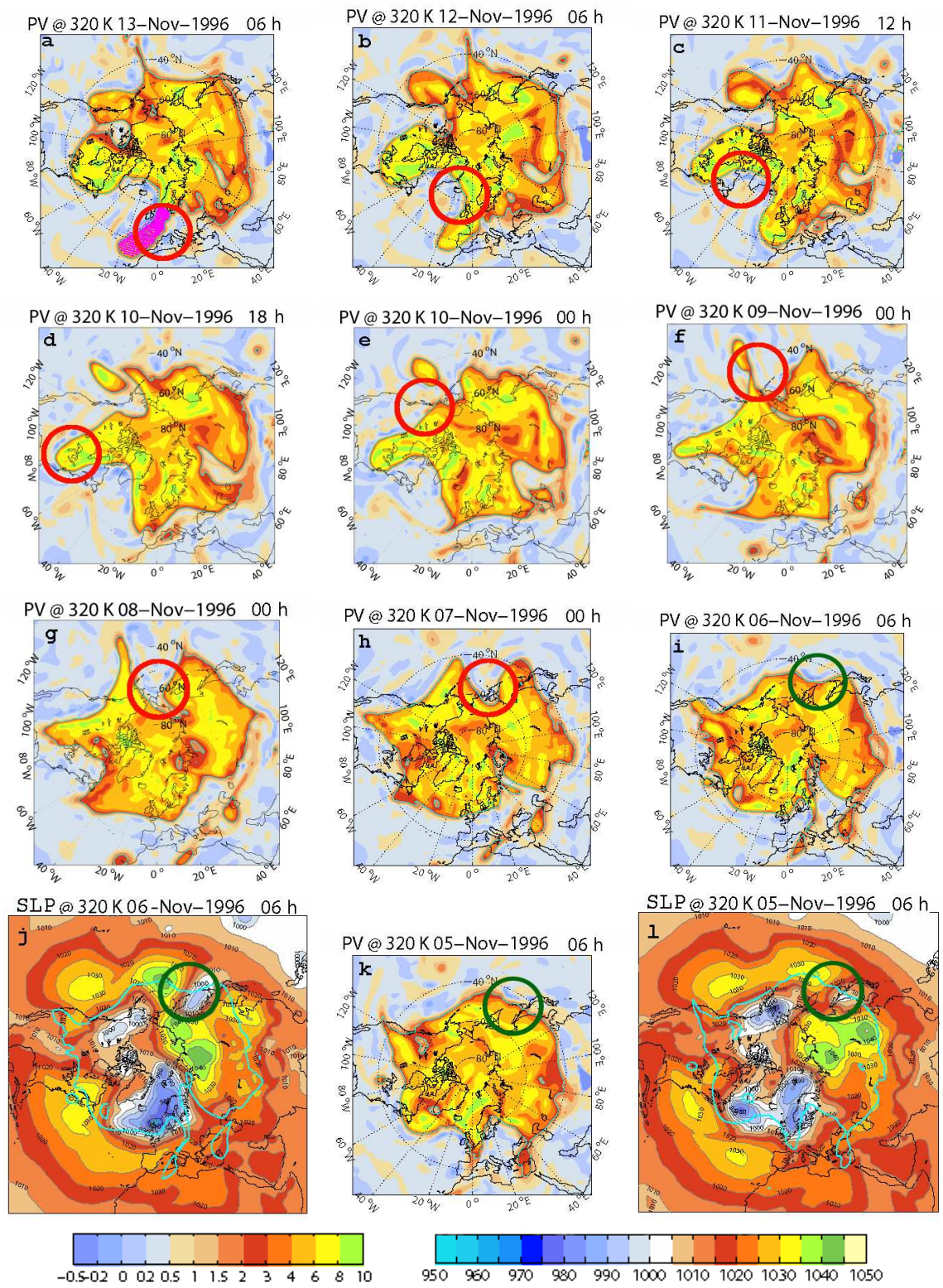

FIGURE 5.2: Isentropic plots starting from the heavy precipitation event on 13/11/1996 to the trigger point on 05/11/1996. Plots a-b, i and k show PV on the 320K isentropic surface. Two sea level pressure plots are included for 06/11/1996 (j) and 05/11/1996 (l) next to their corresponding isentropic plots. Red circle shows movement of wave energy while green circle indicates trigger area. Right colour bar shows PV in PVU while left colour bar shows sea level pressure in hPa.

high intensify around 160°E (green circle in j) and the wave is amplified into a deep trough in subsequent timesteps (h and g).

Looking at potential temperature on PV2 illustrates more information about the wave initiation. The upper-level situation is shown in Figure 5.3. On the 5th, upstream or to the west of the initiation, a trough (a in upper left panel of Figure 5.3) is present on the 315K and 310K isentropes. Downstream to the east, another trough (b) is situated on the 340K and 345K isentropic surfaces. The cross section (middle left) shows the two troughs (a and b) surrounding the area of initiation with high-PV air extending toward the surface on either side. Moist ascending air is present to the east of both of these intrusions (bottom left). The ascending air associated with the trough upstream (a) is part of the deepening low. The feature downstream (b) has ascent ahead of the PV intrusion and descent behind, which is a component of the strengthening anticyclone and high pressure feature.

By the 6th at 06 UTC (Figure 5.3 right hand side) the 320K isentropic surface has begun to take on a wavy pattern. The upstream trough (a) is meridionally aligned and the downstream trough (b) has eroded into a PV streamer. A tropospheric intrusion behind the streamer (c) associated with the high pressure system, also begins to push poleward on the higher isentropic surfaces (330-345K). The PV cross section (middle right) shows that the southward extension of the PV intrusion to the east (b) has been eroded. A positive PV anomaly at the surface (possibly due to diabatic heating downstream from the cyclonic low) beneath the forming ridge is present (d), as well as a small upper-level low PV anomaly (c) contributing to the tropospheric intrusion and enhancing ridge. These characteristics combine to perturb the 320K isentrope into the beginnings of a Rossby wave.

5.2.2 UK precipitation cases

Now that one case has been examined in detail, the UK heavy precipitation cases will be investigated for trigger locations. The number of cases investigated varies for each season (with more in summer (217) and autumn (201), and less in spring (167) and winter(149)) as explained in Table 4.2 in Section 4.6.1. Cases are also omitted when no Rossby wave train is observed before the PV streamer (shown in Table 5.1). When there is no preceding Rossby wave train the PV streamer often forms from re-circulating stratospheric air (such as a cut-off

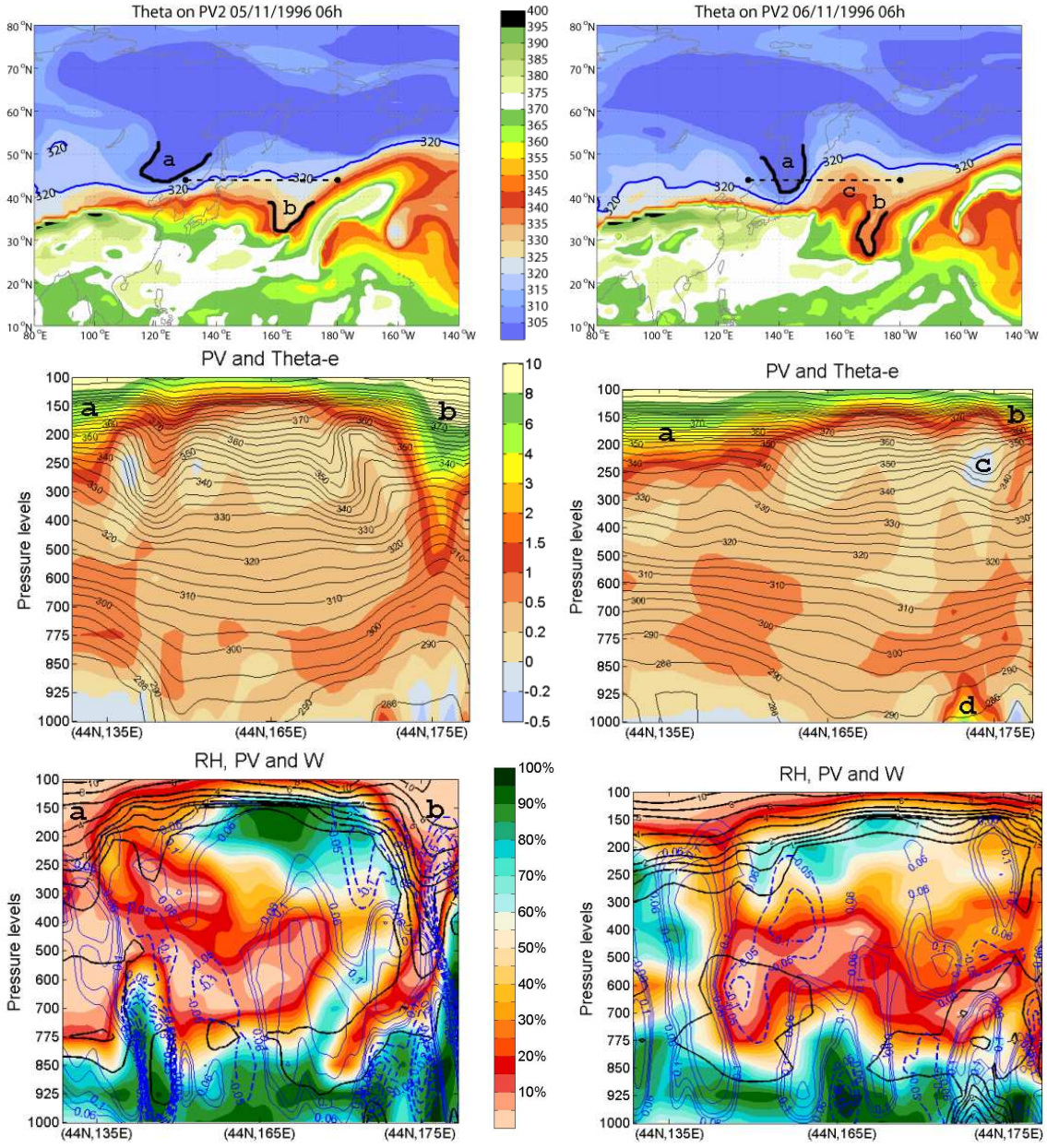

FIGURE 5.3: Situation on 05/11/1996 (left) and 06/11/1996 (right). Theta on PV2 (upper) with 320K isentropic surface as a blue line and cross section selection (black dashed line). Middle plot shows cross section with PV (colour contours) and potential temperature (black contour lines). Relative humidity (colour contours), PV (black contour lines) and vertical velocity (blue contour lines) are illustrated in the lower plots.

re-attaching to the stratosphere). Spring has the most frequent occurrence (70 cases) of no preceding Rossby wave while winter has the fewest (34 cases).

TABLE 5.1: Number of cases where no Rossby wave train is observed

Region	Autumn	Winter	Spring	Summer
NS	2	0	5	6
ES	8	5	7	9
SS	7	3	6	5
NI	3	4	9	7
NWE	10	3	9	6
NEE	6	5	9	3
CE	6	5	7	6
SWE	8	4	9	10
SEE	6	5	9	10
Total	56	34	70	62

5.2.2.1 Trigger locations

The trigger points of the Rossby waves for all of the combined regions in each season are displayed in Figure 5.4. Each figure shows the location of the assessed trigger points marked as circles, while colours represent how much time prior to the heavy precipitation event the trigger occurred in days. Although the locations of the triggers are analysed, the specific source of the wave initiation can not be determined merely by location. With this in mind, some speculative causes based on inspection of potential temperature on PV2 along with the position of the trigger will be proposed.

As expected, waves with triggers found nearer to the UK (over middle to eastern North America) tend to have shorter life times (1-3 days) before the heavy precipitation events while those initiated in the Pacific live longer (5-7 days). The average wave train in autumn and summer lasts 3-5 days, which is shorter than those occurring in winter (4-6 days) and spring (5-7 days).

In autumn, triggers occur in an arc from the western Pacific to the western Atlantic. They are located further north than in other seasons mainly between $50-60^{\circ}$N (over the eastern Pacific and North America). There is a fairly even spread of triggers throughout this whole region, however, a cluster of trigger points is noticeable along the border between North America and the western Atlantic. A possible source of wave initiation could be extra-tropical transition of cyclones as they move up the coast of the United States and interact with the jet exit region in the western Atlantic (Athanasiadis and Wallace, 2010). Also, this is a prime location

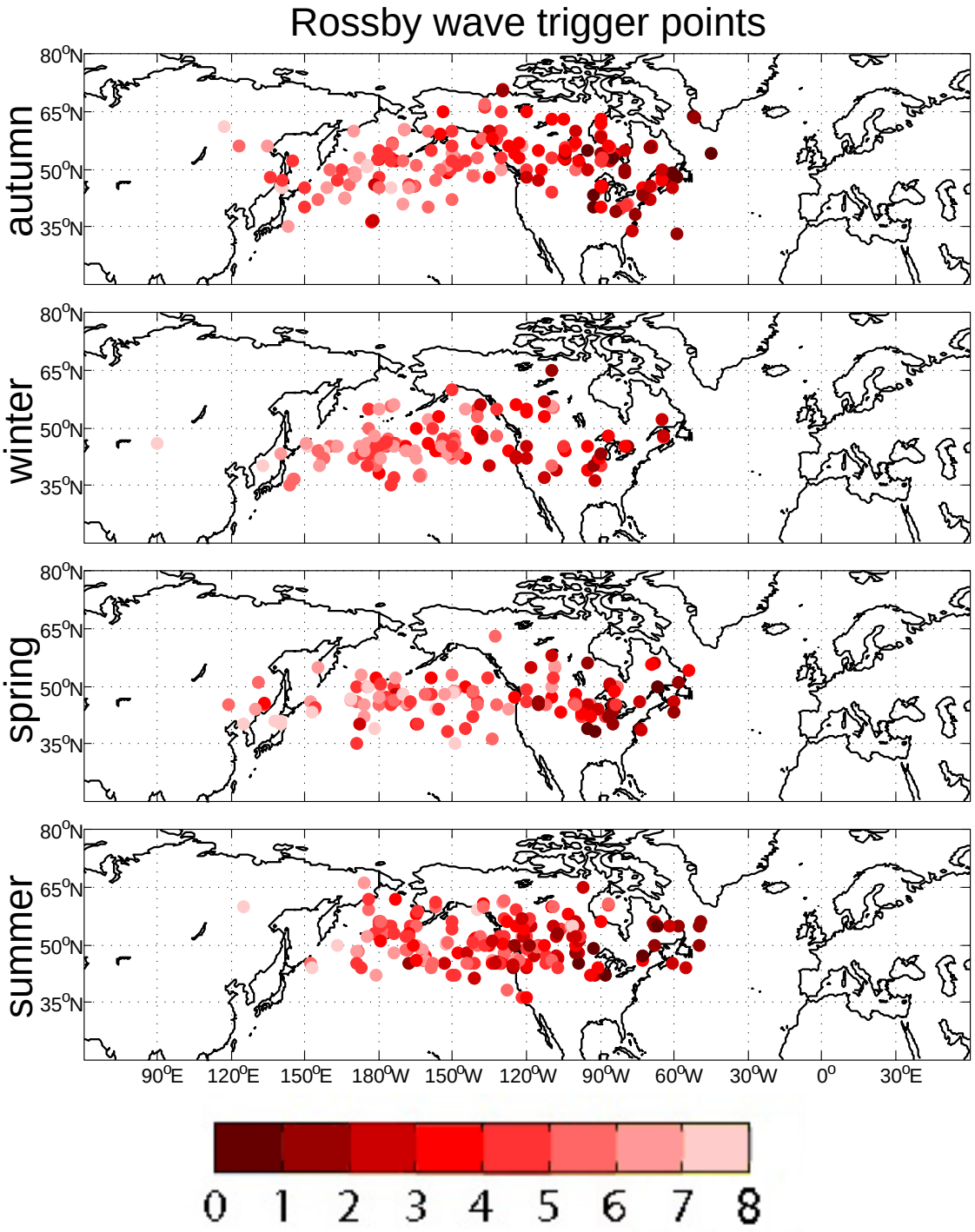

FIGURE 5.4: Trigger point locations of Rossby wave trains in each season. Colours indicate the number of days before the heavy precipitation events in the UK.

for cyclogenesis, which may impact the development of the wave. In the summer the most striking feature is the cluster of triggers on the boundary of the eastern Pacific to mainland North America. Potential temperature on PV2 indicates a deep tropospheric intrusion often occurs as the Rossby waves move over land from the sea in this region, sparking a downstream wave train. Increased evaporation over the ocean in the summer can lead to latent heat energy release during the precipitation process. This feature combined with the position of the Mid-latitude or Polar Jet (positioned further poleward in the summer) may play a role in the generation of triggers within this region.

Winter and spring both have trigger points occurring in a lower latitudinal band than autumn and summer. These are mainly found between $40 - 50°$N. Winter is characterised by clusters in the Pacific with fewer present over the North American continent. Those found over the continent occur in 3 groupings, at the Pacific Ocean/continental border ($45°$N, $120°$W), by the Rocky Mountains and in the Midwest (to the south-west of the Great Lakes). The Polar Jet is located further equatorward in winter so the trigger points across the United States occur on lower latitude levels. The spring season also has triggers which emanate from the Pacific with a second cluster region centred over the Midwest of the United States ($90°$W).

Isentropic gradients over the Asian continent tighten, and as they travel over the coast into the western Pacific Ocean they widen, forming the exit of the Pacific Jet (Athanasiadis and Wallace, 2010). Many downstream waves are initiated in this region. One of the main features of the Pacific, as a trigger generation area, is the presence of tropical and extra-tropical cyclones. Diabatic heating was shown to be present in this region (over the western and middle Pacific) around 2-8 days before the alpine heavy precipitation events by Martius et al. (2008). Triggers in the mid to eastern Pacific are often initiated by a cyclonically breaking Rossby wave or PV streamer (which could be accompanied by a low level cyclone) and hence diabatic heating.

The Polar Jet flows over the continental United States and the orography (Rocky mountains in the west and Appalachian Mountains to the east) frequently creates a trough over the Midwest ($45°$N, $90°$W) (Barry and Chorley, 2003). Breaking Rossby waves and PV streamers form as the trough diminishes and the re-circulation of stratospheric air downstream from the wave can then initiate another wave train. The Midwest is also an area of frontogenesis (cold air from the north meets warm air from the south), which may interact with the wave guide (Martin, 2006).

5.2.2.2 Comparison to Hovmöller diagrams

There are small variations in the trigger point locations in the individual regions of the UK (shown in Appendix B, Figures B.1 - B.4) and this is most pronounced in the spring. Northern Scotland (NS) has most of the triggers located over the Midwest of the United States. Northern Ireland (NI) and Southern Scotland (SS) have 2 cluster regions (in the middle of the Pacific Ocean at $170°$W, and in the middle of the United States $90°$W). While North East England (NEE) has wave trains extending back the farthest, into the Asian continent. The most variation in the combined Hovmöller diagrams (Figure 4.10 in Section 4.4) was found during the spring season as well. It is also significant that the largest number of cases with no preceding Rossby wave occurred during this season.

In general, the individual waves and trigger points vary from the composite of wave trains depicted in the Hovmöller diagrams in Figure 4.10. One possible explanation for this difference is that the composite Hovmöller diagrams contain the consistent wave signal from all the cases, so, differences in the individual wave speed or pattern can affect the final result. In some areas of the diagram waves with altering signs overlap, leading to a cancelation. Only the most consistent portion of the waves (found as those nearest to the heavy precipitation event) remain.

5.2.3 Conclusions

The main locations of triggers for Rossby waves occur in regions known for having an influence on the speed and position of the jet stream. These include, but are not limited to, regions over the Pacific Ocean, near orographic areas (such as the Rocky mountains) in the United States, and on coastal boundaries where the column of air stretches or contracts. Many of the triggers occur within the Pacific basin, and the Alpine case study explored the development of one Rossby wave in this area. Features on nearby isentropic levels (above and below) combine with a surface low, high and PV anomalies within the western Pacific to initiate the Rossby wave train. Although the sources of the Rossby wave triggers have not been explicitly investigated, the seasonal variations in the locations are identified.

In the autumn, wave triggers occur in a more northerly position and the spread of results is wider longitudinally (extending further east and west) than other seasons. The triggers are found

throughout the Pacific, North America and are also frequently found on the border the Atlantic Ocean. The winter and spring are categorised by slightly longer living wave trains. They are more frequent over the Pacific in winter and over the Midwest of the United States in the spring. The summer has the widest latitudinal distribution (stretching north and south) with the largest cluster occurring on the western border between the Pacific and continental North America. Although seasonal variations have been observed, no clear evidence of a particular type of trigger or trigger location associated with waves preceding heavy precipitation events has been found.

5.3 Initiation of PV streamer formation

The location and setting associated with the formation of PV streamers will now be assessed. The UK heavy precipitation events are analysed again, this time for the initiation and amplification area preceding the PV streamer in order to determine seasonal differences in locations where enhancement of the wave guide leads to wave breaking. These locations are related to the cyclonic or anticyclonic shear and hence the classification of the PV streamer type. Initiation locations are identified by pinpointing the first time step when the PV streamer occurs. Potential temperature on the 2PVU surface is then examined preceding the formation in order to determine the position where the wave is enhanced. The main influences are classified into four categories: ahead of the streamer, behind the streamer, both ahead and behind, or recirculation of stratospheric air. A tropospheric intrusion with a strong wave guide and PV gradient is often present either to the east or west of the stratospheric streamer intrusion. If the initiation of the PV streamer occurs in combination with tropospheric air (or an enhanced ridge) upstream of the streamer it is classified as "behind". When the tropospheric intrusion occurs downstream of the PV streamer it is labelled "ahead". The third category comprises a situation when tropospheric intrusions (ridges, or a blocking feature downstream) occur both from the east and west pushing together and squeezing the stratospheric air equatorward. The fourth type occurs when the streamer is formed from re-circulation of stratospheric air (for instance a cut off that eventually rejoins).

Table 5.2 presents the spread of ambient settings for the heavy precipitation cases. Autumn and summer have similar distributions (with a fairly even range between the various categories) as do spring and winter. The most common setting for streamer formation is an enhanced ridge

TABLE 5.2: Percent of each ambient setting impacting streamer development in each season

Season	Ahead	Behind	Ahead and Behind	Recirculated
Autumn	24%	33%	17%	26%
Winter	15%	40%	7%	38%
Spring	14%	41%	9%	36%
Summer	19%	33%	13%	35%

upstream or "behind" (especially in spring and winter). This is closely followed by recirculation of pockets of stratospheric air which remain from previous wave breaking. The location of amplification is related to the classification of PV streamer formed (LC1, LC2 or meridional). When the amplification occurs "ahead" the PV streamer will regularly wrap up cyclonically. Joint intrusions (from upstream and downstream) will often result in a meridionally aligned streamer while rearward amplification generates LC2 type streamers. When stratospheric air circulates and re-attaches the resulting streamer is not predisposed to any classification type.

The distribution of the ambient settings related to streamer amplification are displayed in Figure 5.5. The locations in each figure relate to the position where the amplification begins but in a large-scale setting these areas encompass a much broader range so should not be interpreted as exact points. Most PV streamer initiation occurs over the Atlantic Ocean to the west of the UK, as expected. Autumn has the widest spread of results with the main cluster centred around 53°N, 30°W while summer has the smallest distribution with initiation localised around 53°N, 20°W. Spring has a similar pattern to summer with a slightly wider spread and southward placement. In winter, the locations are further south due to the equatorward position of the isentropes during this season. Amplification behind the PV streamer (blue) occurs further to the west than other setting types as they are positioned upstream from the streamers (and streamers impacting the heavy precipitation in the UK tend to form in the eastern Atlantic). Downstream amplification (red) has a more eastern location in spring and summer with a slightly northern position in autumn. The increased zonal winds in the winter and stronger waveguide moving from the west appears to prohibit the likelihood of downstream amplification and when this does occur it is initiated mainly from the south. Joint amplification (yellow) has a much wider spread throughout the distribution while recirculated air has a central location (especially in the summer) and coincides with the position of the PV streamer. Regions of wave enhancement are influenced by both local and remote sources, so the wave perturbation areas reveal limited information. Identification of these sources needs further investigation in order to determine the main cause of the PV streamer formation.

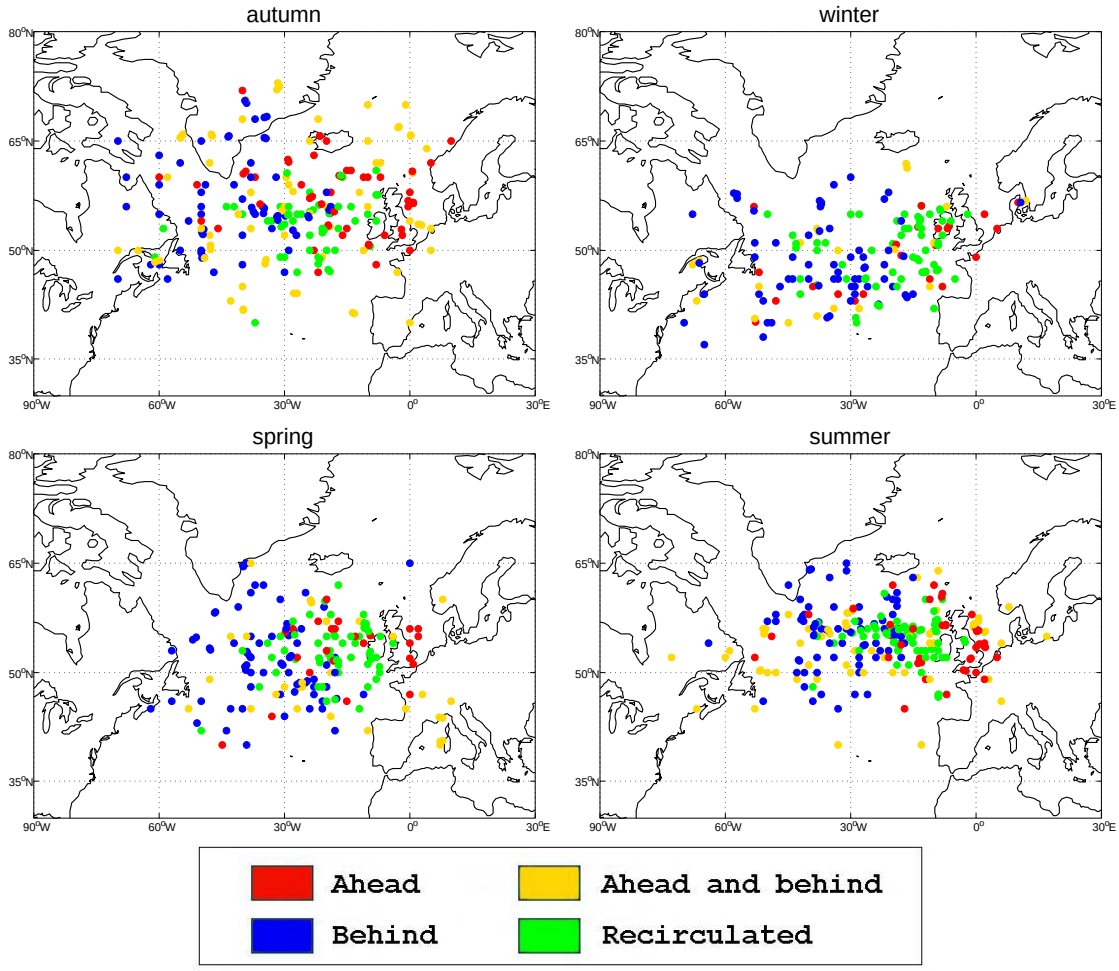

FIGURE 5.5: Locations of PV streamer amplification in each season. Colours represent the type of ambient setting.

5.4 Adjoint sensitivity study

As illustrated in Section 5.2 the initial trigger of a Rossby wave can lead to downstream evolution of streamers and high-impact weather. The initiation of the PV streamer is more localised however (Section 5.3), and factors such as diabatic heating events (for instance extra-tropical transition of tropical cyclones) can specifically cause PV streamer formation. Current forecasts and models of extra-tropical transition often do not accurately depict the subsequent downstream evolution and impacts (Jones et al., 2003; Hakim, 2005). In order to better understand the development of the streamers a case of extra-tropical transition of a tropical storm is investigated during the THORPEX Pacific Asian Regional Campaign (TPARC). TPARC took place from August to October 2008 with a primary aim of investigating tropical cyclones and extra-tropical transition. The dynamical causes for the formation of a PV

streamer downstream of a tropical cyclone undergoing extra-tropical transition is investigated in this study through the use of an adjoint sensitivity model. This investigation was carried out at the University of Wisconsin, Madison with the working group of Professor Michael Morgan.

The goal of an adjoint sensitivity study is to evaluate how small modifications to the initial conditions or model forecast state can alter a specified function of the forecast model's output (the response function). The response function, R, must be a first order differentiable function of forecast model output. The adjoint to a numerical weather prediction (NWP) model is the transpose of the tangent linear model which is linearized about a full-physics nonlinear trajectory. The adjoint model uses the gradient of R with respect to the model forecast state and is integrated backward in time. The "sensitivity gradients" or gradient of the same response function to the model state at earlier times is thus calculated. Assuming a perfect model, an adjoint model allows for the identification of analysis errors that contributed to a specific forecast error (Kleist and Morgan, 2005b,a). The adjoint of an NWP model is the most efficient means of identifying the sensitivity gradients and thus how small perturbations to the initial conditions would impact the response function (Errico, 1997).

Adjoint sensitivity studies have been utilised to examine various aspects of atmospheric dynamic flow. Upper-level precursor troughs were studied ahead of heavy precipitation from a Mediterranean mesoscale cyclone by Martin et al. (2007) and Homar and Stensrud (2004). Similarly, Lazear (2007) used an adjoint sensitivity study to investigate the amplification of a ridge associated with a blocking anticyclone and explosive cyclogenesis. Various studies have also investigated the importance of synoptic-scale features in the development of extratropical cyclones (Vukicevic and Raeder, 1995; Langland et al., 1995) as well as sensitivity gradients involved in tropical cyclone steering (Wu et al., 2007, 2009; Hoover and Morgan, 2011).

Limitations exist in the use and interpretation of adjoint models and the sensitivity gradients they produce. As the adjoint states are tangent linear, the nonlinear evolution of perturbations and sensitivities are not addressed. The validity of the linear results in the nonlinear evolution should be tested especially if moist physics or convection strongly influence the response function (Errico and Raeder, 1999). Martin et al. (2007) found that the tangent linear model produced perturbations with amplitudes of the typical analysis error for an intense cyclone over the Mediterranean, however the convective scheme introduced small but important nonlinearities. Diabatic heating from stratiform condensation also hampered the accuracy of the linear model. Evidence from the study by Homar and Stensrud (2004) suggests that important

nonlinear effects can be traced to the moist processes, although the main results of the adjoint had acceptable accuracy. When the moist physical processes were included in the adjoint sensitivity study of cyclone intensity by Langland et al. (1996), the results indicated that sensitivity magnitudes increased, however the spatial pattern of the sensitivities was not altered.

Testing of the sensitivity gradients to determine their accuracy is important as well as the dynamical interpretation of the results. Hoover (2009), and Hoover and Morgan (2010) found that many studies were flawed due to methodology and interpretation errors. Although the sensitivity patterns illustrate areas where changes to the initial conditions will impact the response function, they do not provide any explicit information on which initial condition changes will have the largest contribution to the response function in the basic state (Langland et al., 1995; Langland and Errico, 1996). With these factors in mind, the adjoint sensitivity study of PV streamer formation during the TPARC field study has been investigated.

5.4.0.1 TPARC case background

On the 12th of September 2008, during the TPARC field campaign, a tropical cyclone (TCS037) underwent extra-tropical transition. Figure 5.6 illustrates the position of the cyclone off the coast of northern Japan.

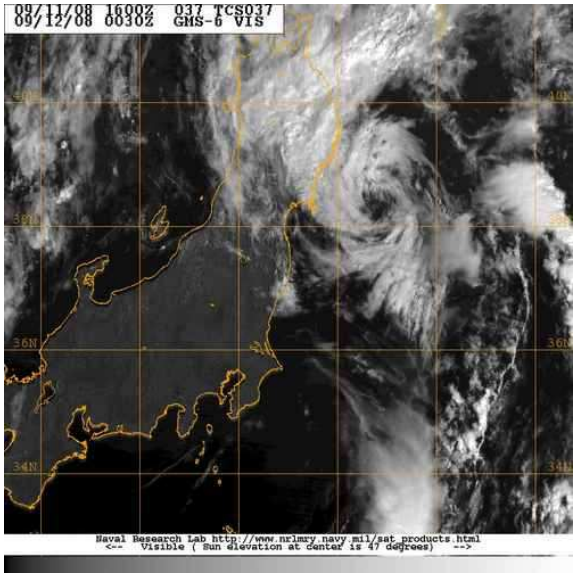

FIGURE 5.6: Satellite imagery of TCS037 over Northern Japan (depicted at 40N, 140E).

As TCS037 moved northward it interacted with the right hand side of an upper-level Rossby wave trough (depicted by the blue coloured contours in Figure 5.7). Over the next 3 days,

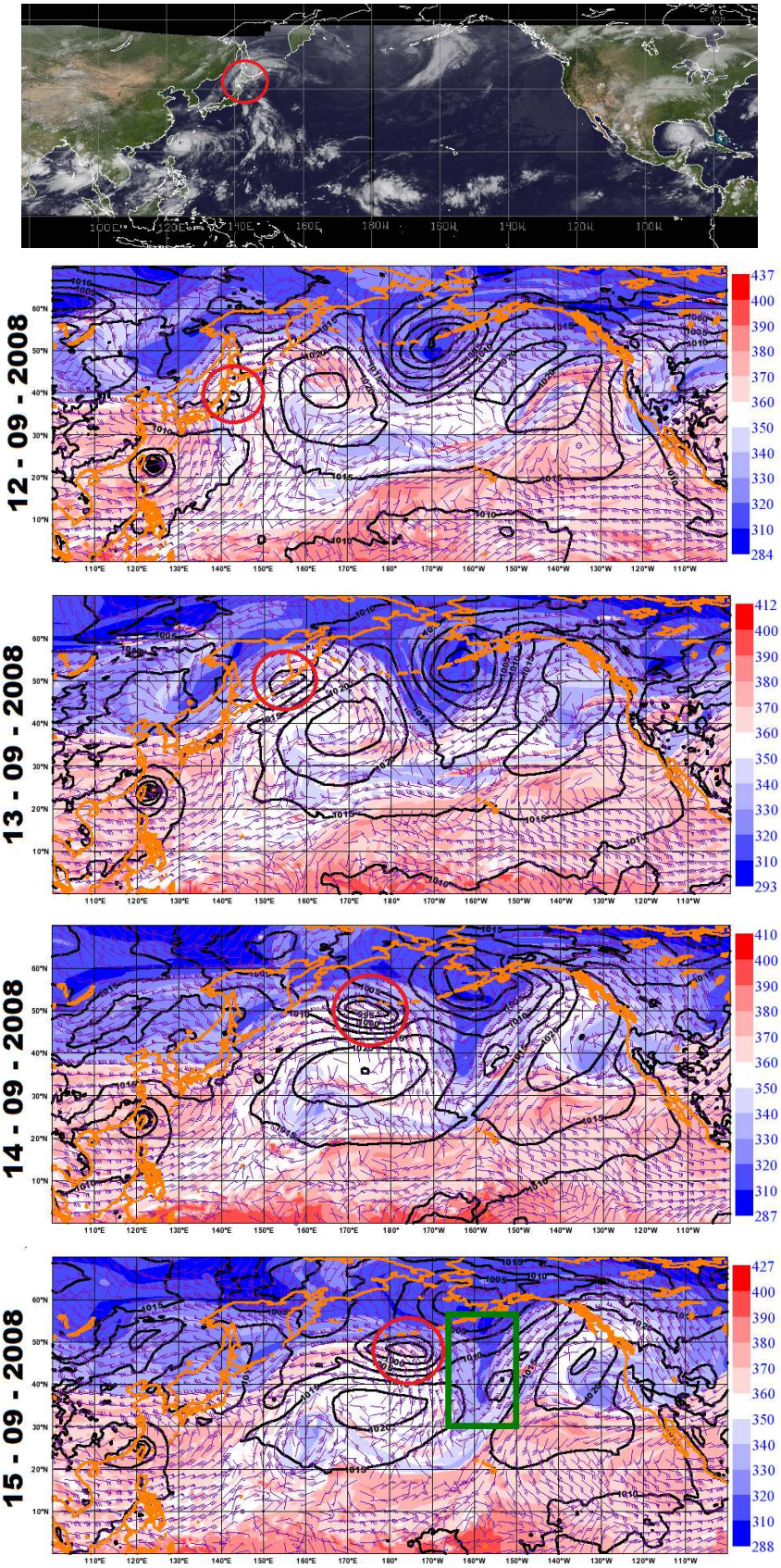

FIGURE 5.7: Upper figure shows infrared image of the Pacific on 12/09/2008. Each following figure depicts 2PVU on potential temperature (colour contours) with sea level pressure (black lines) and winds at 00UTC for 12-15/09/2008. TCS037 is depicted by a red circle and the green rectangle highlights the PV streamer formed.

from the 12th to the 15th, the upper-level flow field formed an enhanced ridge and finally a downstream PV streamer highlighted by a green square in Figure 5.7 (bottom). The development of the streamer is investigated by performing an adjoint sensitivity study. This study aims to diagnose the regions of dynamical influence affecting the formation of the streamer.

5.4.0.2 Adjoint models and response functions

For this case study, the adjoint to the version two MM5 (fifth generation mesoscale model) (Zou et al., 1997; Zou and Huang, 1998) developed at the National Center for Atmospheric Research (NCAR) was used. In addition, similar experiments were run with the Navy Operational Global Atmospheric Prediction System (NOGAPS) global spectral model (Hogan and Rosmond, 1991; Rosmond et al., 2002) by Professor Michael Morgan. For each of the sensitivities performed, the nonlinear version of each model is initialized with the ECMWF final analysis. This creates the basic state that the tangent linear model and adjoint models are linearized upon. The adjoint codes have been modified as described by Kleist and Morgan (2005a) to include the full physics basic state and eliminate the non-physical oscillation in the sensitivity gradients. This allows the evaluation of time evolution for forecast sensitivities. The nonlinear MM5 integrations use the Grell convective scheme, however, the tangent linear model and adjoint model use dry dynamics integrated about the moist basic state. The NOGAPS adjoint model includes large-scale precipitation within the physics scheme and is used as a comparison tool. In order to obtain information about whether the results are quantitatively accurate perturbations would need to be applied to the initial fields. This study does not employ that technique, so the results should be viewed as a qualitative assessment of the case study only.

The forecast lead time chosen was 72 hours starting at 12/09/08 12UTC at the point where TCS037 intercepted the Rossby wave and ending at 15/09/08 12UTC when the PV streamer formed. The tangent linear model and adjoint integrations are spaced over 20 sigma levels in the vertical with a top pressure level in the model of 100 hPa. A box was selected around the tip of the downstream PV streamer (Figure 5.8) as identified in the MM5 (green box) and NOGAPS (yellow box) models as well as over the position where the analysis (purple box) streamer (as defined by the ECMWF final analysis) was located, but using the MM5 forecast output. The box was selected around the tip in order to investigate the equatorward extension of the PV streamer and to examine an area of the streamer known for influencing convective available potential energy and precipitation events (Schlemmer et al., 2010). The sensitivity

to the vorticity (the chosen response function within each box) was investigated for vorticity, winds and divergence in order to understand the movement of the flow field and interaction of atmospheric variables around the time when the streamer formed. The sensitive regions were examined at 6 hourly time steps from 0 to 72 hours and so the progression of perturbations impacting the response functions are assessed.

5.4.0.3 Sensitivity Analysis

When performing a sensitivity study, the assumption is that the forward run model output is "perfect" so an assessment of the quality of the forecast is only briefly discussed. The three PV streamers (MM5, NOGAPS, and analysis) have small differences as shown in the vorticity in Figure 5.8. The NOGAPS is most similar to the analysis in position and magnitude while the MM5 PV streamer extends further equatorward and is located south-west of the analysis and NOGAPS streamers. The sensitivity gradients related to the vorticity within the tip of each streamer at 300mb have been investigated.

The sensitivity analysis reveals regions where positive or negative perturbations in the initial conditions or basic state would increase the vorticity within the chosen response function box. Figure 5.9 shows the sensitive regions for all three boxes at the initial time of 12/09/2008 at 00UTC on the 300mb level. The colour contours with a green or blue shade indicate a negative perturbation would increase the vorticity while the red and yellow shades show areas where positive perturbations would increase the final vorticity. A broad range of influences are identified, mainly to the west of the streamer (due to the westerly flow at upper-levels).

The NOGAPS adjoint model (Figure 5.9a) has lower magnitudes for the sensitivity gradients, but similar features to the analysis streamer sensitivity regions (Figure 5.9b), especially near the position of the tropical cyclone (illustrated with a black circle). Increasing the vorticity near the tropical cyclone for both of these cases would increase the vorticity in the developed streamer. The forecast streamer within the MM5 model (Figure 5.9c) displays an almost opposite pattern to that of the analysis streamer box (as both of these use the same forward run model). The MM5 forecast PV streamer would be enhanced if the tropical cyclone was placed further northward (shown by the yellow and red contours to the north and north-east of the cyclone position). The MM5 gradients also indicate that decreasing the vorticity within

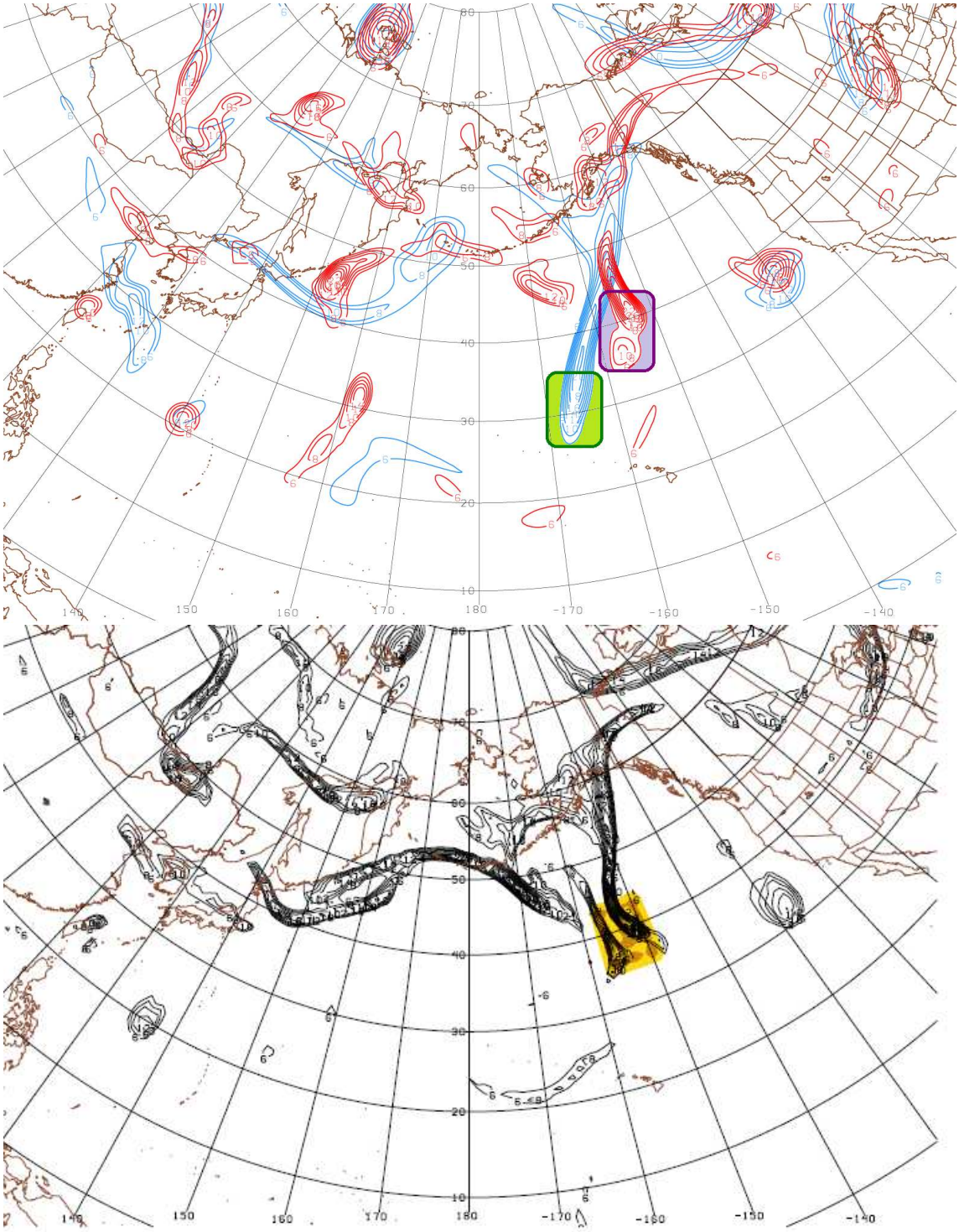

FIGURE 5.8: 72 hour forecast time with response function box at 300mb positioned around final streamer tip shown by vorticity contours. MM5 adjoint model (upper figure) with forecast (blue contours) and analysis streamer (red contours) and response function boxes (green for forecast and purple for analysis). NOGAPS adjoint model (lower figure) with forecast streamer (black contours) and response function box (yellow).

the ridge (illustrated by the purple and blue contours to the north-east of the cyclone) would amplify the ridge and enhance the vorticity within the final streamer.

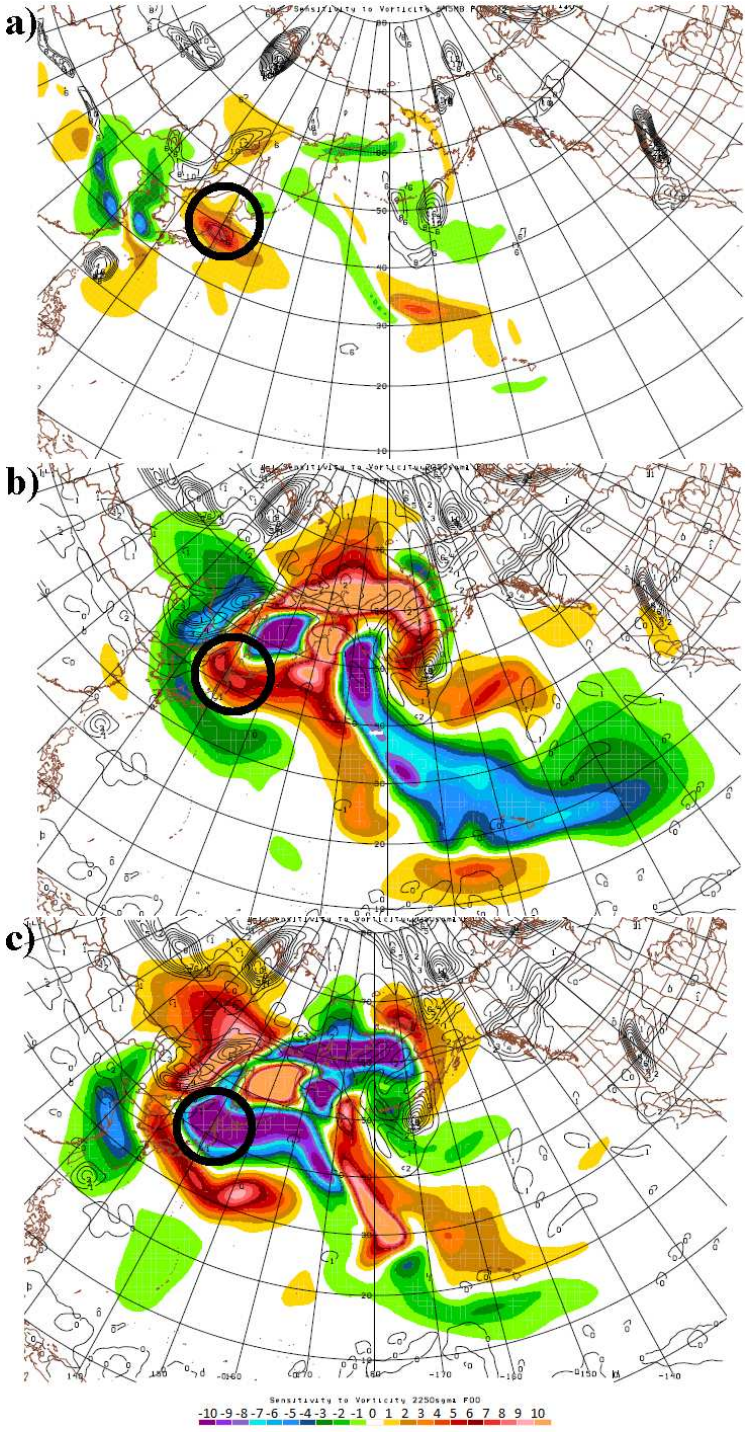

FIGURE 5.9: Sensitivity to vorticity at initial time of 12/09/2008 at 00UTC on the 300mb level. Negative perturbations (blue shades) and positive perturbations (red shades) to the vorticity at this time step would increase the vorticity within the final box (see Figure 5.8). The black circle illustrates the postion of TCS037 within the NOGAPS forecast (a) analysis position within MM5 forecast (b) and MM5 forecast (c). Black contours represent the vorticity in panel (a) and potential vorticity in panels (b-c).

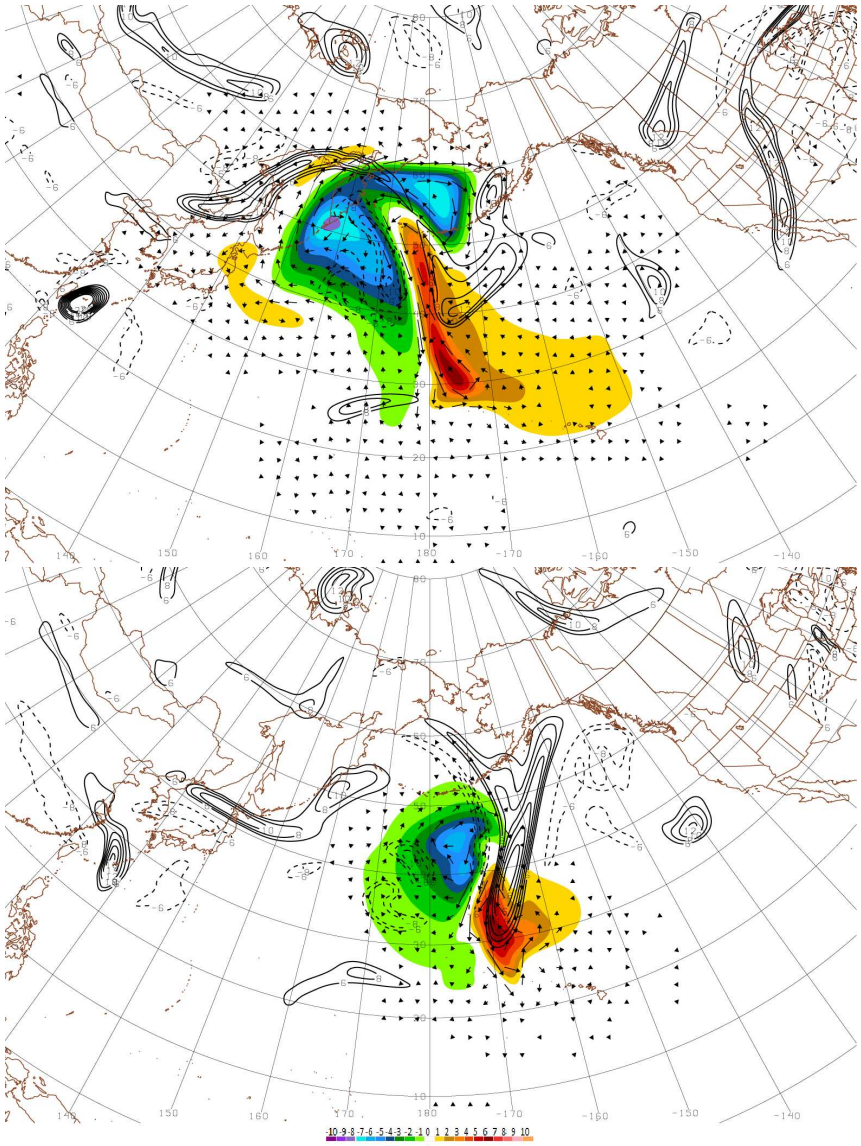

FIGURE 5.10: Sensitivity to vorticity within the MM5 adjoint model at 24 hour forecast on 13/09/2008 at 00UTC (upper) and 60 hour forecast on 15/09/2008 at 12UTC (lower). Negative perturbations (blue shades) and positive perturbations (red shades) to the vorticity at this time step would increase the vorticity within the final box (see Figure 5.8). Wind fields are demonstrated as arrows and the forecasted vorticity is displayed as black contour lines.

Local influences near the response function box also have an impact in the vorticity amplification. As the sensitivity gradients progress through time, they become more focussed on the area surrounding the streamer tip (shown for the MM5 forecast streamer in Figure 5.10). As the streamer develops, the sensitive regions are located within the immediate upstream ridge (negative perturbations or enhancing the ridge) as well as near the tip of the streamer (positive perturbations or increasing the vorticity near the streamer tip). Examining other variables such as divergence and wind reveal similar results. Enhancing cyclonic (anticyclonic) rotation

in areas where negative (positive) vorticity perturbations should occur enhance the vorticity in the PV streamer. Similarly, decreasing (increasing) divergence where positive (negative) vorticity perturbations occur also increases the vorticity within the streamer. In later forecast times similar patterns are also observed in the analysis positioned box and NOGAPS model (not shown), with sensitive areas located in the upstream ridge and around the streamer tip.

5.4.1 Discussion and conclusions

The main influences on the developing streamer come from the enhancement (MM5 forecast) or reduction (analysis box position) of the preceding ridge in earlier forecast times. The position of the tropical cyclone in this case interacts with the poleward moving airflow of the Rossby wave trough and enhances this wind field. A stronger vorticity centre in the tropical cyclone as well as a more northward placement of the cyclone would have enhanced the downstream streamer feature further by increasing the strength of the Rossby wave airflow. In later forecast times, the local circulation directly around the streamer tip has the main influence on the development. A comparison with the NOGAPS adjoint model, which includes moist processes, reveals a similar pattern to the analysis streamer sensitivity gradients. The non-linear model captures the structure and magnitude of the PV streamer more accurately and subsequently the sensitivity pattern has more similarity to the position of the analysis streamer within the MM5 forecast. The gradients have a smaller magnitude than in the MM5 and are more localised initially near the position of the tropical cyclone. Again, in later timesteps the sensitivities shift nearer to the tip of the streamer.

The adjoint sensitivity study highlights areas where targeted observations would be beneficial in order to improve the analysis. This study also demonstrates the potential for using these models to study the dynamical processes contributing to the streamer development. Limitations in the use of this method include problems with the model's ability to reproduce moist processes and diabatic characteristics. In order to make a complete study, perturbations to the initial conditions should be made and the changes to forecast results should be checked (not done for this case). The use of the adjoint model on more cases and for streamers causing heavy precipitation would be beneficial in understanding the predominant influences on streamer formation and in aiding in the predictability of these events. Evidence suggests the local influences of wave enhancement nearer to the streamer formation are an important factor in predicting where the PV streamer will occur.

Chapter 6

Forecast quality and predictability of PV streamers

6.1 Introduction

An important aspect of weather prediction is identifying when and where high-impact weather, such as strong winds or heavy rainfall which leads to flooding, will occur. As the large-scale flow is intrinsically related to precipitation events, the ability of numerical models to represent upper-level Rossby waves is crucial. The characteristic structures and orderly propagation of baroclinic waves give them properties conducive to enhanced predictability over 1-2 week time-scales (Hoskins, 2006). Grazzini (2007) found this to be the case for medium-range predictability of wave packet amplification and downstream southerly flow toward the Alps leading to heavy precipitation events in the autumn. Low predictability issues still remain for some aspects of Rossby wave train progression. The interaction between Rossby waves and tropical or extratropical systems, especially on the western side of an ocean basin (Pacific and Atlantic), contribute to forecast errors (Harr and Dea, 2009; Anwender et al., 2008). The errors continue downstream within the ridge formation, breaking of the Rossby wave and evolution of PV streamers.

Atmospheric blocking features, associated with breaking Rossby waves, were found to be represented well in ECMWF models up to 4 days in advance by Pelly and Hoskins (2003). However, a study by Dirren et al. (2003) revealed that some aspects of breaking Rossby waves and PV

streamers need improvement in more recent prediction models. The correct phasing and orientation of streamers were not captured accurately which in turn led to misforecasts of associated severe weather events. Similarly, a study by Grazzini and Van der Grijn (2003) found that a wave packet emanating from eastern Asia to the Alps, and the associated trough, were well simulated but there was a phase shift in the wave in 3 to 5 day forecasts affecting the placement of the trough and impacting the precipitation forecasts. The meso-scale structure of a PV streamer can determine the location and intensity of precipitation (Fehlmann and Quadri, 2000), hence the ability to clearly forecast the specific internal structure and placement is critical for accurate heavy precipitation forecasts.

Quantifying the predictability of PV streamers, and identifying typical forecast errors may help to improve predictive capabilities of high-impact weather events. To this end, a novel feature-based method is proposed and studied here, which aims at verifying a range of streamer quantities. The method is exemplified for a set of heavy precipitation events on the Alpine south side, a class of streamer-induced events that is well-studied in terms of physics, dynamics and climatology. After applying the feature error method to the deterministic forecast it is also applied to a single case using the THORPEX Interactive Grand Global Ensemble (TIGGE).

6.2 Methodology

Potential misforecasts of PV streamers during Alpine heavy precipitation events are investigated by comparing ECMWF deterministic forecasts and analysis data. Five forecast times are investigated 6 (FC06), 30 (FC30), 54 (FC54), 102 (FC102) and 126 (FC126) hours ahead. Thirteen case studies occurring in the autumn season have been examined (dates listed in Appendix C Table C.1). Each streamer in the analysis and forecast time is defined using the streamer identification routine described in Section 3.1. PV streamers occurring on 310K, 315K, 320K and 325K isentropic surfaces are selected. Similar to the study by Martius et al. (2006b), streamers affecting the Alpine region are extracted if they overlap with the rectangle region of $43 - 50°$N, $5°$W$-10°$E in either the forecast or analysis time. Each time step and isentrope is checked for streamer matches by identifying the closest streamers (occurring in the forecast and analysis data) at a maximum distance of 500km. In addition, if the distance between the line points, marking the connection to the main body of stratospheric air, is more than 2000km away, the streamers are considered to be different systems. Figure 6.1 shows the

selected forecast (red) and analysis (blue) streamers for an FC102 case. Cutoffs and larger troughs of stratospheric air are not included in the comparison.

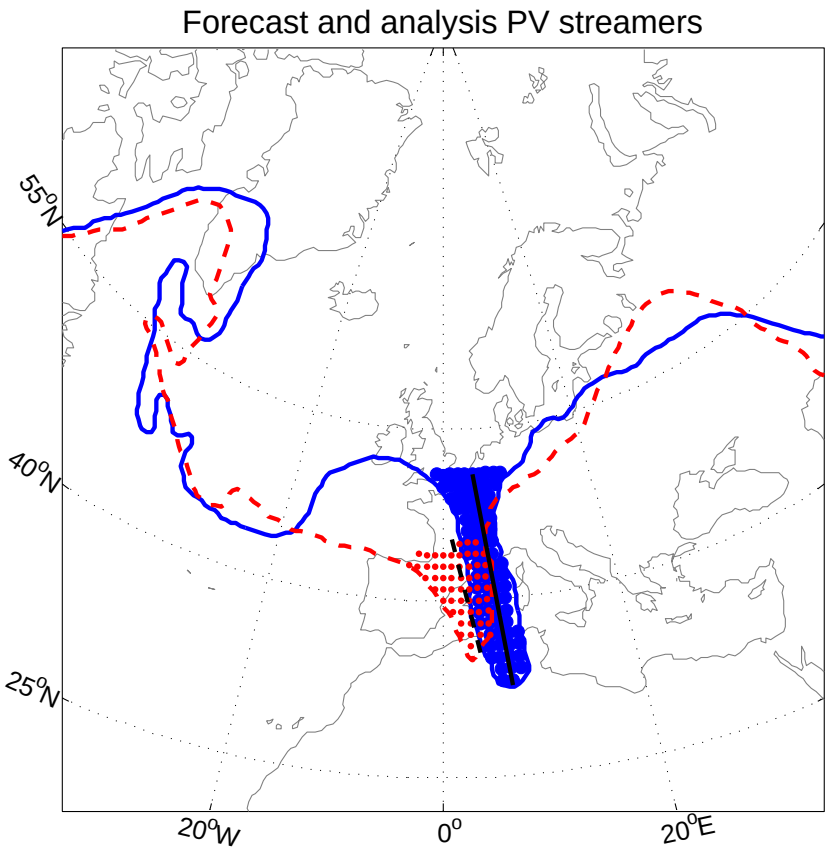

FIGURE 6.1: 2PVU contour lines with analysis (blue) and forecast (red) streamer for a 102 hour forecast. Lines of elongation (dashed black - forecast and solid black - analysis) are displayed.

Not only is the presence and location of a similar feature important in determining the accuracy of the forecast but also the distinctive structural anomalies. In order to evaluate the differences in streamers, several feature-based components are analysed. The position of the streamer is determined by using the centre of mass and depicts the shift in location of the forecast in relation to the analysis. The differences in the shape and size of the streamer are analysed by comparing the width, length and area of the features. Tilting angle and streamer classification (LC1, LC2 and meridional) are also calculated and compared. An assessment of the PV amplitude and distribution is carried out by investigating the mean, maximum (95% quantile) and minimum (5% quantile) PV within the interior of the streamer. The spatial configuration of PV differences are also examined through a four-quadrant technique based on the line of elongation and central width line. In this way, upper and lower portions of the streamer can be compared, as well as right and left hand sides.

6.3 Deterministic forecast results

All of the following results are presented in the format of forecast minus analysis. Positive values indicate that the forecast PV streamer is longer, wider, or has higher PV amplitude while negative values show shorter, narrower or smaller PV amplitudes.

6.3.1 Structural differences

The size of the PV streamers are compared by analysing the differences in elongation and width. Figure 6.2 shows histograms of the differences in length (left) and width (right) for all the forecast times. The FC06 forecasts have a narrow and symmetrical shape (centered near 0km difference) and the size of the PV streamers are very similar to the analysis counterparts with differences in the range of -250km (shorter) to 250km (longer). In the FC30 time there are also mainly small differences between the forecast and analysis. A few outliers occur in the distribution and these are usually longer than the analysis (by up to 1000km). These large differences at a short lead time are not very frequent. The FC54 forecasts have fewer streamers that are the same in length, with most differences around -250km or 250km. There are slightly more shorter streamers in these forecasts and the largest outliers in the distribution reach -750km (shorter) and 750km (longer). The FC102 and FC126 forecasts have much wider distributions (with outliers reaching -1500km and 1500km). There is a slight skew towards longer streamers in the FC102 forecasts while the FC126 has an uneven distribution but overall more forecast streamers are longer than the analysis.

The differences in the widths are also accentuated as the forecast time increases. Most of the PV streamers in the FC06 and FC30 have small or no deviations from the analysis. Streamers range from -75km (narrower) to 150km (wider) with a slight skew towards wider streamers. This pattern remains in the FC54 forecasts (where the most typical streamer differences are -75km to 75km), but with a flatter curve and wider overall distribution (-225km to 300km). The FC102 and FC126 forecasts have a similar arrangement with most of the streamers either being much wider (150km) or narrower (-150km to -225km) than their analysis counterparts. There is a tendency towards wider streamers in both of the later forecast times and outliers range from -375km to 375km. Surprisingly, both the elongation and width of the forecast streamers have a bias toward larger features at longer lead times.

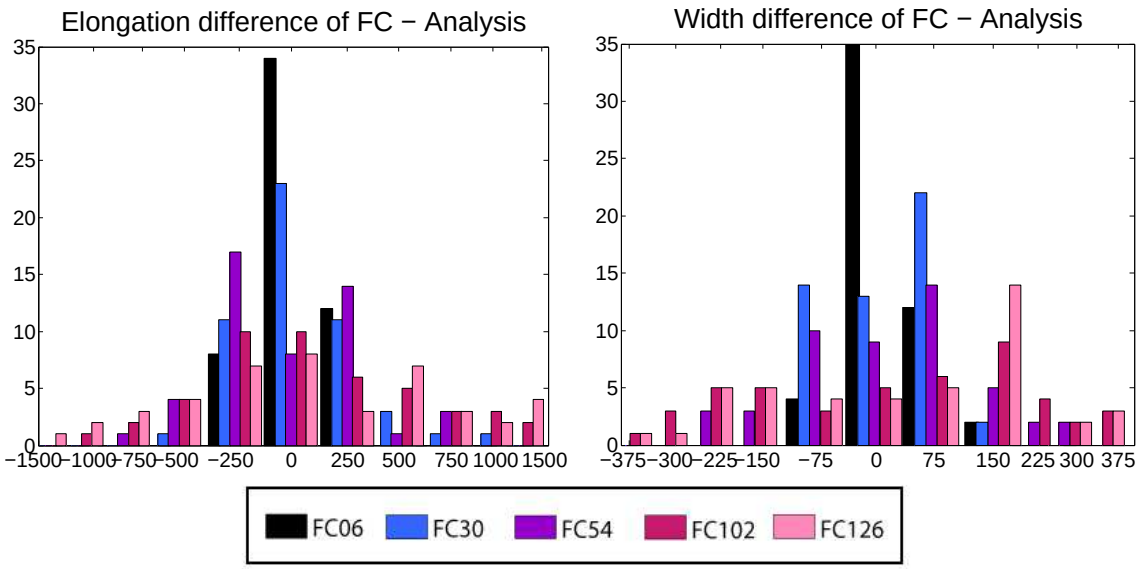

FIGURE 6.2: Histograms of the elongation (left) and width (right) differences (km) for the five forecast times. Negative (positive) values illustrate shorter (longer) or narrower (wider) streamers.

6.3.2 Error relationships

The links between structural differences, position and mean PV are illustrated in Figure 6.3. Each square within the diagram represents the position of the forecast streamer in relation to the analysis streamer. Vertical lines indicate differences in elongation while horizontal lines show width changes. If the lines are coloured red (blue), the forecast streamer is wider or longer (narrower or shorter) than the analysis counterpart.

As forecast lead times increase the streamers spread further outward away from the analysis streamer (positioned at 0,0). The FC06 cases are all found very close to the analysis with only a few outliers. FC30 and FC54 are similar but with more outliers especially to the north-east. In the later forecast times (FC102 and FC126) the streamers are shifted as much as 1200km to the east and west (mainly to the east and the direction of propagation in the FC102 cases). Less northward and southward shifting is detected, although FC102 and FC126 have larger distributions in these directions (mostly southward in FC126) than earlier forecast times.

The position of the streamers have a tendency to be related to their overall size (as the position is identified as the centre of mass) in earlier forecast times. Because of this, streamers with larger elongation and width differences are often found further away from the analysis centre. An example of this can be seen in the FC30 time (Figure 6.3) where the north-east outliers are

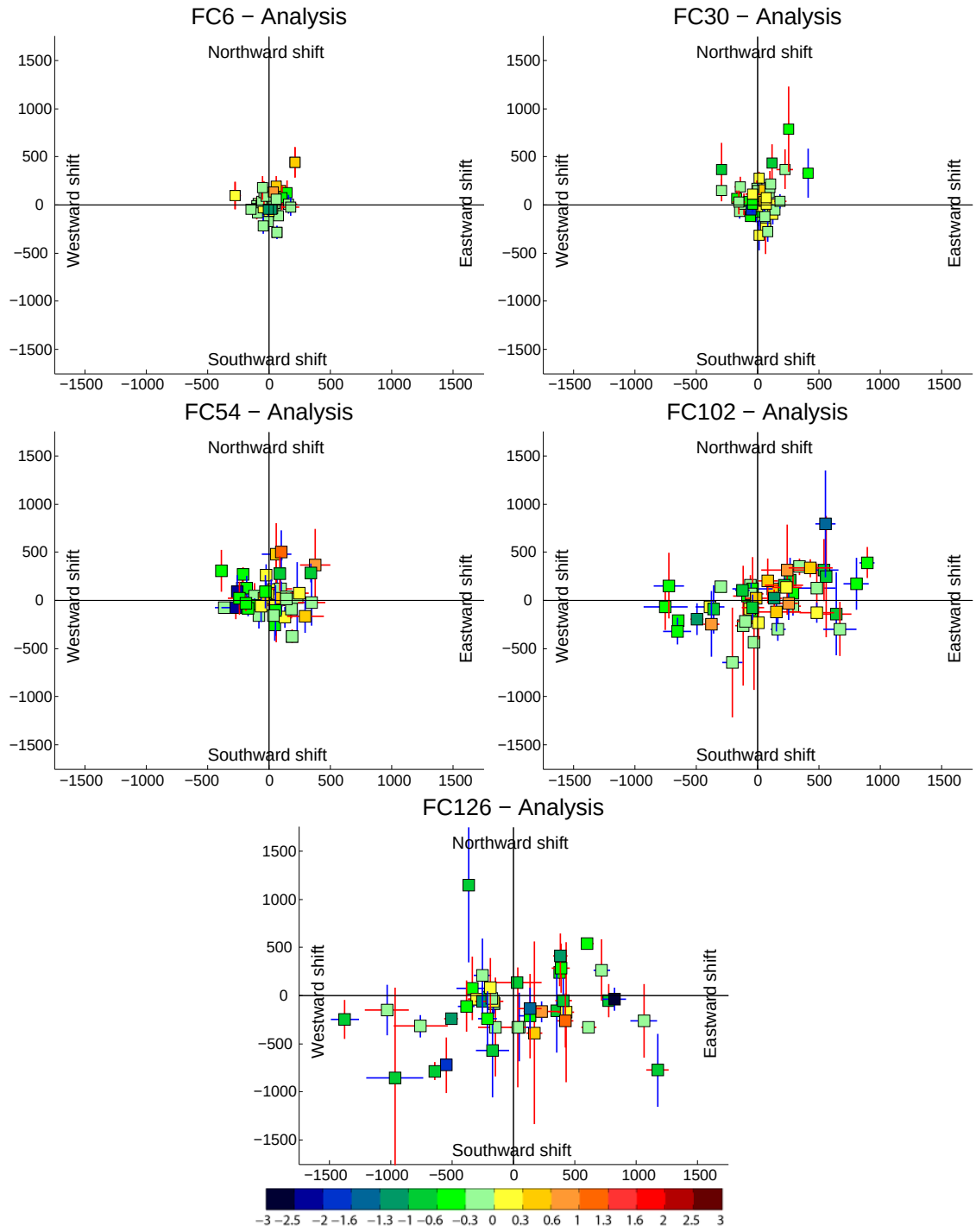

FIGURE 6.3: Difference of forecast in relation to analysis streamer (positioned at 0,0) for FC06, FC30, FC54, FC102 and FC126 times. Elongation (vertical lines) and width (horizontal lines) differences are shown, red indicates positive values (wider or longer streamers) while blue indicates negative changes (shorter or narrower streamers). Colour of square illustrates difference in mean PV, blue (red)shades show lower (higher) PV.

longer than the analysis streamers. In later forecast times, the link between position and size is not distinct. An attribute of the identification routine in selecting the PV streamers also has an impact on the relationship between the errors found. It only captures portions of the 2PVU contour that have a width across the "neck" of $\leq$800km. This means that if the streamer grows wider nearer to the stratosphere, less of the feature will be selected (resulting in shorter, wider features). These wider and shorter streamers are evident by the points in Figure 6.3 that have opposite coloured horizontal and vertical lines (blue vertical with red horizontal). Additionally, as a single PV contour is analysed, the vertical position of that contour could result in observed errors. Depending on the gradient of the 2PVU contour, errors in vertical displacement could lead to a horizontal shift in the contour and hence a shift in the position of the identified PV streamer.

There is also an indication of a relationship between position and the mean interior PV difference within the streamers. In earlier forecast times (FC06, FC30 and FC54) streamers found closest to the analysis have slightly higher mean PV values (0.3 to 1PVU). Higher PV means are also found in the northward placed outliers in FC06, FC54 and to the east in FC102. In spite of these cases, no significant link between position, elongation or width and the PV amplitude has been identified.

6.3.3 PV amplitude differences

A comparison of the PV amplitudes within the entire forecast and analysis streamer show that the forecast streamers exhibit a bias towards lower PV values (Figure 6.4). This is evident in the mean and maximum (95% quantile). The PV minimum value differences for the forecast and analysis streamers have a much smaller range (-0.5 to 0.5PVU) than the mean or maximum differences. This can partly be explained by the asymmetric PV distribution between the stratosphere and the troposphere as well as the fact that the selection criterion follows the 2PVU contour line. The FC06 forecast time has similar mean interior PV to the analysis streamers and 70% of values differ by less than 0.15PVU. Lower values are dominant in all of the other forecast times with values normally falling between -1 and 0.5PVU.

The maximum PV within the forecast streamers have a clear predominance towards lower values in all the forecast times. The FC06 streamers are mainly distributed between -0.45 and -0.15PVU (less). Only 5% of the maximum values are higher in the FC30, FC54 and FC126

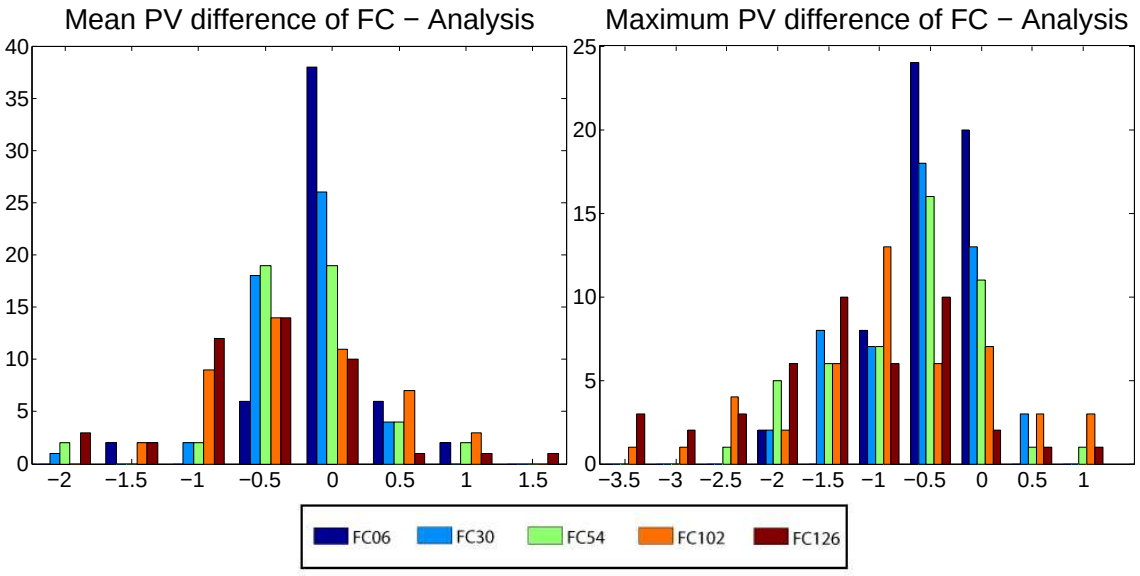

FIGURE 6.4: Difference of mean (left) and maximum 95% quantile (right) PV (in PVU) for the five forecast times (forecast - analysis data).

forecasts (with 13% in FC102). Maximum values are lower by an average of -0.5PVU in FC30 and FC54 while this increases to -1PVU in the FC102 and FC126 times. Outliers also increase with longer lead times with a range from -3.5PVU to 1PVU.

The distribution and significant locations of the PV differences within the streamer are investigated by dividing the streamer into 4 quadrants. Quadrant 1 comprises the upper left hand portion, quadrant 2 is the upper right, quadrant 3 makes up the lower right and quadrant 4 is the lower left portion of the streamer. Figure 6.5 and 6.6 show the distributions of the mean and maximum (95% quantile) PV differences arranged in their closest geographical positions.

Quadrant 1 (Figure 6.5) has a fairly even distribution of mean PV differences (centered around 0PVU) with a balanced range of higher and lower values in all forecast times. Similarly, the maximum PV differences (Figure 6.6) in quadrant 1 show only a slight bias toward lower PV (centered at -0.5PVU) with an even spread of outliers. Quadrant 2 demonstrates the most significant variations within the PV streamer. This quadrant has a slight skew towards lower PV means (most fall between -1 to 0PVU) while maxima are highly skewed towards lower values (ranging from -5 to 1PVU). Quadrant 3 (Figure 6.5) has a Gaussian spread centered around -0.25 to 0PVU especially for the lower forecast times (FC06, FC30, and FC54). The later forecast times (FC102 and FC126) have additional outliers giving these curves a slight skew towards lower values. This trend continues in the differences in PV maximum (Figure 6.6) where FC06 has an even distribution and the other forecast times are skewed toward marginally

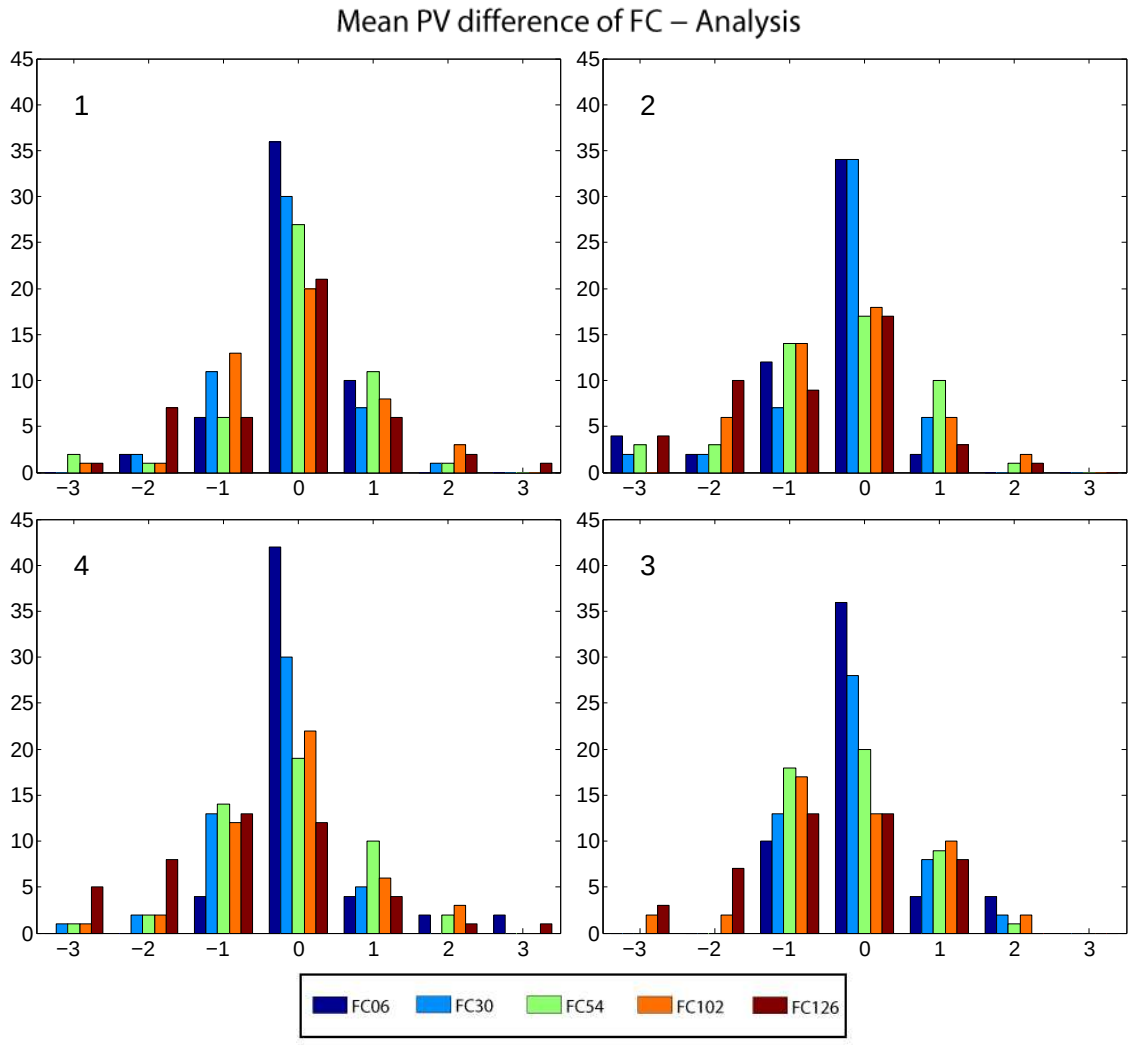

FIGURE 6.5: Difference in mean PV within each quadrant (1 to 4, arranged in their geographical position) in PVU for the five forecast times (forecast - analysis data).

lower values (centered around -1PVU and ranging from -3 to 2PVU). Quadrant 4 has more outliers than the other quadrants for both the mean and maximum. The mean spread is fairly evenly distributed except for FC126 which has a higher portion of low values (-1 to -3PVU). This is also true in the maxima where the FC126 forecasts display more negative values (-1 to -5PVU) and earlier forecast times show a skew towards lower maxima (centered at -1PVU).

Overall forecast streamers tend to exhibit lower PV mean which is directly related to the maximum values also having lower quantities. The lower maxima in Quadrant 2 suggests that the PV gradient at the tropopause boundary on the eastern flank may be weaker in the forecast streamers. These lower values may also indicate insufficient influx of high-PV air from the main body of the stratosphere. The narrower "neck" near the stratosphere, which causes longer streamers in the forecasts, could lead to less downward influx of the stratospheric air.

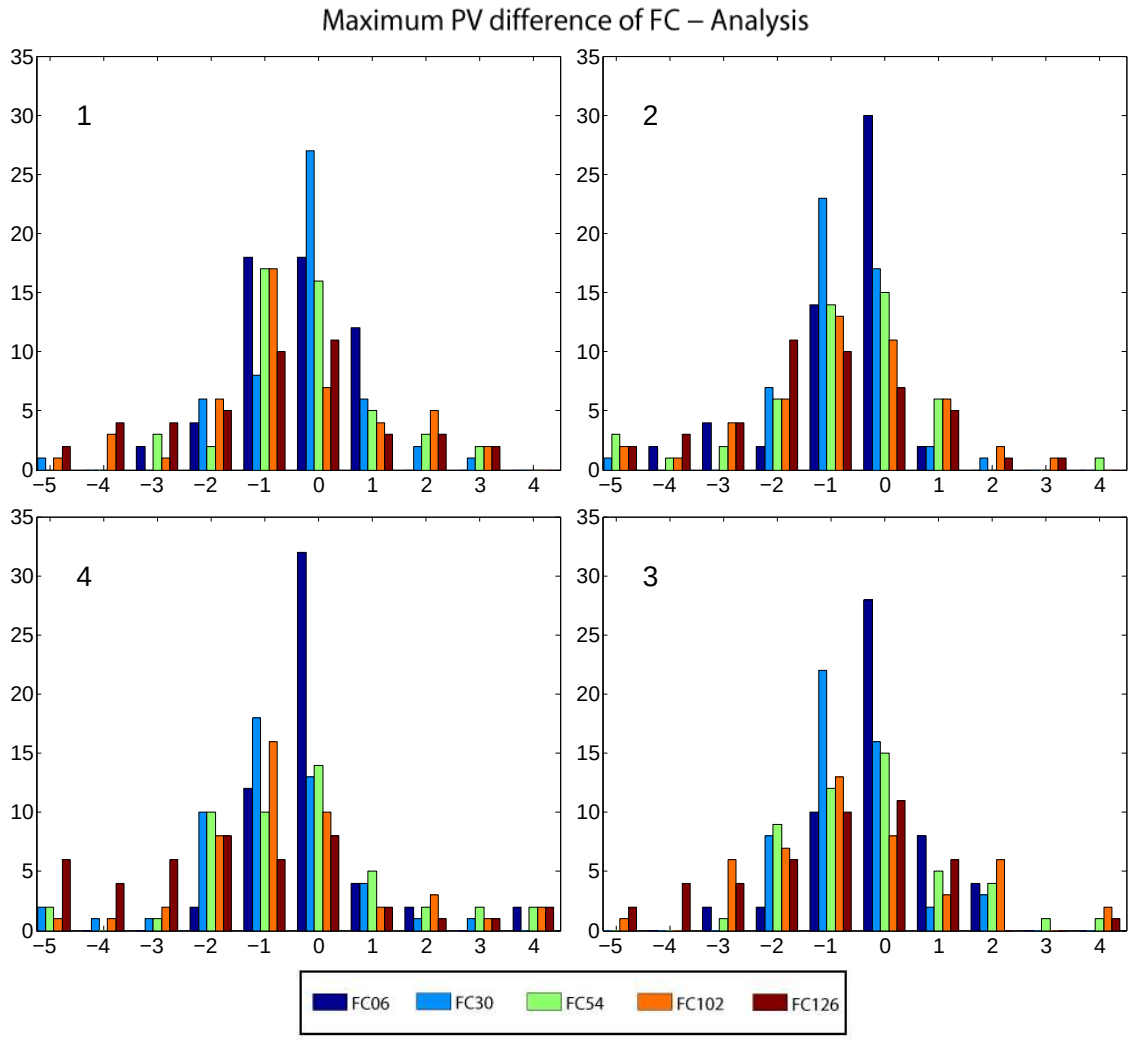

FIGURE 6.6: Difference in maximum 95% quantile PV within each quadrant (1 to 4, arranged in their geographical postion) in PVU for the five forecast times (forecast - analysis data).

6.3.4 Angle and tilt

The percentage of angle or tilting differences between the streamers are displayed in Figure 6.7. The change in angle of the streamer is often related to whether the streamer breaks sooner or later than the analysis. It can also be impacted by the development of a preceding ridge (especially in LC1 classifications), by tropospheric intrusions ahead or by how the streamer wraps up (in LC2 classifications). The FC06 forecast time has little variation from the analysis with most forecast streamers (75%) having less than 2.5° differences. Angle differences are also very small in the FC30 forecasts and both FC06 and FC30 have an even split of forward (larger angles) and backward tilting (smaller angles). As the forecast time increases, so does the magnitude of differences. The FC54 have more forward tilted streamers with outliers

reaching -20 and 20°. By the FC102 and FC126 lead times, the angle differences are fairly evenly spread between the backward and forward tilting and the maximum angle differences increase to $+/-30°$.

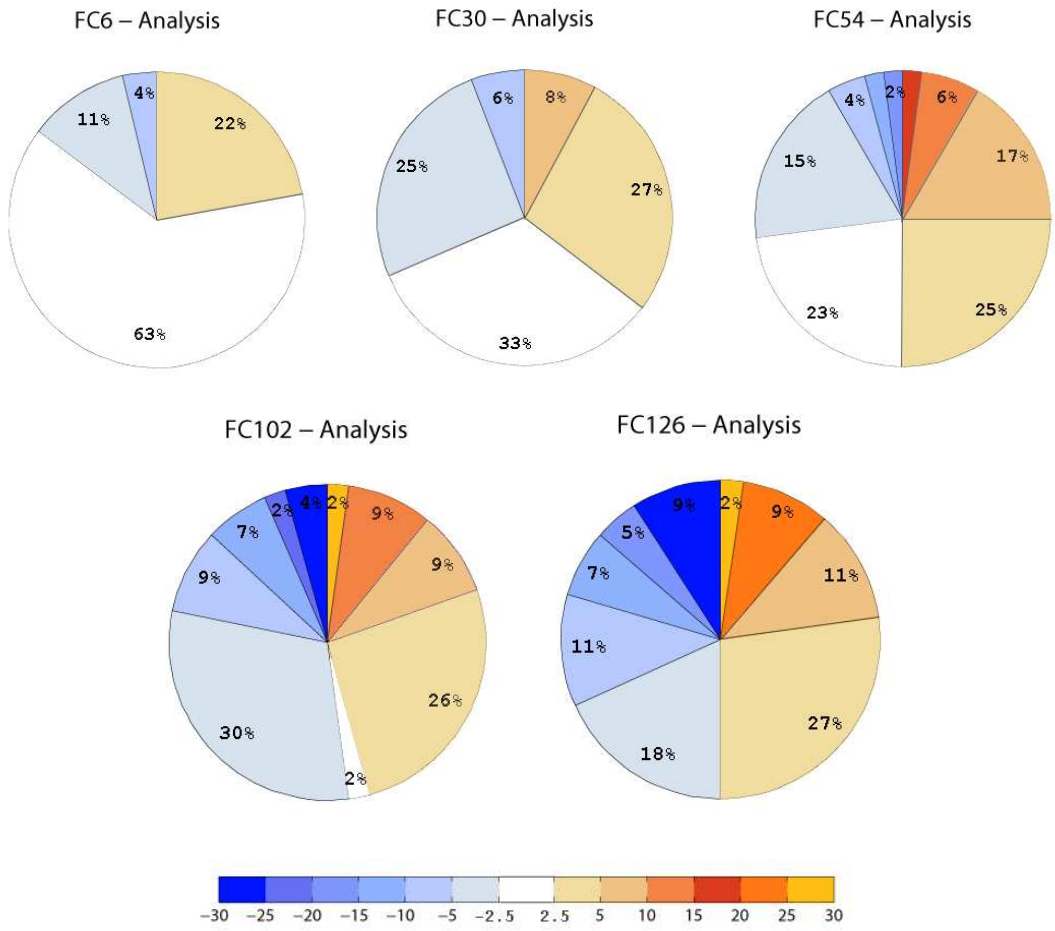

FIGURE 6.7: Angle differences between forecast and analysis streamers. Blue shades indicate backward tilt while orange shades show forward tilt (in degrees).

Small differences in angle (less than 10°) have no apparent relationship with the other streamer attributes (elongation or width). Larger angle differences are associated with a shift in the position of the streamer. Forward tilting results in a westward movement from the analysis while backward is associated with eastward movement. Although there is a growth in error as the forecast lead time increases, there is no specific reason for the variations (ie enhanced ridges or increased tropospheric intrusions). Instead the spread of results is quite varied and is based on each particular case.

6.4 TIGGE ensemble study

The streamer feature error technique will now be applied to a single case study by analysing ensemble forecast data. There are two main sources of error in numerical weather prediction: 1) initial condition uncertainties (due to a deficiency in the information available or poor meteorological observation coverage); and 2) model errors (due to approximations in physical processes). Perturbing each member by simulating alternative (yet similar) initial conditions, as well as using stochastic physics schemes addresses both initial condition and model errors within the ensemble prediction system. Ensemble systems enable probabilities to be calculated for weather events, which enhances the forecast.(Buizza, 2006).

The Observing System Research and Predictability Experiment (THORPEX) Interactive Grand Global Ensemble (TIGGE) was initiated in 2005 (Richardson et al., 2005) and consists of 10 operational weather forecasting centres. These include the Australian Bureau of Meteorology (BoM), Chinese Meteorological Agency (CMA), Canadian Meteorological Centre (CMC), the Brazilian Centre for Weather Prediction and Climate Studies (Centro de Previsao de Tempo e Estudos Climticos, CPTEC), the European Centre for Medium-Range Weather Forecasts (ECMWF), the Japan Meteorological Agency (JMA), the Korean Meteorological Administration (KMA), the United States National Centers for Environmental Prediction (NCEP), the Met Office (UKMO), and Meteo-France (not used in this study due to its lack of long-range forecasts). Figure C.1 in Appendix C shows a table from Froude (2010) that details the main differences between the ensemble models at the various forecast centres (including horizontal resolution, number of levels and members, initial perturbation techniques and data assimilation). By utilising the TIGGE ensemble data not only can an examination of the forecast and analysis streamers be undertaken but also a multi-model intercomparison can be conducted.

6.4.1 Data and methodology

The TIGGE data for nine ensemble prediction systems, as detailed above, are used throughout the investigation. Forecast lead times of 24, 48, 72, 96, 120, 144 and 168 hours are studied. The TIGGE data is stored on limited pressure levels (200, 250, 300 and 500 hPa) so vertically averaged upper-level PV (UPV) is calculated as described in Wiegand et al. (2011). The PV streamers are then extracted using the same technique as for the deterministic model (see Section 6.2) with the exception that the 1.5PVU contour line is used (as lower absolute values

of PV are produced with the UPV). The forecast PV streamers are then matched and compared to the ECMWF analysis data (using the same method described in Section 6.2). Table 6.1 illustrates the number of members in each lead time that do not have matching streamers due to cutoffs, larger troughs or dissimilar stratospheric development. The distribution between these three types within the centres will be discussed later, however, centres with more members (ECMWF and JMA) tend to have more spread and hence increased numbers of non-matches. In general, more cases of non-matched PV streamers occur once the 120-h forecast time is reached. A comparison of the forecast precipitation on the same day as the assessed streamer (26/05/2008) is also examined in this study and verification data is from the ENSEMBLES E-OBS dataset (Haylock et al., 2008). All fields are interpolated onto 1°x1° grids.

TABLE 6.1: Numbers of EPS members that do not match the analysed PV streamer.

Model	Members	24 h	48 h	72 h	96 h	120 h	144 h	168 h
BoM	32	0	0	0	0	12	1	2
CMA	14	0	0	0	3	3	2	3
CMC	20	1	7	7	5	7	10	12
CPTEC	14	0	0	0	0	0	1	0
ECMWF	50	5	10	5	7	4	4	22
JMA	50	0	7	2	8	14	10	12
KMA	16	0	0	6	5	5	2	4
NCEP	20	0	0	6	4	6	5	9
UKMO	23	0	1	2	2	10	8	6

6.4.2 Case study overview

This study focuses on a PV streamer that formed over the UK and western Europe on the 26th of May 2008 and extended down to northern Africa. The synoptic situation leading up to the creation of the streamer is illustrated in Figure 6.8. The streamer was produced by an upper level disturbance that began on the 20th of May, initiating in the North Atlantic. On the 21st of May (Figure 6.8a) an injection of high PV stratospheric air, which later formed the PV streamer on the 26th, travelled from an upper level trough (positioned at $50°$N, $65°$W) and moved toward the Mediterranean Sea. Over the next few days (Figure 6.8b-d) an enhanced ridge formed over the North Atlantic, associated with a high pressure system. On the 25th (Figure 6.8e) the trough, positioned at $45°$N, $10°$W, began to elongate resulting in a PV streamer on the 26th (Figure 6.8f). A low-pressure system at the surface was found directly to the east of the streamer tip and several high-impact weather events occurred.

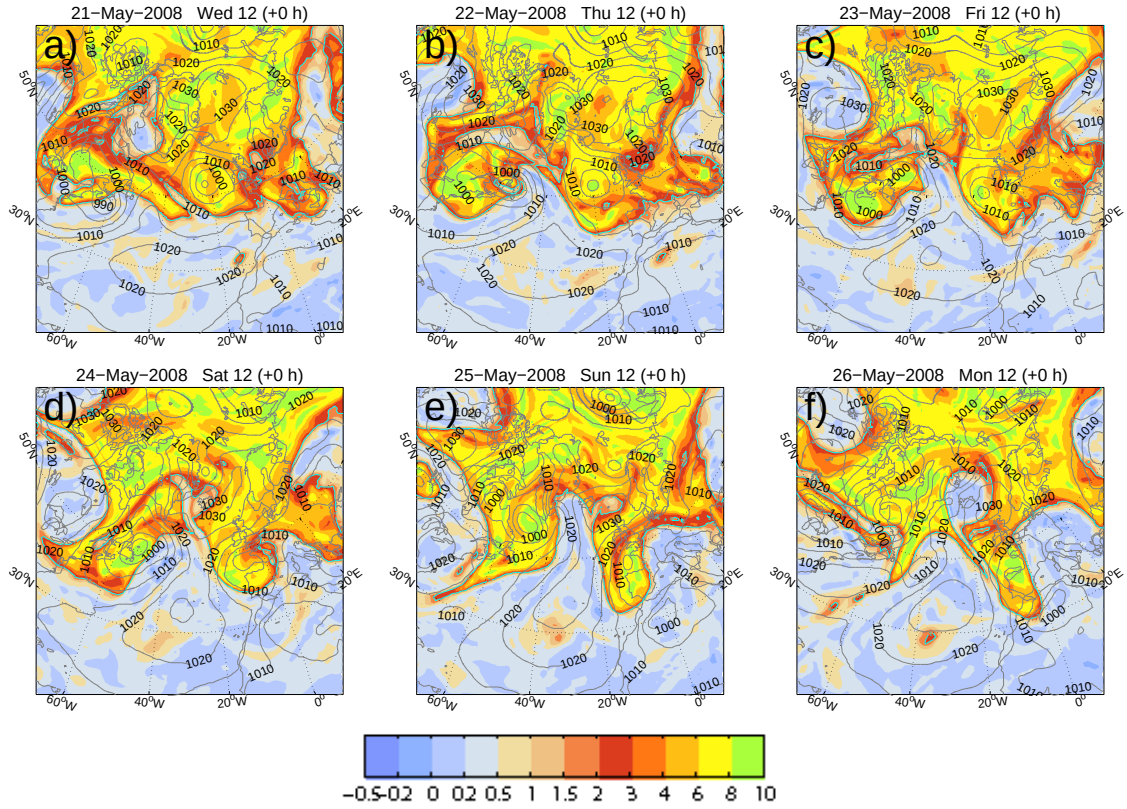

FIGURE 6.8: Synoptic situation occurring from the 21-26 of May 2008 12UTC. PV (colour contours) in PVU and SLP (grey line contours) in hPa are shown.

Strong winds in the northern Sahara caused dust mobilization and transport across the Mediterranean Sea into central Europe leading to a significant dust event in Germany (Klein et al., 2010). Several flooding events within Europe also occurred during this time period. Heavy precipitation began on the 23rd of May and the saturated soil received more precipitation from the 26th through to the 28th of May. Recorded daily accumulations of over 100mm were observed in southern Switzerland and northern Italy (Murcia et al., 2008). The rapid influx of precipitation resulted in runoff and flooding on the Alpine south side of Switzerland and Italy.

6.4.3 PV streamer structural differences

Differences between matched PV streamers within the forecasts and ECMWF analysis will now be investigated. Figure 6.9 shows the location error for the nine TIGGE centres with each lead time represented by a surrounding ellipsoidal envelope. The center of the ellipse is the mean over all matched ensemble members and the orientation of the main axis is determined by linear regression. The length of this axis is calculated, so that the ellipse encompasses either

90% of the forecast streamer center points, or the point with the maximum distance away from the ECMWF analysed center is reached (which ever occurs first). In this way, the ellipses are sensitive to outliers in order to represent the range of forecasts. The standard deviation of the distance between the forecast PV streamer center points and the center point of the ECMWF analysis PV streamer gives the ratio of the major to the minor axis.

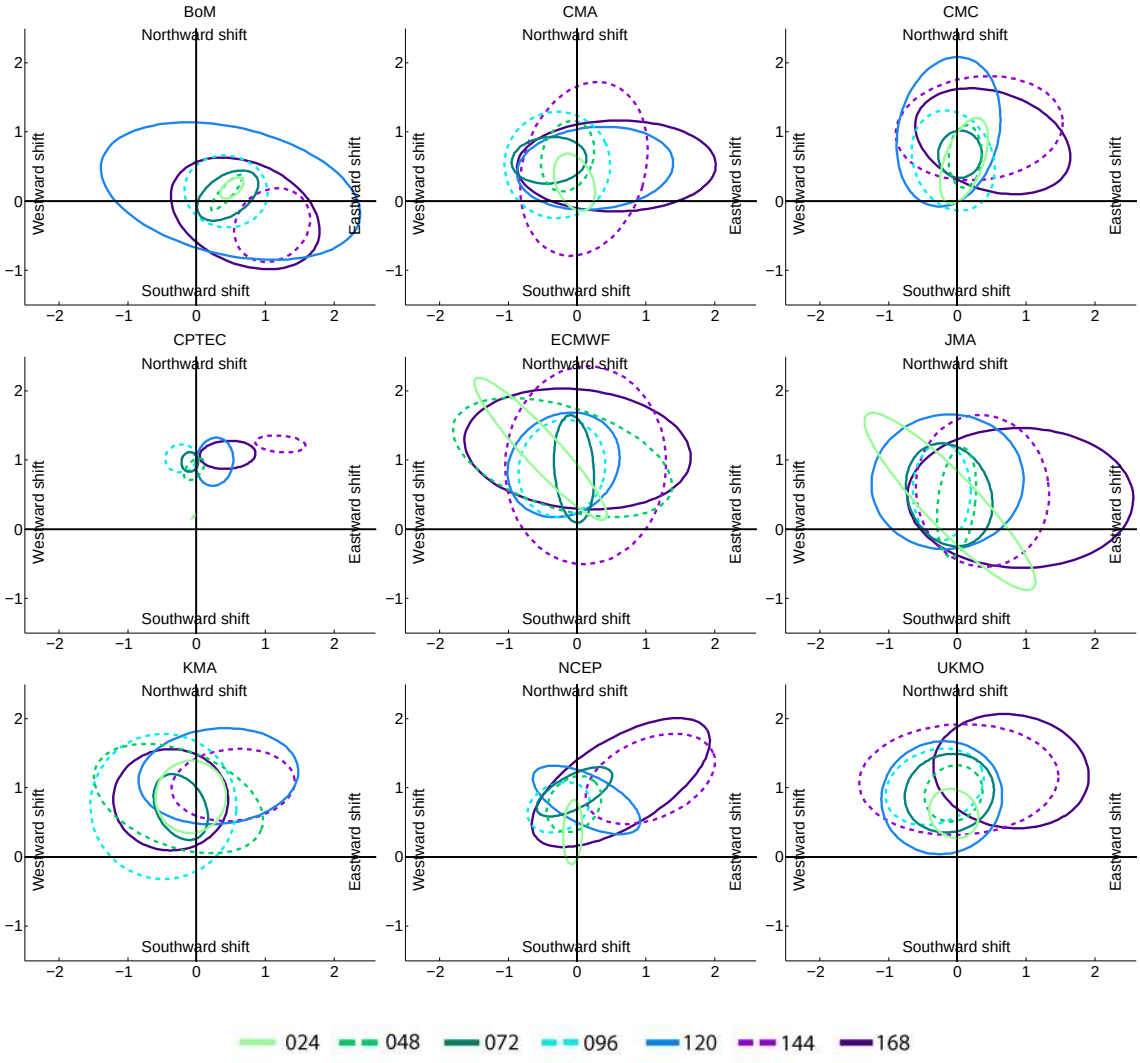

FIGURE 6.9: Position error (in 1000km) of the streamer ensemble forecasts based on UPV from nine TIGGE forecast centres. Ellipses surround the position of forecasts members (see text for details) at 1200 UTC 26 May 2008. Coloured dashed and solid lines indicate lead time ranging from 24 to 168 hours (see legend). Center of the coordinate system is the PV streamer position as analysed by ECMWF in all panels.

Figure 6.9 illustrates the differences in the positions of the forecast streamers from the analysis streamer (situated at 0,0) and demonstrates the dispersive nature of each model over the increasing lead times. Smaller ellipsis show smaller spread of forecast streamer position errors

while wider ellipsis show larger errors and wider dispersion of results. The results indicate a small spread for all centres at shorter lead times (green colours) and a slight northward shift of the forecast PV streamers. The spread does not increase substantially over the first four forecasting days while larger spreads are found from the 120-h forecasts onwards (dark blue and purple ellipse colours) for all models. This coincides with the increase in the number of non-matched streamers in the 120, 144, and 168-h forecasts (as shown in Table 6.1). The non-matched members are due to 1) cutoffs; 2) wider stratospheric troughs which do not fulfil the PV streamer definition; or 3) no stratospheric disturbance in the region. The third type of member applies in half of the cases for the 144 and 168-h non-matches for CMA, CMC, and NCEP, and in one third of the cases for UKMO. The BoM non-matched members all fall into the first group and the lack of spread in the CPTEC model (Figure 6.9 coincides with few non-matched cases. As lead times decrease from 96 to 24-h, most of the members belong to group 1 and the position and size of the cutoffs get closer to that of the streamer. This is also the case for the JMA, KMA, and ECMWF models. The five non-matched members in the 24-h forecast for ECMWF coincide with cutoffs that are very similar in size and structure to the analysed PV streamer, with only a thin gap to the main body of stratospheric air (illustrated in Figure 6.11). These cut-off features create a narrow diagonal ellipse in the 24-h ECMWF and JMA models (Figure 6.9 light green solid line). The JMA, KMA, and ECMWF models all show a much wider range of ensemble spread throughout all lead times than the other centres. The structure of the stratosphere-troposphere interface often differs completely from that in the analysis for the 144 and 168-h forecasts for JMA and ECMWF. The 168-h forecast ellipsis are also largest for these two regions, indicating that there is increased dispersion in these models.

The elongation and width differences in the PV streamers are displayed in Figure 6.10. Each figure shows the nine TIGGE ensemble members, as well as each of the seven forecast lead times. The boxes represent the upper and lower quartile with the median (highlighted as a black line as well as a notch), minimum and maximum (upper and lower whiskers). The length of forecast PV streamers (based on the line between the southernmost and northernmost points) tend to be shorter than the analysis for most of the lead times and do not capture the extent of the southward penetration of the streamer (Figure 6.10 upper). Shorter lead times (24, 48 and 72-h) have lower spread especially in BoM, CPTEC, and NCEP and are often slightly longer than the analysis. Many of the ensembles capture the length of the streamers well in the 24-h forecast time, ECMWF, CMC, JMA and KMA have the median very near to the zero line (for JMA this continues to the 72-h forecast). Notably the ECMWF and CMA ensembles

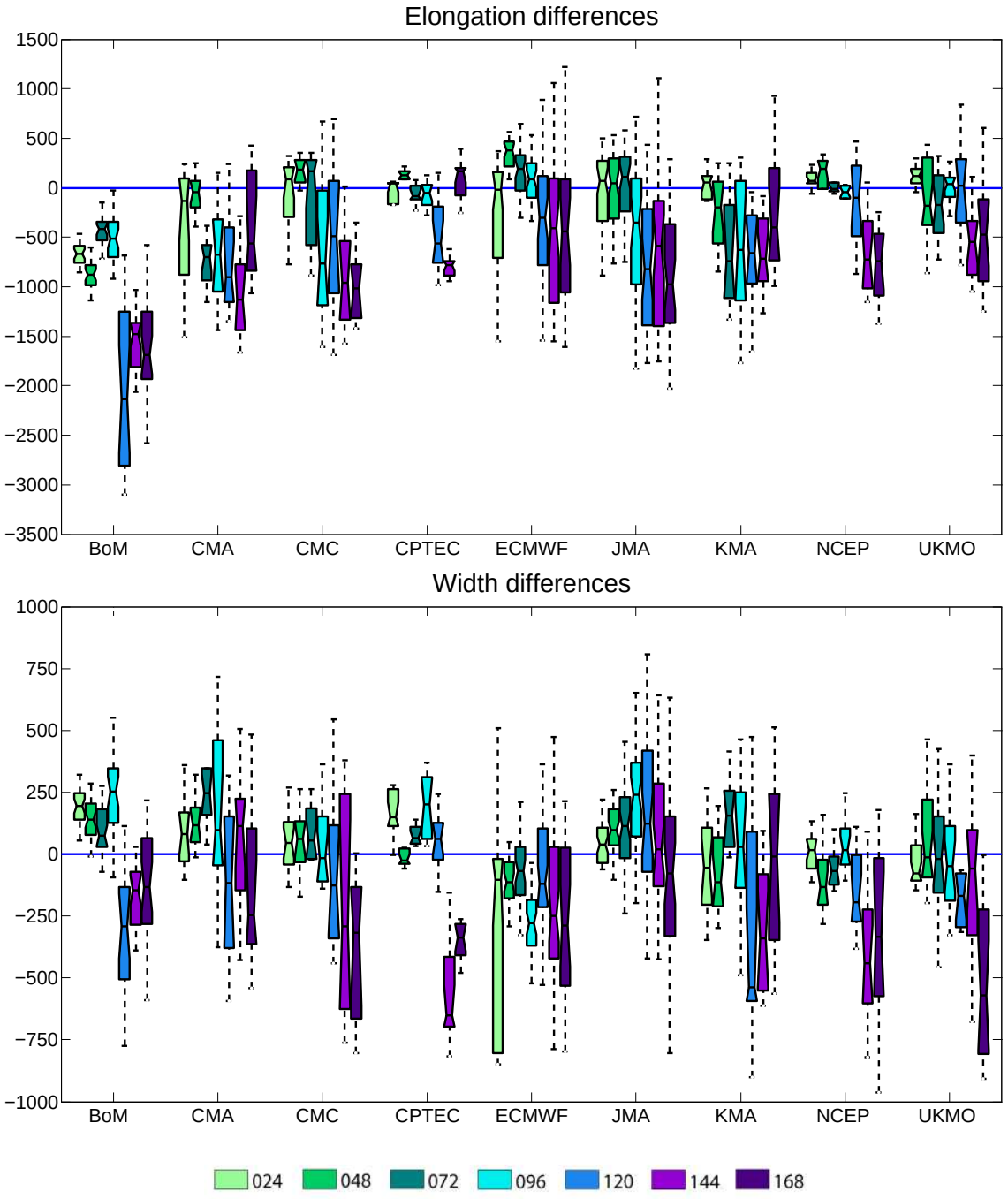

FIGURE 6.10: Length errors (upper) based on line of elongation between southernmost and northernmost points and width errors (lower) in km. Nine TIGGE forecast centres are displayed ranging from 24 to 168 hours (see legend). Box-and-whisker plots show the lower and upper quartiles (coloured portion) with a black line (as well as notch) indicating the median, and dashed lines for the minimum and maximum. The blue line highlights the comparison to the ECMWF analysis, and negative (positive) values demonstrate shorter/narrower (longer/wider) forecast PV streamers.

are up to 750km shorter (as well as 750km narrower for ECMWF) in the 24-h forecasts. These cases are similar to the 5 unmatched ECMWF 24-h cases in that a cutoff is situated in place of the streamer. The shorter and narrower PV streamers are identified as the small portion of stratospheric air which almost attaches to the cutoff (shown in Figure 6.11).

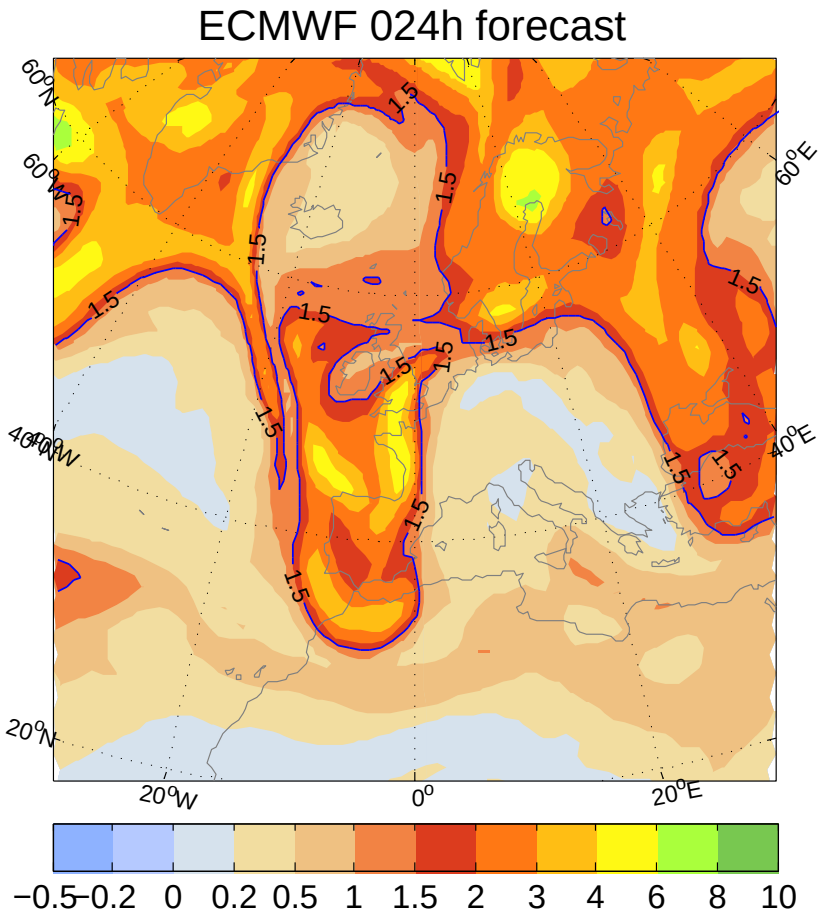

FIGURE 6.11: 24 hour forecast from an ECMWF ensemble member (in UPV). Blue line represents 1.5UPV contour, which is used to identify streamers.

NCEP, BoM and CPTEC all have low ensemble spread up to 96-h, however they have low length error and capture the feature well up through this time. The UKMO and NCEP have overall the best performance up to the 120-h lead time. Once the 120-h forecast time is reached there is a noticeable increase in spread in most centres. This coincides with the spread of PV streamer positions widening at this lead time (Figure 6.9). A similar scenario is observed for the widths of the streamers (Figure 6.10 lower). The forecast streamer widths are slightly wider in earlier lead times (24 to 96-h) with spread increasing at 120-h and average streamer width decreasing until the 168-h lead time. The interrelation of width and length illustrates that shorter and narrower PV streamers are predicted at longer lead times. This streamer type

combined with the northward shift in most models suggests that the amplitude of the Rossby wave is too small and/or the RWB too weak.

6.4.4 PV amplitude differences

Examining the UPV amplitude within the PV streamers reveals similar results to the deterministic forecasts. The forecast streamers again tend to have lower PV amplitudes in the maximum (Figure 6.12) and mean values (not shown). Typical differences range from -0.25 to -0.5PVU for short lead times and increase to -0.75 to -1.5PVU for later forecast times. The UKMO has the best performance regarding UPV amplitude (until the 168-h lead time) as most forecast times have a reasonable spread and the ensemble mean falls near the observed PV in the ECMWF analysis. In general, most of the centres have only small differences in the maximum and mean with the largest aberrations found in the later forecast times. The main exception to this is found in the ECMWF ensemble during the 24-h time. Much lower values are displayed, again caused by the thin northward placed stratospheric air situated above the main cutoff (see Figure 6.11). The analysis streamer in this case held a pocket of high-PV stratospheric air on its eastern flank (shown in Figure 6.8f). As the forecast streamers tend to be shorter and narrower (especially with increasing lead time) the influx of high-PV stratospheric air is also reduced. This may play a part in the lower forecast values.

6.4.5 Precipitation forecasts: May 26th

An analysis for the heavy rainfall on the 26th of May (0600 UTC 26 to 0600 UTC 27 May) has been carried out. A box from $43 - 46°$N and $3 - 7°$E was defined where the maximum precipitation over the 24 hours occurred (see Figure 6.13). Box-and-whisker plots are used to show the predicted precipitation with median and spread from every EPS as well as the observed 24 hour sum of precipitation of 11.82mm as a blue line (Figure 6.14). The observed value is much smaller than the 100mm mentioned in Section 6.4.2 due to the area averaging in the gridded ENSEMBLES data (see details in Haylock et al. (2008)). KMA had to be excluded in this analysis, as it does not provide precipitation data.

The 24-h lead times predict the mean rainfall amount well for the BoM, ECMWF, JMA and NCEP ensemble systems. The UKMO under-predicts precipitation in the 24-h forecast as does

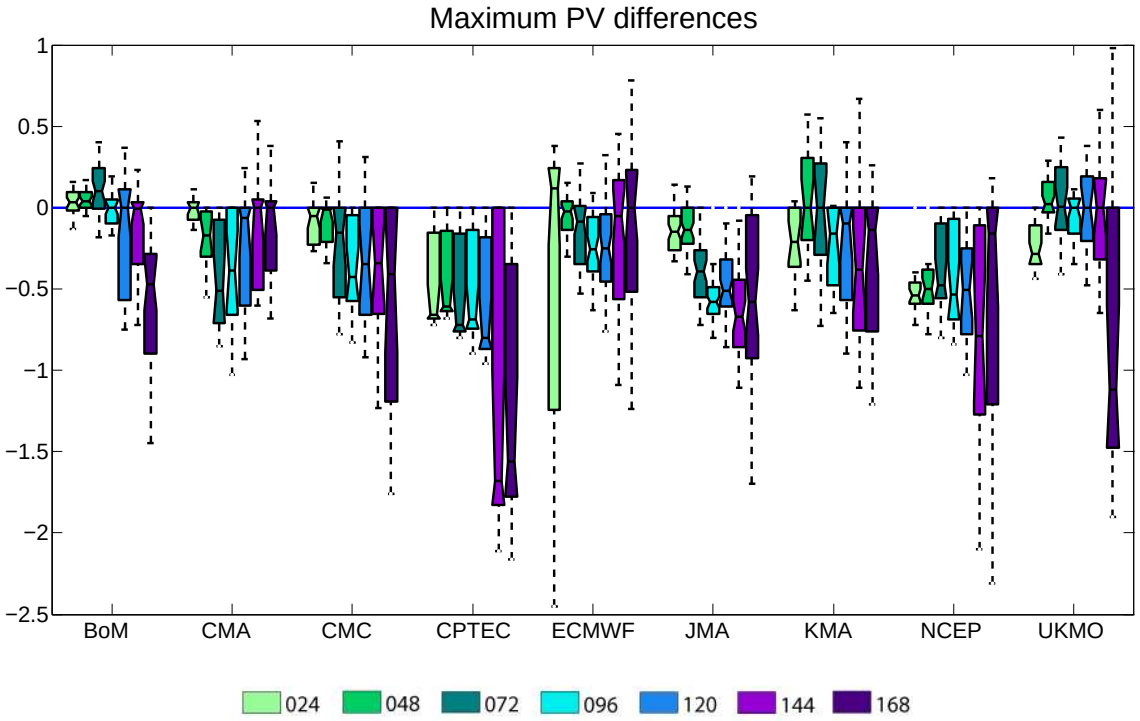

FIGURE 6.12: Same as Figure 6.10 but for PV maximum (95% quantile) errors (in UPV) from nine TIGGE forecast centres. Coloured boxplots show lead times ranging from 24 to 168 hours (see legend).

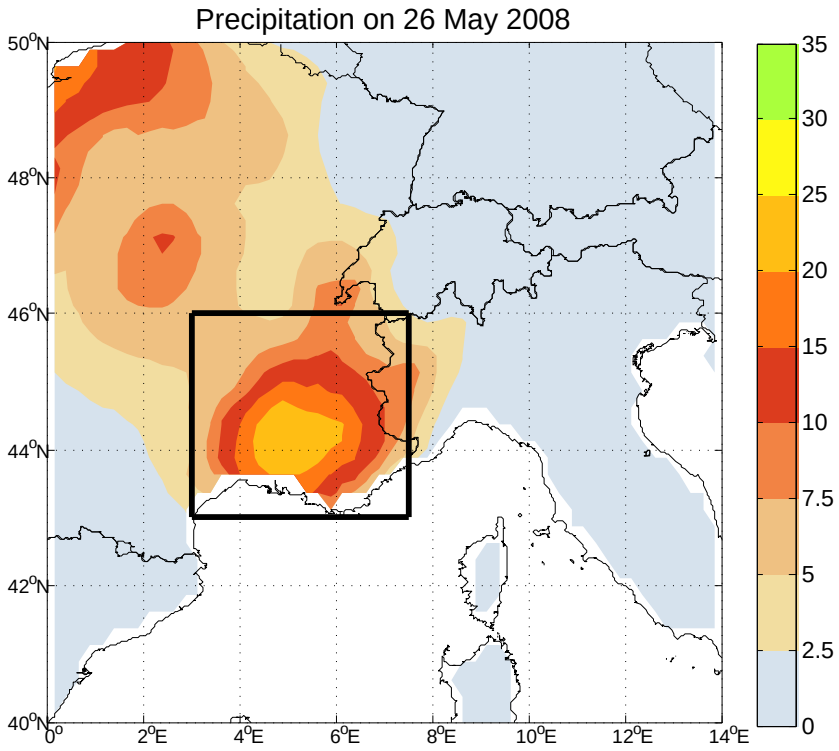

FIGURE 6.13: Observed precipitation on 26/05/2008. Black rectangle ($43 - 46$°N and $3 - 7$°E) shows the area used for the investigation of precipitation forecast performance.

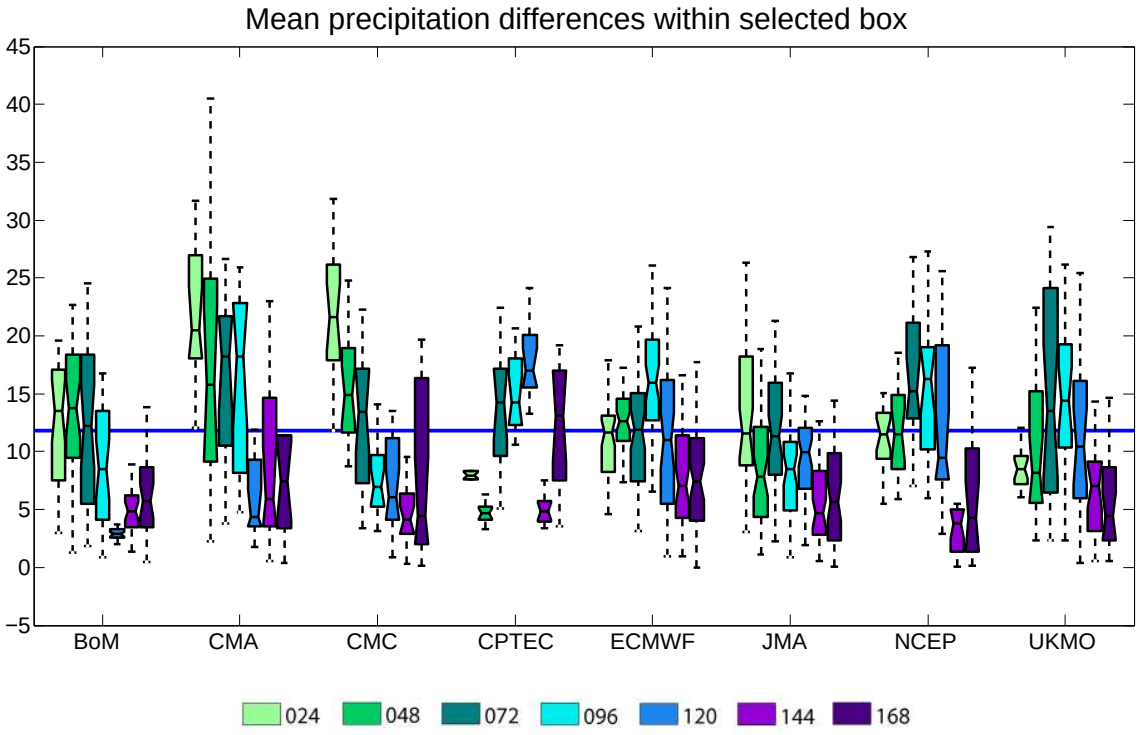

FIGURE 6.14: Same as Figure 6.10 but for mean precipitation within box ($43-46$°N and $3-7$°E). Blue line illustrates observed mean precipitation.

CPTEC and both of these centres display low spread at this forecast time. CPTEC also has low spread in the 48 and 144-h forecasts, similar to the low spread observed in the streamer feature errors. CMA and CMC resemble each other with over-prediction of the rainfall at earlier lead times and under-prediction of rainfall with increasing forecast length. Similarly, JMA shows decreasing rainfall predictions with lead time, however, the 24 and 72-h forecasts have good skill with the mean of the ensemble close to the observed rainfall.

Interestingly, ECMWF, NCEP, and UKMO have higher rainfall predictions in middle range forecasts (72 to 96-h) with a drop in accuracy once the 144-h forecast is reached. BoM also has skillful rainfall predictions with large spread until the 120-h forecast. At this point the spread and skill drop dramatically, this coincides with the increased PV feature errors around 120-h. Overall ECMWF has the best skill at predicting the rainfall with four of the forecast times (24, 48, 72 and 120-h) close to the observed mean and the lowest decrease in skill at longer lead times (144 and 168-h). Similarly, exceptionally good predictability of heavy precipitation events on the Alpine south side in general was shown in Jenkner et al. (2008) for the mesoscale model COSMO.

6.4.6 PV streamer and precipitation error relationships

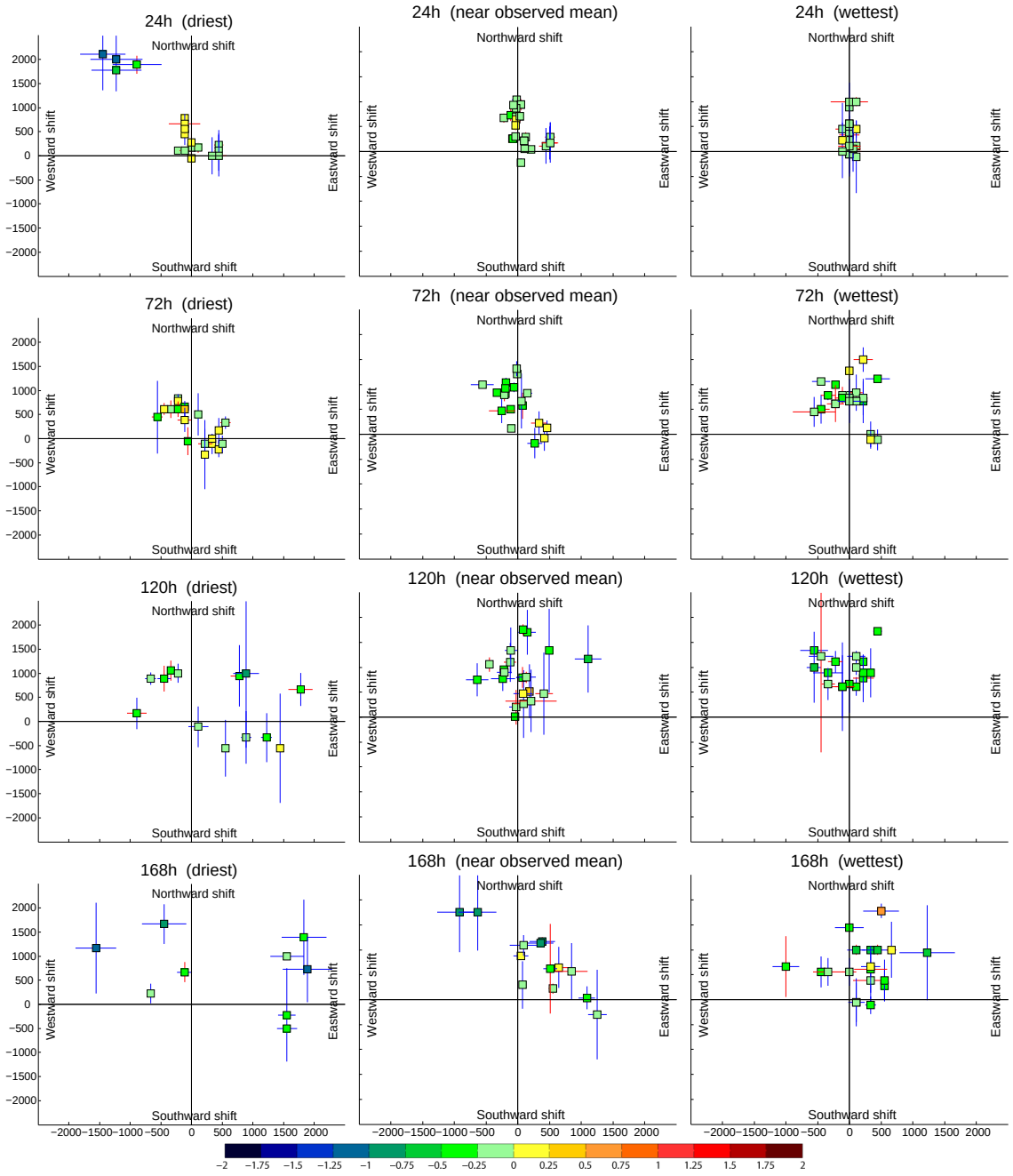

FIGURE 6.15: Difference of forecast in relation to analysis streamer in 24, 72, 120 and 168-h lead times for all nine TIGGE ensemble systems. Each square represents a PV streamer with forecasted precipitation in driest (left) near observed mean ($+/-1$mm) (middle) and wettest (right) members. Differences in elongation (vertical lines) and width (horizontal lines) are displayed, red shows positive values (wider or longer streamers) while blue indicates negative changes (shorter or narrower). Colour of square illustrates mean UPV difference.

Relating the skill in the precipitation and PV streamer forecasts is accomplished by analysing the streamer features during precipitation forecasts which occur close to the mean ($+/-1$mm),

as well as for the wettest (90% quantile) and driest (10% quantile) members. All of the individual centres members are combined in order to identify the low and high quantiles and extract the associated PV streamer information. Figure 6.15 shows the PV streamers related to the driest (left), wettest (right) and observed mean (middle) precipitation forecasts. The structural differences such as elongation (vertical lines - red indicate longer and blue shorter) and width (horizontal lines - red indicate wider and blue narrower), as well as the shift in relation to the analysed streamer is shown. The difference in mean UPV is also displayed as the colour within each square. The streamer features and placement of all the PV streamers from all TIGGE members can be viewed in Figure C.2 in Appendix C for comparison.

The 24 hour forecasts (Figure 6.15 - top) show that the position of the PV streamers occurring during skilled precipitation forecasts (middle) are near to or slightly northward of the analysis streamer. These also have very small elongation and width differences (except for a small cluster to the east). Similarly, the over-predicted and under-predicted (right and left) precipitation forecasts have streamers which occur in a similar location to the analysis (the driest forecasts have some members associated with the cutoff/small stratospheric tendril of air to the north-west observed in 24-h forecasts). The streamers coinciding with the wettest forecasts have larger elongation and width differences than the near-mean streamers, but are shifted the least. This could indicate that the streamer is extending further toward the surface rather than to the south, producing increased ascent to the east and causing more precipitation to fall.

Except for the north-west streamers, the driest category is associated with streamers that have higher mean UPV. The differences in PV could affect the forecast by creating a shift in the precipitation pattern (in a similar manner as described by (Fehlmann and Davies, 1999)) moving the rainfall out of the analysed box. This trend continues through to the 72-h forecasts where the driest group again has a tendency towards higher mean UPV. The placement of the streamers at this forecast time begin to spread outward from the centre and are usually found just north (in all groups) or to the south-east (mainly in the under-prediction group). Again the PV streamers linked to skilled precipitation forecasts have lower elongation and width differences.

As the lead time increases the spread of results also grows leading to a wider distribution. This happens earlier (in the 120-h forecasts) in the under-predicted cases. The wettest forecasts maintain a slightly northward position while the near-mean streamers exhibit the closest position to the analysis streamer (with some outliers). By the 168-h forecast time, the driest

cases occur either to the north-west or to the east, well ahead of the analysis streamer, and have the likely effect of shifting the precipitation out of the investigated box. Several cases in this time are also linked to unmatched members. The over-predicted precipitation cases have increased spread but maintain their position to the north and east (with only a few outliers), while the skillful precipitation forecasts have streamers with a mainly eastward shift. The limit of predictability has probably been reached by this point (as observed by the much larger spread of streamer feature errors). The skilled forecasts could be attributable to influences from other conditions (e.g. moisture influx into the region). In all of the forecast times the wettest and near-mean cases are more similar than the driest precipitation cases.

6.5 Conclusions

The forecasts of streamers within the ECMWF deterministic model at early lead times capture the location and the structure of the PV streamers well (with low angle, width, elongation and PV differences in the 6 and 30 hour forecasts). These results are in agreement with previous work by Pelly and Hoskins (2003), Dirren et al. (2003) and Grazzini (2007). As the lead time progresses the forecasts become less like their analysis counterparts with the position, width and elongation differing by values up to $+/-1500$km ($+/-375$km for width). There is a slight tendency towards longer as well as wider streamers in later times. These are mainly distributed between either shorter and wider streamers or longer and narrower with only one quarter of cases that are larger in width as well as length. The maximum (95% quantile) PV differences have a distinct tendency towards being lower than analysis values by an average of 1PVU (with differences as much as -3.5PVU). These anomalies are predominantly located in quadrant 2 (the upper right hand portion) of the streamer but are also observed in quadrant 3 and 4 (the lower half of the streamer). The PV streamer feature errors in later forecast times do not demonstrate a specific trend in angle differences or directional shift other than those attributable to increased variability with lead time.

The TIGGE EPS study revealed some similar features to the deterministic model analysis. An increase of forecast errors were found with longer lead times as well as a similar trend towards lower PV values in forecast PV streamers. This case dealt with an elongated PV streamer with deep southward penetration into northern Africa. Early lead times (24, 48, and 72-h) forecasts show small variations in width, elongation and position compared to the analysis and

generally the PV streamer feature is captured well up until this point. ECMWF displays some discrepancies in the 24-h forecasts where the intrusion was not attached to the main body of stratospheric air creating thin, low PV, north-eastward placed streamers. There was an abrupt shift in errors and PV streamer placement after the 96-h forecast onward indicating a limit of predictability at this time. The northward shift in position errors as well as the shorter streamers predicted at longer lead times (96 hours onward) indicate that models did not sufficiently capture the intensity of the wave breaking. This resulted in a curtailment in the southern meridional extent of the forecasted PV streamer. A complimentary RMSE error study based on upper-level PV and including ensemble spread calculations was performed by Wiegand et al. (2011) for this streamer case. Results concluded that using the individual centres' own analysis rather than that of the ECMWF decreased the RMSE for all models and that there was a tendency for under-dispersive behaviour in many of the model systems. Limited predictability was also found within the upstream ridge as well as areas of large PV gradients along the midlatitude jet.

The forecasted precipitation assessment shows some variations in model skill at predicting the rainfall on the 26th. Many of the models show a good level of spread and skill up until the 96-h lead time; there is then a decrease in spread and a distinct drop in skill in later forecast times (120-h onwards). The streamers associated with the near-mean forecast members show a slight northward placement but small variation in elongation and width, especially for earlier times. Spread of placement and feature errors increase with lead time, however the PV streamers still maintain similarities with the analysis streamer. A comparison with under and over-predicted rainfall reveals that streamers associated with higher rainfall amounts are more similar to the analysis as well as the skillful precipitation members. The evidence suggests that the position and structural features of the PV streamer within the model has an effect on the quality of the forecasted precipitation. This corroborates previous studies by Fehlmann and Quadri (2000), Gheusi and Davies (2004) and Schlemmer et al. (2010).

Chapter 7

Conclusions

The linkage of PV streamers to high-impact weather in the UK, their initiation and their predictability within current weather models has been investigated. In this chapter a summary of the main findings is presented along with suggestions for further research required.

7.1 Summary of main findings

The United Kingdom was highlighted as an area of interest for investigating Rossby wave breaking and PV streamer formation. Its position on the eastern side of the Atlantic Ocean means that it is highly influenced by the midlatitude jet stream associated with synoptic-scale weather systems. It is surrounded by climatological hotspots of cyclones (low-pressure systems near Iceland), anticyclones (high-pressure systems in the Atlantic to the west of Europe and northern Africa) (Wernli and Schwierz, 2006) as well as stratospheric and tropospheric PV streamers (each with clusters positioned over or to the west of the UK and Europe) (Martius et al., 2006b). This unique situation, along with the fact that ocean basins are generally linked to limited predictability in Rossby wave amplification and breaking (Harr and Dea, 2009; Anwender et al., 2008), made it an ideal location for investigations into the role of PV streamers in heavy precipitation high-impact weather events. The primary results are detailed below with reference to the questions posed in Section 1.3.

1. What are the main synoptic influences on heavy precipitation in different parts of the UK?

a) Autumn is characterised by stratospheric intrusions to the west (85%) in combination with cyclones to the north-west of the UK.

b) Winter is dominated by cyclones to the north west, while anticyclones over northern Africa or central Europe (in northern regions) help to steer the systems further northward.

c) Spring has an east/west split with stratospheric combined with tropospheric streamers in eastern regions and cyclones paired with anticyclones in western regions. Larger troughs are also found on non-streamer days in western regions.

d) Summer has the fewest cyclones (especially in southern regions) and the highest frequency of stratospheric streamers (88%). Anticyclones are more frequent and can be found in their climatological position in the Atlantic. There are also anticyclones positioned over eastern Europe, which, combined with tropospheric streamers to the east, may be part of a blocking feature.

e) Regional differences indicate that Scotland is dominated by orographic influences. These influences work in conjunction with upper-level features in eastern Scotland, which has the longest Rossby wave trains and the most consistent frequency of stratospheric intrusions in all seasons. In northern Scotland upper-level features are reduced in the 99% cases.

2. What are the differences in heavy precipitation days with and without an overlying PV streamer?

a) Winds take on a westerly component during streamer days while non-streamer days have a tendency towards south-westerly winds with greater velocities.

b) Relative humidity peaks earlier on the days associated with PV streamers. Ascent to the east of the streamer lowers surface level moisture saturation while this remains higher for longer on non-streamer days. This indicates that the upper-level forcing is enhanced on days with a PV streamer.

3. Is there an archetypal stratospheric PV streamer that occurs on the heavy precipitation days?

a) Stratospheric streamers are primarily split between LC1 and LC2 classifications (see Section 2.4.1 for an explanation). The higher isentropic levels in the winter lead to

the emergence of more LC1-type streamers, while increased zonal wind contributes to more LC2 PV streamers in autumn.

b) The PV streamer feature investigation has uncovered a wide distribution of sizes and types. The non-uniformity of the features as well as regional differences raises issues related to their ultimate predictability.

The genesis of preceding Rossby waves and the resultant PV streamers were also investigated with the following major results:

1. Where are the main trigger localities to precursor Rossby waves?

   a) In autumn, triggers span from the Pacific through the North American continent to the Atlantic Ocean coast.

   b) In winter and spring, longer living wave trains are initiated with clusters located within the Pacific Ocean basin (winter) and over the Midwest of the United States (spring).

   c) Summer has the widest latitudinal distribution with a cluster of triggers found on the Pacific Ocean and North American coastal region.

   d) Potential sources of the triggers based on the location and case study evidence include: interaction from breaking Rossby waves on other isentropes, exit regions of the Pacific jet, extra-tropical transition of tropical cyclones and diabatic heating, areas of frontogenesis and cyclogenesis as well as orographical influences.

2. Where do the dominant influences on PV streamer formation occur?

   a) The PV streamers related to the UK heavy precipitation cases are all initiated within the Atlantic Ocean basin.

   b) Seasonal differences include a wider spread of locations in autumn with a narrower distribution in the summer. Spring and winter both have a slightly southward placement (especially in winter where the streamers occur on lower isentropes).

   c) Amplification occurring downstream of the streamer coincides with LC2 classification and cyclonic wrapping while upstream initiation produces enhanced ridges and usually LC1 type streamers. The most common formation type is from upstream influences closely followed by recirculation of stratospheric air.

d) The adjoint sensitivity case study found that the upstream interaction of the extra-tropical cyclone with the wave guide had an influence on ridge enhancement and downstream PV streamer production for all three streamers analysed. The point at which the interaction occurred in the wave created larger or smaller quantities of vorticity and potential vorticity downstream and had an influence on the ultimate location of the PV streamer tip.

e) Localised influences within the immediate ridge and near the streamer tip also affected the extent and placement of the resultant streamer.

The predictive capabilities of NWP models in resolving the PV streamer features was outlined in Chapter 6 with the use of a novel feature error measure technique.

1. How well are PV streamers predicted in forecast models?

   a) ECMWF deterministic models capture the structure, location and angle of streamers well at 6 to 30 hour lead times.

   b) As forecast time increases so do the feature errors with elongation errors up to 1500km and width errors up to 750km by 126 hour lead times.

   c) PV amplitudes are usually lower in forecast streamers with differences in maximum values of as much as -3.5PVU.

   d) Similarly, the TIGGE EPS investigation showed fewer errors at shorter lead times (up to 72 hours) with increased differences at later forecast times. Maximum and mean PV amplitudes were also lower than the analysis (by up to -1.5PVU).

2. Do the errors in PV streamers have a relation to the heavy precipitation forecasts?

   a) Precipitation forecasts were near the observed mean for many of the TIGGE centres up to 72 hours. Most centres over-predicted rainfall at 96 hours and then under-predicted from the 120 hour forecast onward. ECMWF showed the best over-all precipitation forecast skill.

   b) Ensemble members that over-predicted rainfall or were close to the observed mean had fewer PV streamer feature errors than those that had under-predicted rainfall in early forecasts.

c) Longer lead times maintained this pattern but the spread of results widened with larger PV streamer errors observed in all the categories.

7.2 Relation to other work

Several studies have investigated PV streamers related to Alpine precipitation events (e.g. (Massacand et al., 1998; Fehlmann et al., 1999; Martius et al., 2006b; Grazzini, 2007; Hoinka and Davies, 2007)). Much of the work done in analysing the influence of streamers on extreme weather events in other locations has taken the form of individual case studies (e.g. (Krishnamurti et al., 2003), (Krichnak et al., 2004) and (Tripoli et al., 2005)). The seasonal and regional differences within the UK shown in this PhD thesis have highlighted some interesting variations in comparison to the study by Martius et al. (2006b). The percentage of heavy precipitation days in connection with a PV streamer is higher in this study than in the Alps in the summer and autumn. Also, typical PV streamer orientations have the tendency to be more cyclonic over the UK instead of meridional as they are on a majority of Alpine precipitation days. Due to the variations in topography, it is noteworthy that regions similar to the south side of the Alps (eastern Scotland) as well as flatter areas (central England) both had a significant link with these features (up to 95% of cases in the summer had an overlying streamer for CE). The dynamic forcing mechanism which enhances the precipitation therefore impacts frontal, orographic as well as convective events (reinforcing previous work by Schlemmer et al. (2010) that linked streamers with enhanced convection).

Vast regional differences within the UK itself were also found in flow structure and upper-level influence between northern and eastern Scotland in most seasons as well as eastern and western regions across the whole UK in the spring. These regional differences were also observed by Maraun et al. (2011) in a study investigating typical airflow patterns over the UK. However, the intense link to PV streamers especially in the autumn, summer and eastern regions in the spring has not been previously identified. When trying to define a "typical" PV streamer for the UK heavy precipitation days little evidence emerged of deviations to "average" PV streamers. Further investigation into each case revealed that the streamer types had large variations, so other influences such as moisture influx could help to determine whether or not a PV streamer leads to a heavy precipitation event (even though it may provide the dynamic forcing).

Investigating the precursor wave trains leading to the precipitation events also produced results that differed from the Alpine cases. For instance, the wave signals were greatly reduced in winter for the UK cases in comparison to the long wave trains observed in Alpine winter events by Martius et al. (2008). This can partly be explained by the inclusion of cases not linked with a PV streamer. Because of this, many events were included which had no wave train at all and were associated with strong zonal winds, as well as high and low pressure systems, leading to frontal precipitation. This eliminated any coherent wave signal, however, it also illustrated that wave packets are not always present as precursors to heavy precipitation in the UK winter season. On the contrary, signals from longer waves were visible in some regions in the spring and summer cases (in the 99% and 95% quantiles) than those found for the Alps by Martius et al. (2008). This means that in seasons where it is less typical to have long wave trains, when these are observed, there is an increased likelihood that heavy precipitation events will occur downstream.

The locations of the wave triggers displayed large variations with only a few small clusters noticeable in each season. These locations were in good agreement with previously identified initiation areas such as the Pacific Ocean basin (Chang and Yu, 1999; Danielson et al., 2004; Martius et al., 2008), and near orographic regions (Aebischer and Schär, 1998). Unfortunately, no main specific location of Rossby waves could be identified for waves which lead to heavy precipitation in the UK. Examining the local influences on wave breaking and streamer formation also produced results which corroborate current understanding. A climatological peak of PV streamer frequency stretches from the eastern Atlantic Ocean into Europe (Martius, 2005). Based on the westerly flow at upper-levels, it is therefore expected that most wave breaking occurs over the Atlantic Ocean (as found by this study in Section 5.3 as well as by Postel and Hitchman (1999), Wernli and Sprenger (2007) and Frhlich and Knippertz (2008)). The impacts of extra-tropical transition of tropical cyclones and the downstream influence on wave amplification and PV streamer formation (found in this study in Section 5.4 and previously by Harr and Dea (2009) and Anwender et al. (2008)) make the wave amplification in the Atlantic less predictable and so could also affect the predictability of downstream heavy precipitation events.

This was found to be the case in the TIGGE ensemble study where reduced wave amplification greatly affected the placement and size of a PV streamer. Overall the results of the novel feature-based assessment of the PV streamers are in agreement with Grazzini (2007) and

Dirren et al. (2003). The ECMWF deterministic and TIGGE ensemble systems had good skill in representing the features of the PV streamers at shorter forecast times (6 to 30 hours) with larger errors at increasing lead times. A new outcome of the study was the discovery that PV amplitude was typically lower in forecast streamers with maximum values as much as -3.5PVU lower. The main region where these differences occurred was in the upper right hand side of the PV streamer. This could mean that the PV gradient near the tropopause boundary on the eastern flank of the PV streamer is not captured correctly or that the influx of high-PV stratospheric air into the streamer is not sufficient in forecasts. Representing the PV field correctly is important as Rosting and Kristjansson (2008) found with their method of PV modification where small PV changes lead to significantly different cyclone forecasts in the North Atlantic.

The associated precipitation forecasts showed good skill at early lead times, which was also the outcome of a study by Jenkner et al. (2008) who investigated precipitation forecasts over the Alps. The PV streamers linked to the best precipitation forecasts (defined as closest to the observed mean within a selected area) also had the least structural differences to the analysis streamer. Forecast streamers with higher than analysed PV tended to produce much drier precipitation forecasts in the chosen area, so there may have been an associated shift in the placement of rainfall (determined by the interior PV amplitude as shown in Fehlmann and Davies (1999). The wettest forecasts also had similar attributes to the near-mean and analysis streamers. The position of these streamers seemed to be the dominant characteristic, with the likely effects including ascent of moist air and downstream rainfall. This leads to the conclusion that correctly forecasting the structure and PV amplitude within the streamer is important in order to interact correctly with the local and meso-scale influences and produce reliable forecasts of heavy precipitation.

7.3 Implications

Seasonal and regional differences in the structure of the upper-level influences on heavy precipitation in the UK were explored. The variability within the results for the nine regions highlights potential difficulties for forecasting these events. The preceding Rossby waves do not have a uniform trigger or wave train with only a few regions and seasons demonstrating a clear representative signal. Trigger locations emanate from the Pacific Ocean, over the continental

United States, and Atlantic Ocean coast but each case develops differently so that one specific cause has not been identified. With the long distance to travel and the potential for multiple factors to influence the wave between the trigger and the heavy precipitation event, identifying more localised influences is also important. The ambient setting for the PV streamer events was identified within the Atlantic Ocean basin, however, the spread of results again was rather broad.

In spite of these potential uncertainties both the ECMWF deterministic model and TIGGE ensemble prediction systems resolved the PV streamers well with similar positioning, length, width and angle at short lead times (6 to 30 hours). As lead times increased, the range of errors also widened with a limit of predictability evident around 96 hours for the TIGGE case study. Precipitation was also resolved well and members who captured the observed mean had fewer streamer feature errors. This demonstrates a clear link with improved prediction of heavy precipitation events when PV streamers are correctly forecast.

7.4 Further research

Additional questions were raised during this study which would benefit from further investigation. There is a link between heavy precipitation events in the UK and stratospheric streamers especially in the summer and autumn months (88% and 85% of cases have an associated streamer, respectively). A typical orientation of the PV streamer in autumn and summer (except for eastern regions) on UK heavy precipitation days is a NW-SE alignment with cyclonic wrapping. Blackburn et al. (2008) carried out 3 case studies for flooding events in the UK, which linked upper-level cyclonically breaking PV anomalies with persistent rain in the summer due to static or blocked Rossby waves. The slow movement of the trough, streamer or cut-off promotes the instability of the atmosphere for longer, which can lead to higher accumulation of precipitation in the same region and hence flooding events. Downstream blocking has also been linked to cyclonically breaking Rossby waves as well as streamers to the south west of these features (Altenhoff et al., 2008). Evidence from the UK heavy precipitation study reveals possible blocking features in the summer season. Further studies into the role of downstream blocking for sustained heavy precipitation and flooding within the UK would be beneficial.

Also, as not all PV streamers are linked with heavy precipitation events, a more detailed investigation into the moisture sources and how they interact with the streamers to the west of the UK would be useful.

There are open questions regarding Rossby wave breaking and the initiation and formation of PV streamers in the Atlantic. The main source of error within the TIGGE streamer study was found in the diabatic ridge amplification through latent heating leading to shorter and less intense PV streamers. Identifying the sources of PV streamer formation in the Atlantic as well as further study on the interaction between extra-tropical cyclones and Rossby wave amplification could improve predictability of these features in the future.

PV amplitudes were also highlighted as problematic areas within forecasts. When assessing the capabilities of models in representing PV streamer features (Dirren et al., 2003) found the largest error growth occurred in areas with the highest PV gradients (near the jet stream). Examining the interior PV of the forecast streamers illustrated that maximum values were generally lower than in the analysis. Further study related to the cause of these errors would be beneficial. It would also be interesting to discover whether or not these errors impact the predictability of downstream upper-level activity.

Appendix A

UK heavy precipitation linked to upper level features

A.1 Frequency plots for 95% and 90% quantile days

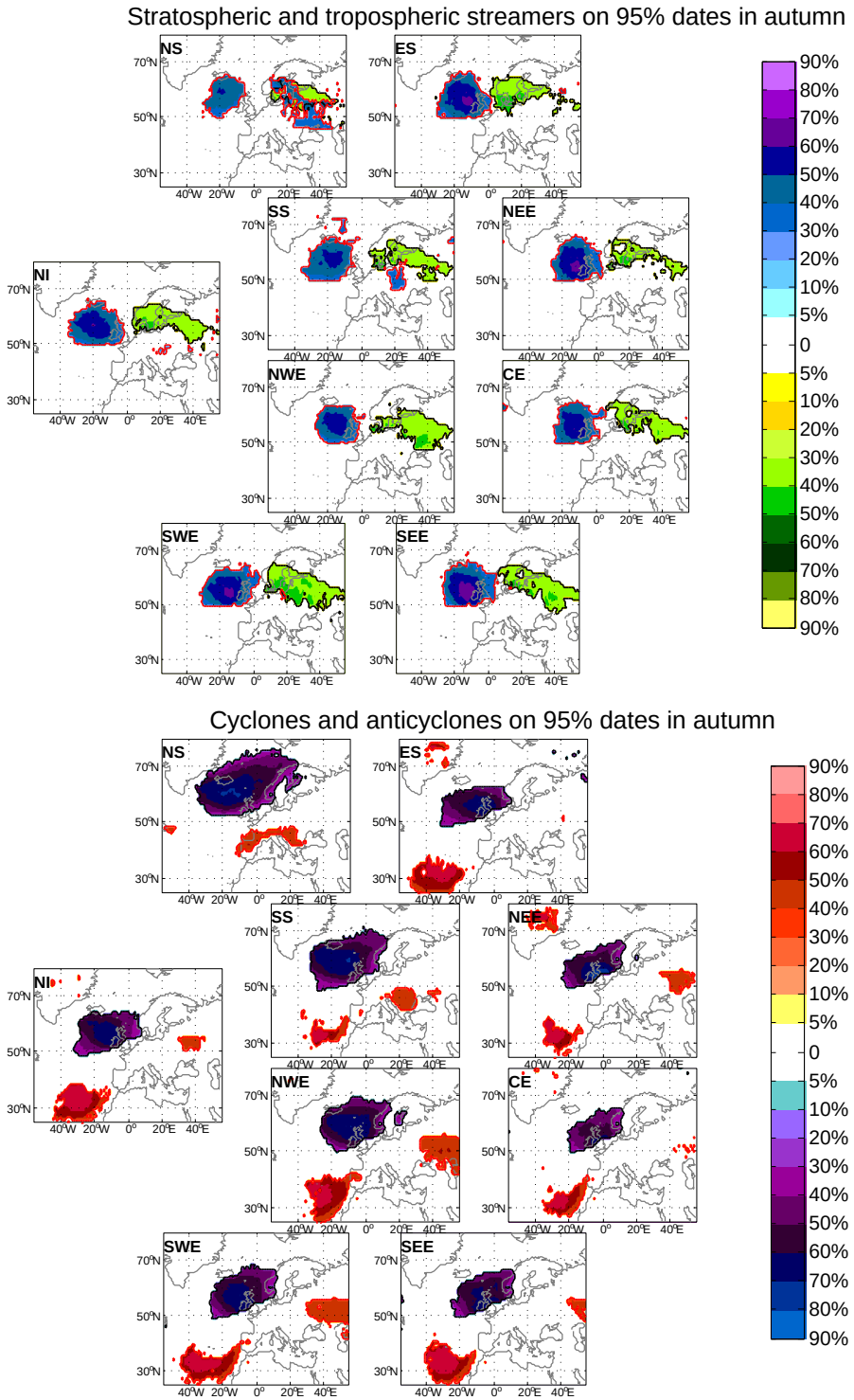

FIGURE A.1: Frequency of significantly more features than the climatological comparison (to the 95% confidence level) for the 95^{th} percentile cases. Top: stratospheric streamers (blue scale) and tropospheric streamers (green scale) in autumn, bottom: cyclones (blue scale) and anticyclones (red scale) in autumn.

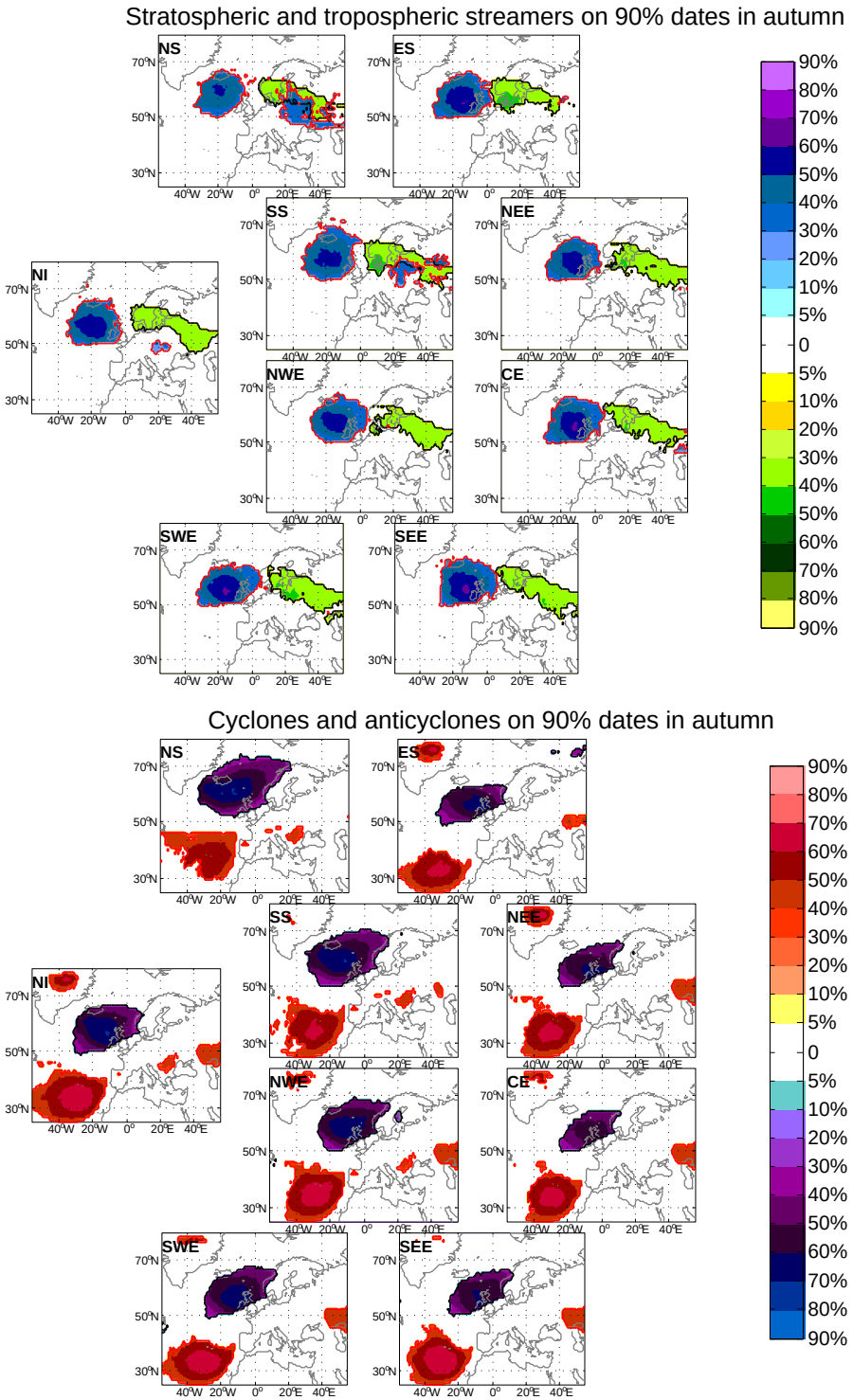

FIGURE A.2: Frequency of significantly more features than the climatological comparison (to the 95% confidence level) for the 90^{th} percentile cases. Top: stratospheric streamers (blue scale) and tropospheric streamers (green scale) in autumn, bottom: cyclones (blue scale) and anticyclones (red scale) in autumn.

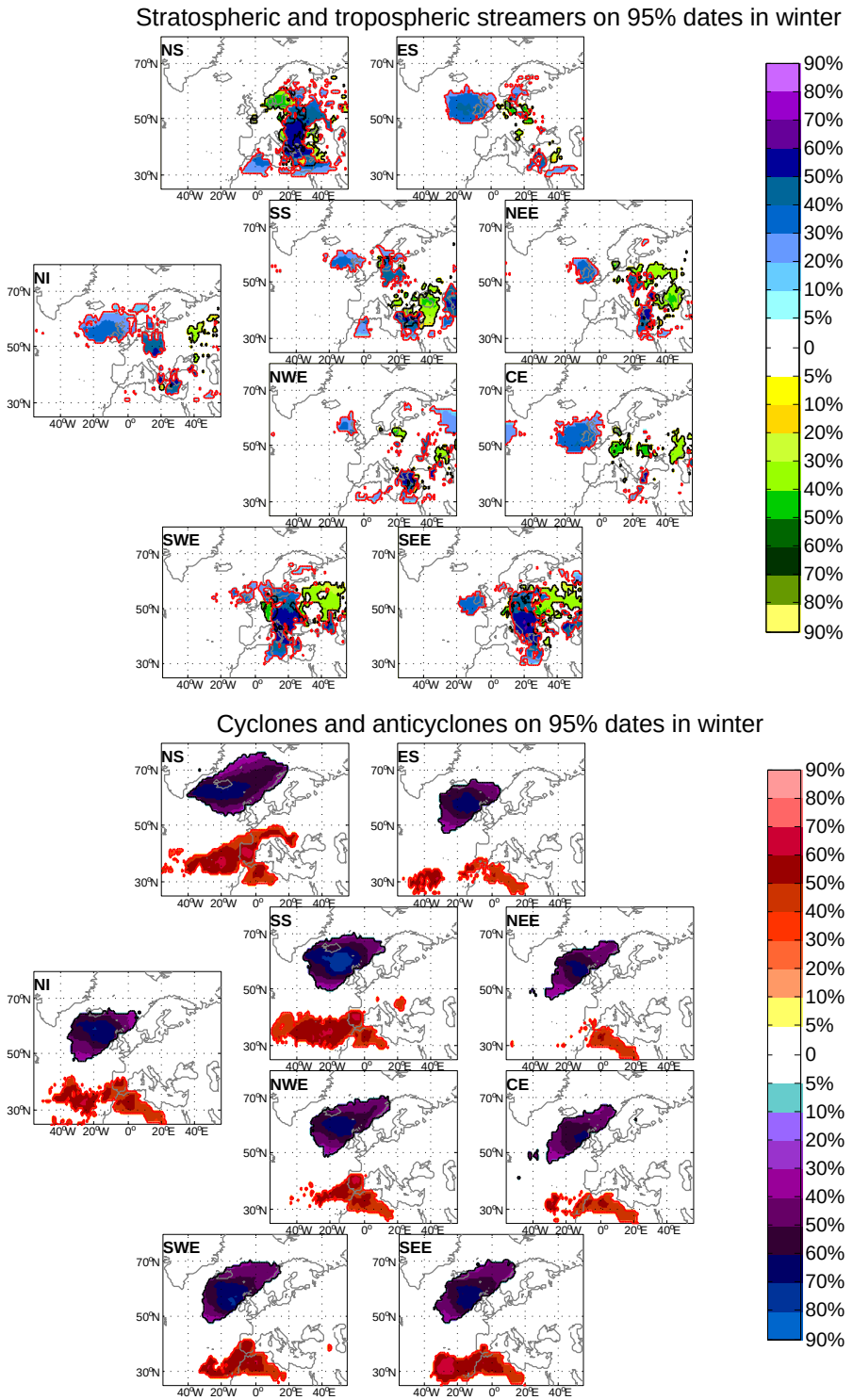

FIGURE A.3: Frequency of significantly more features than the climatological comparison (to the 95% confidence level) for the 95^{th} percentile cases. Top: stratospheric streamers (blue scale) and tropospheric streamers (green scale) in winter, bottom: cyclones (blue scale) and anticyclones (red scale) in winter.

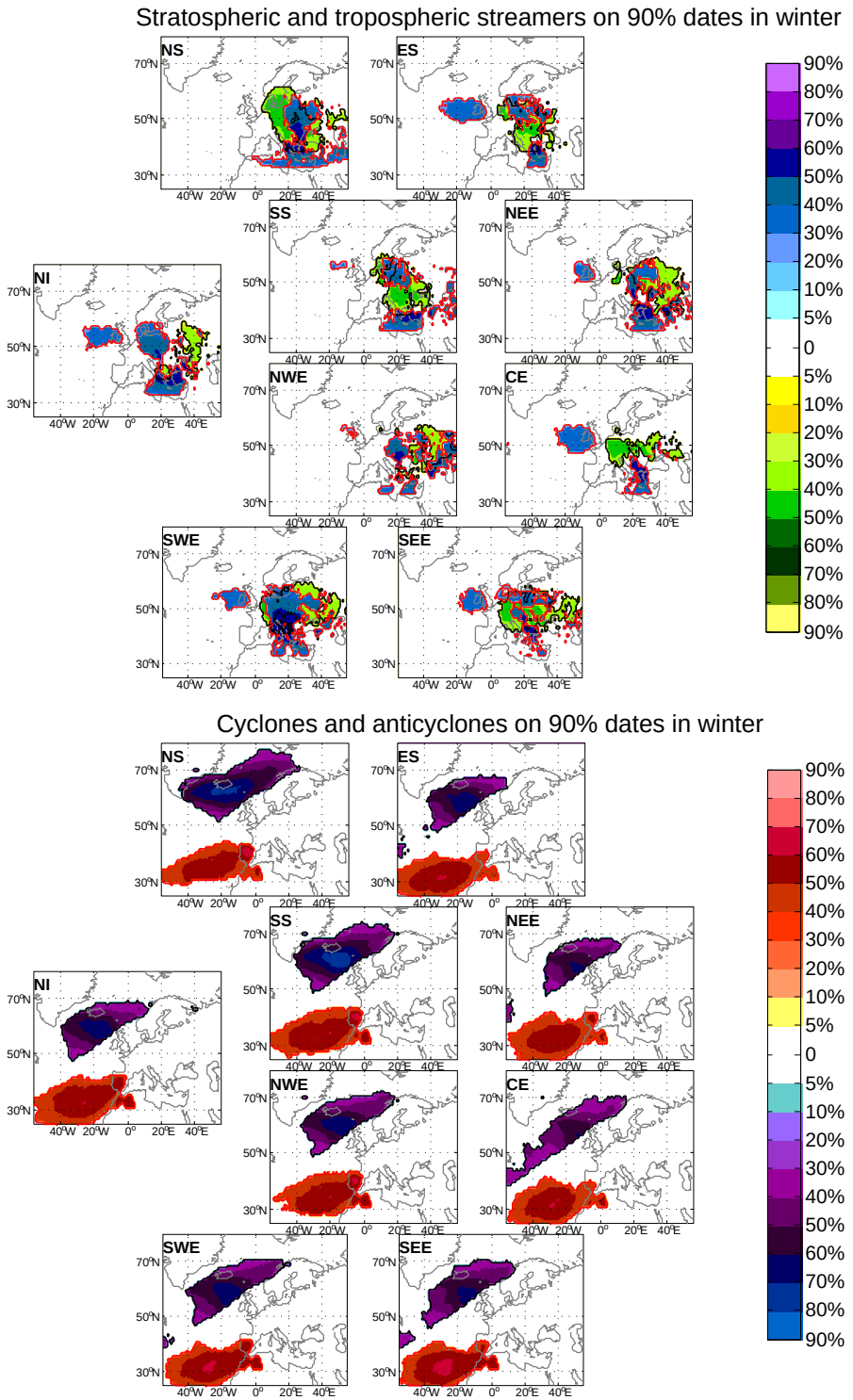

FIGURE A.4: Frequency of significantly more features than the climatological comparison (to the 95% confidence level) for the 90^{th} percentile cases. Top: stratospheric streamers (blue scale) and tropospheric streamers (green scale) in winter, bottom: cyclones (blue scale) and anticyclones (red scale) in winter.

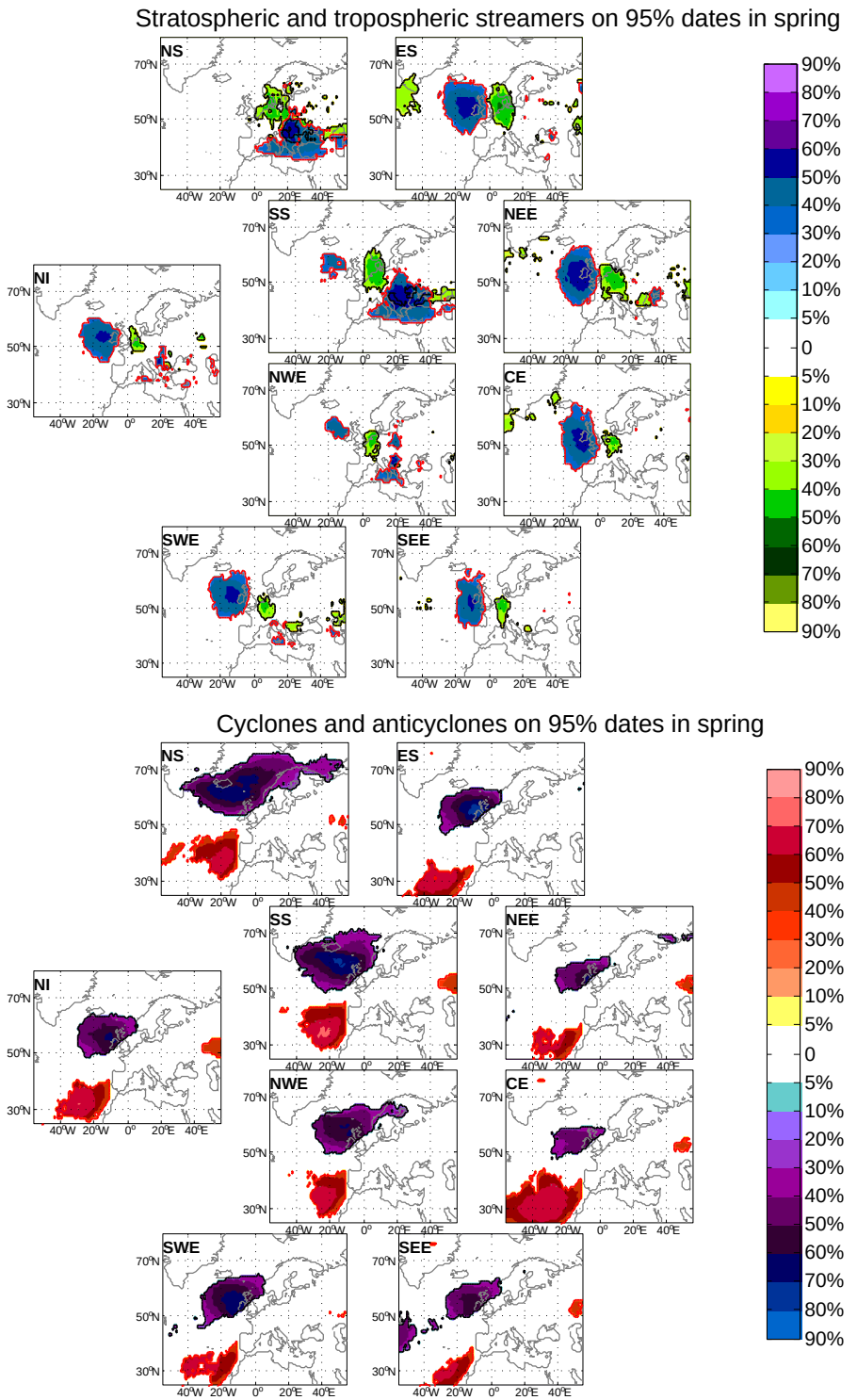

FIGURE A.5: Frequency of significantly more features than the climatological comparison (to the 95% confidence level) for the 95^{th} percentile cases. Top: stratospheric streamers (blue scale) and tropospheric streamers (green scale) in spring, bottom: cyclones (blue scale) and anticyclones (red scale) in spring.

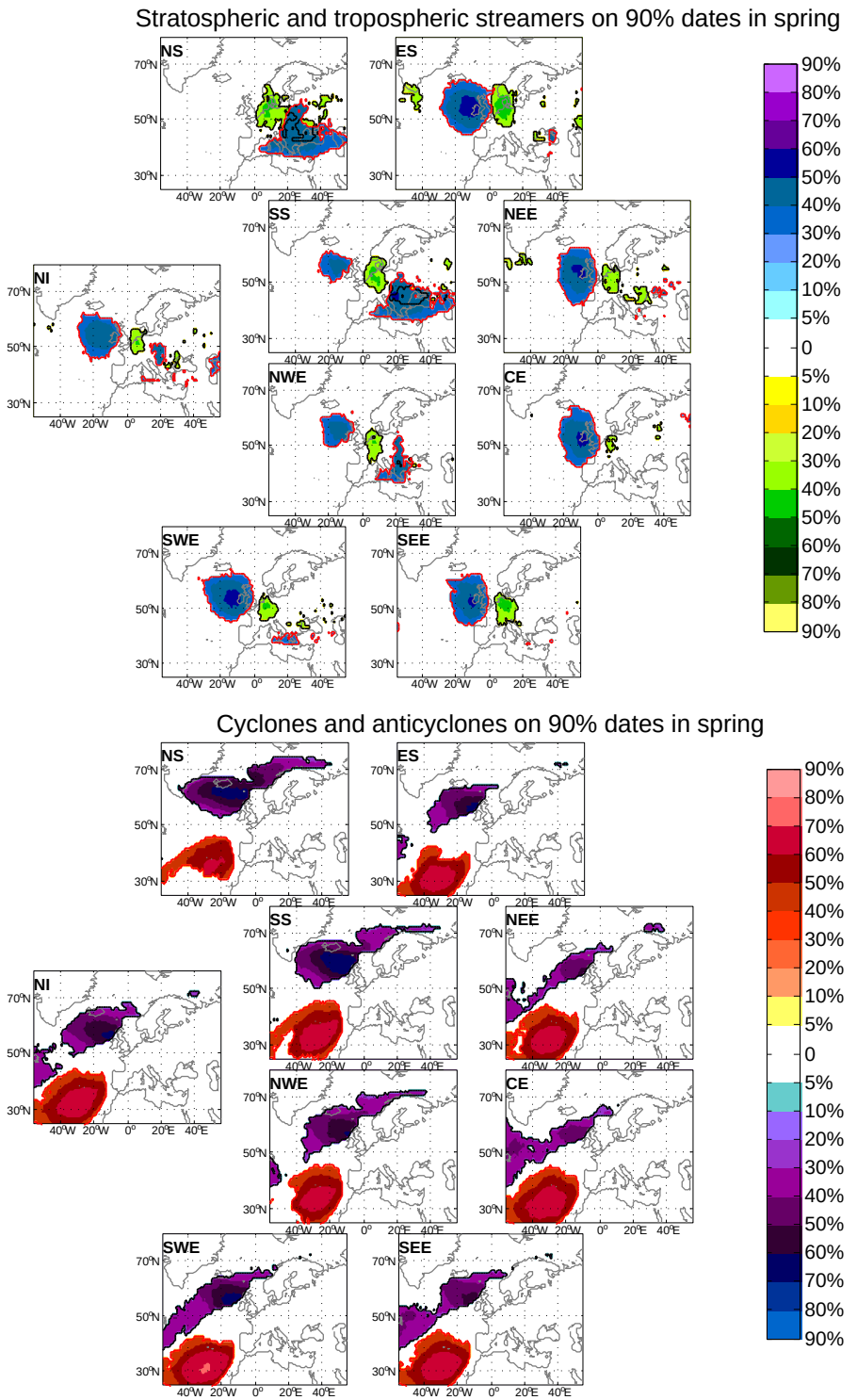

FIGURE A.6: Frequency of significantly more features than the climatological comparison (to the 95% confidence level) for the 90^{th} percentile cases. Top: stratospheric streamers (blue scale) and tropospheric streamers (green scale) in spring, bottom: cyclones (blue scale) and anticyclones (red scale) in spring.

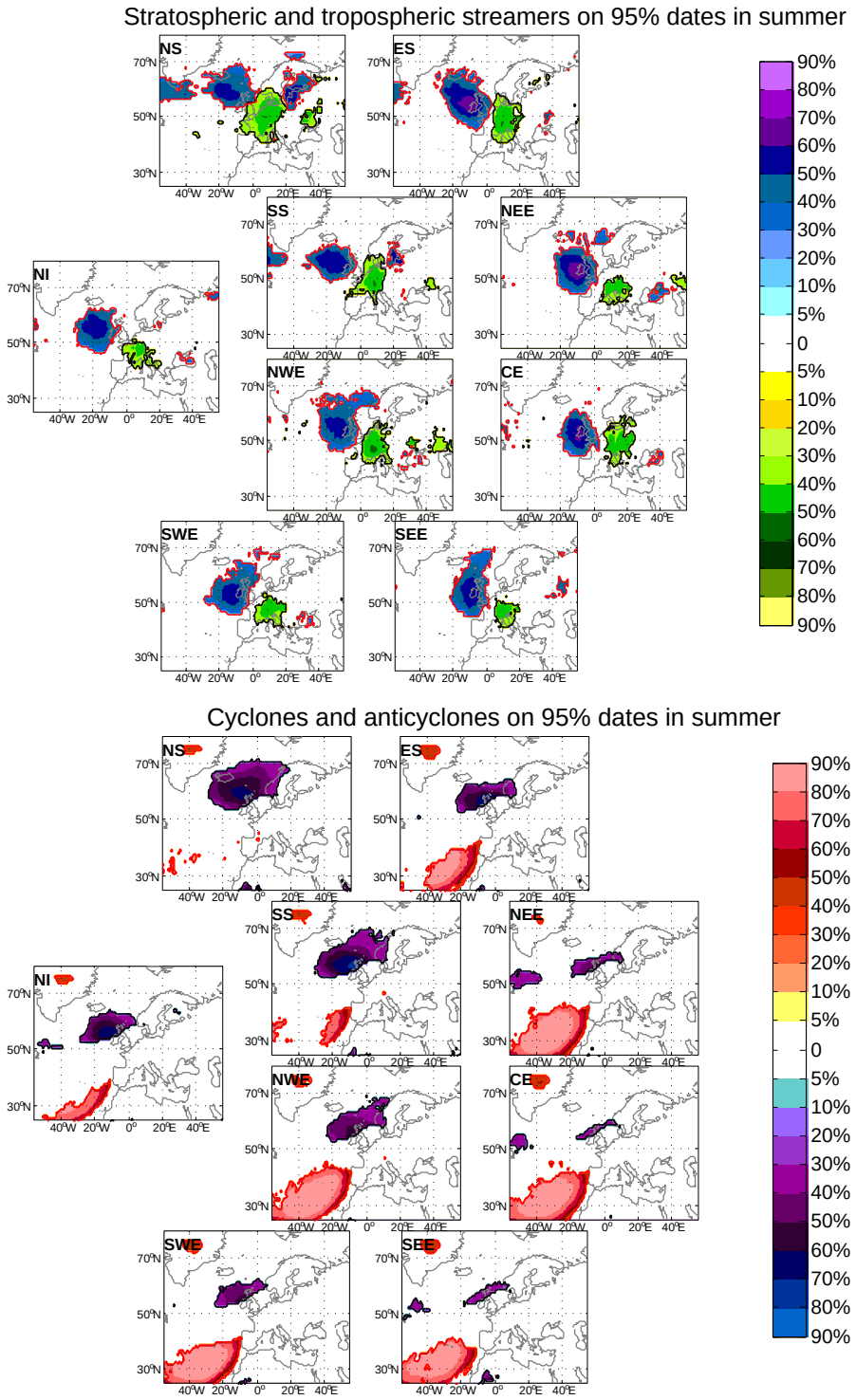

FIGURE A.7: Frequency of significantly more features than the climatological comparison (to the 95% confidence level) for the 95^{th} percentile cases. Top: stratospheric streamers (blue scale) and tropospheric streamers (green scale) in summer, bottom: cyclones (blue scale) and anticyclones (red scale) in summer.

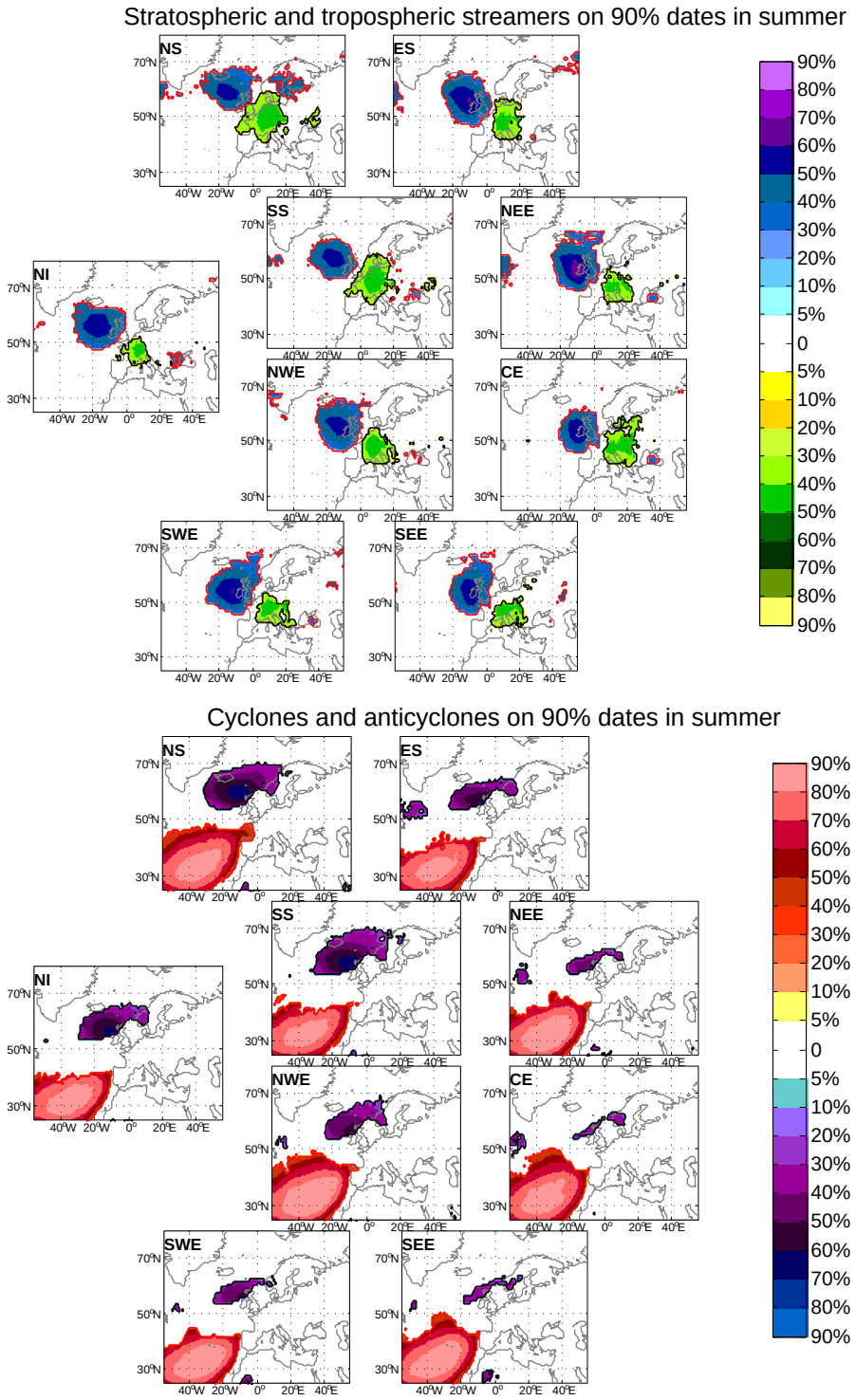

FIGURE A.8: Frequency of significantly more features than the climatological comparison (to the 95% confidence level) for the 90^{th} percentile cases. Top: stratospheric streamers (blue scale) and tropospheric streamers (green scale) in summer, bottom: cyclones (blue scale) and anticyclones (red scale) in summer.

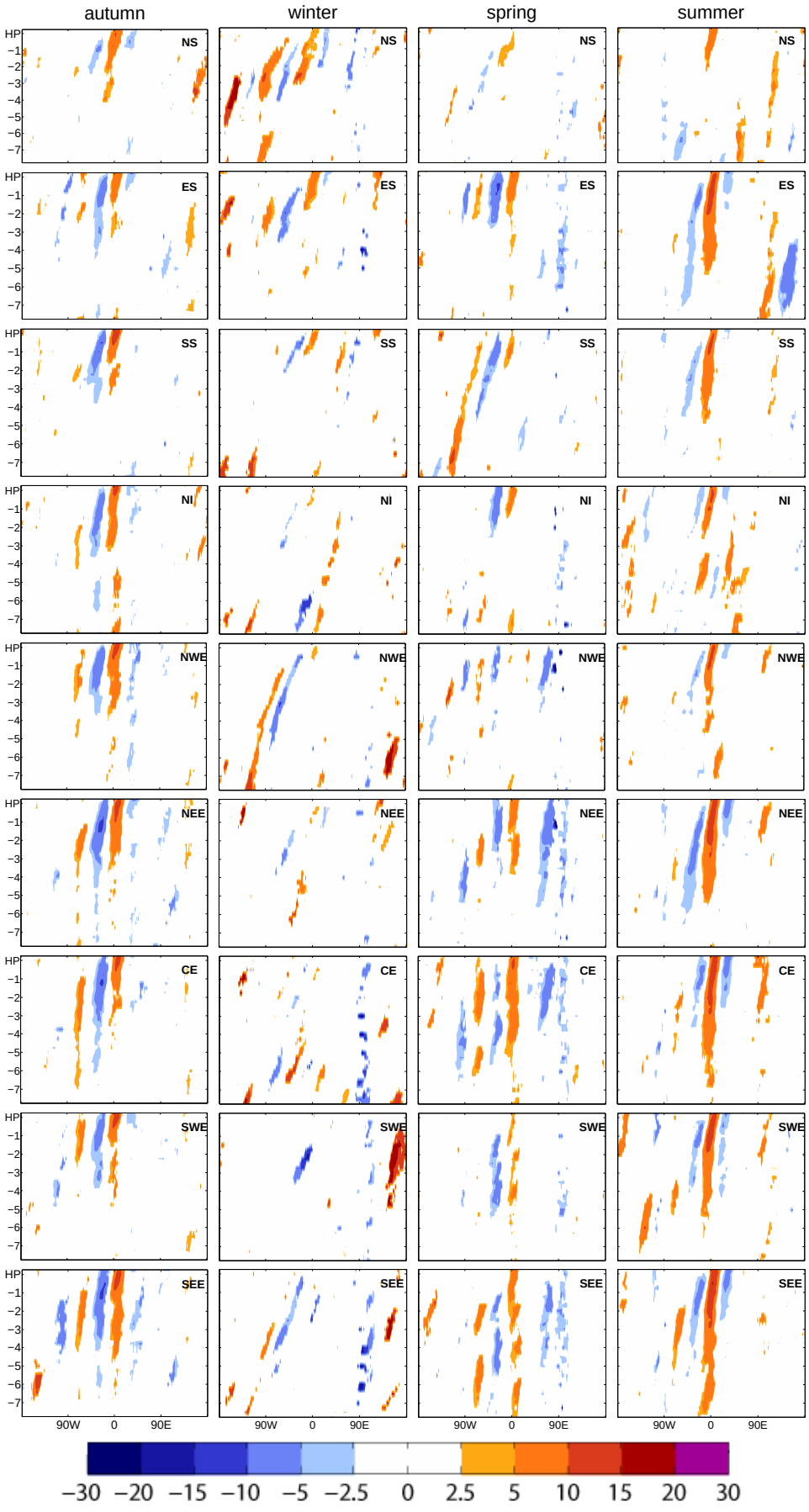

FIGURE A.9: Hovmöller plots of preceding Rossby waves (precipitation day to 7 days prior) for 95% cases in all regions (northern: top to southern: bottom) and seasons. One isentropic level is used for each season: 320K for autumn, winter and spring and 330K for summer.

Appendix B

Triggers of Rossby waves and PV streamer formation

B.1 Rossby Wave trigger plots for individual UK regions

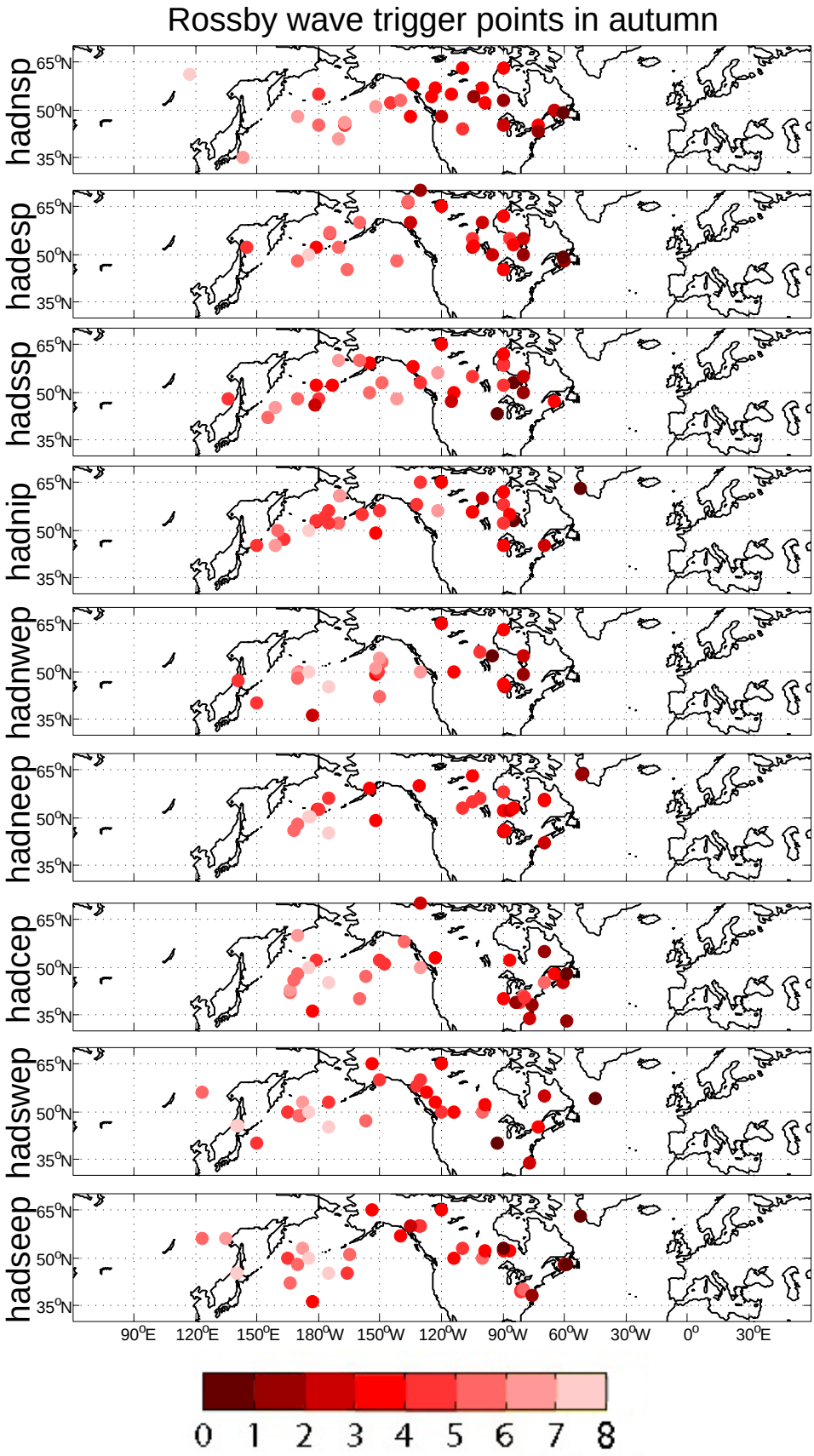

FIGURE B.1: Trigger points of Rossby wave trains preceding heavy precipitation events in the UK for autumn (colours represent number of days prior to the heavy precipitation event).

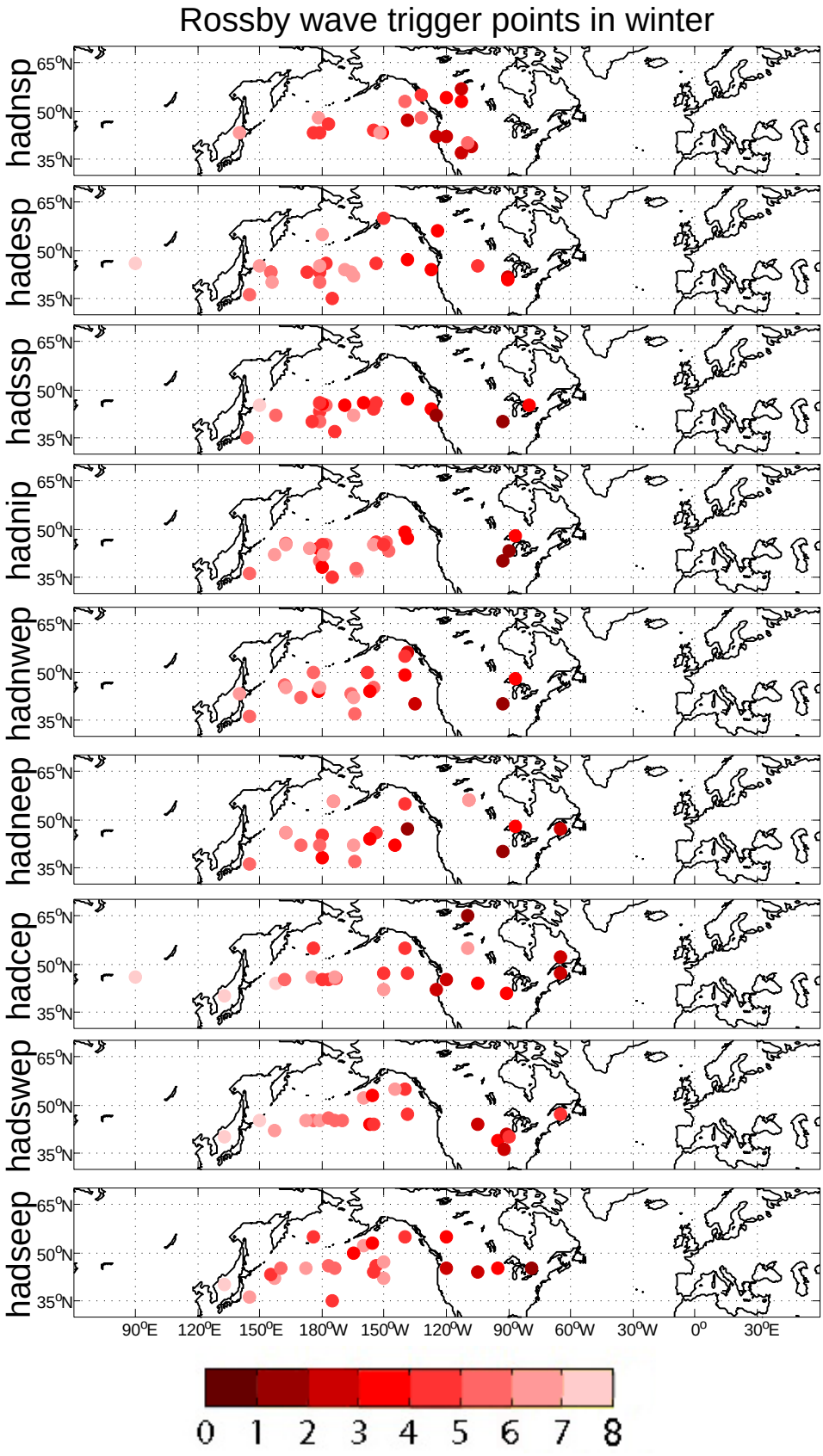

FIGURE B.2: Trigger points of Rossby wave trains preceding heavy precipitation events in the UK for winter (colours represent number of days prior to the heavy precipitation event).

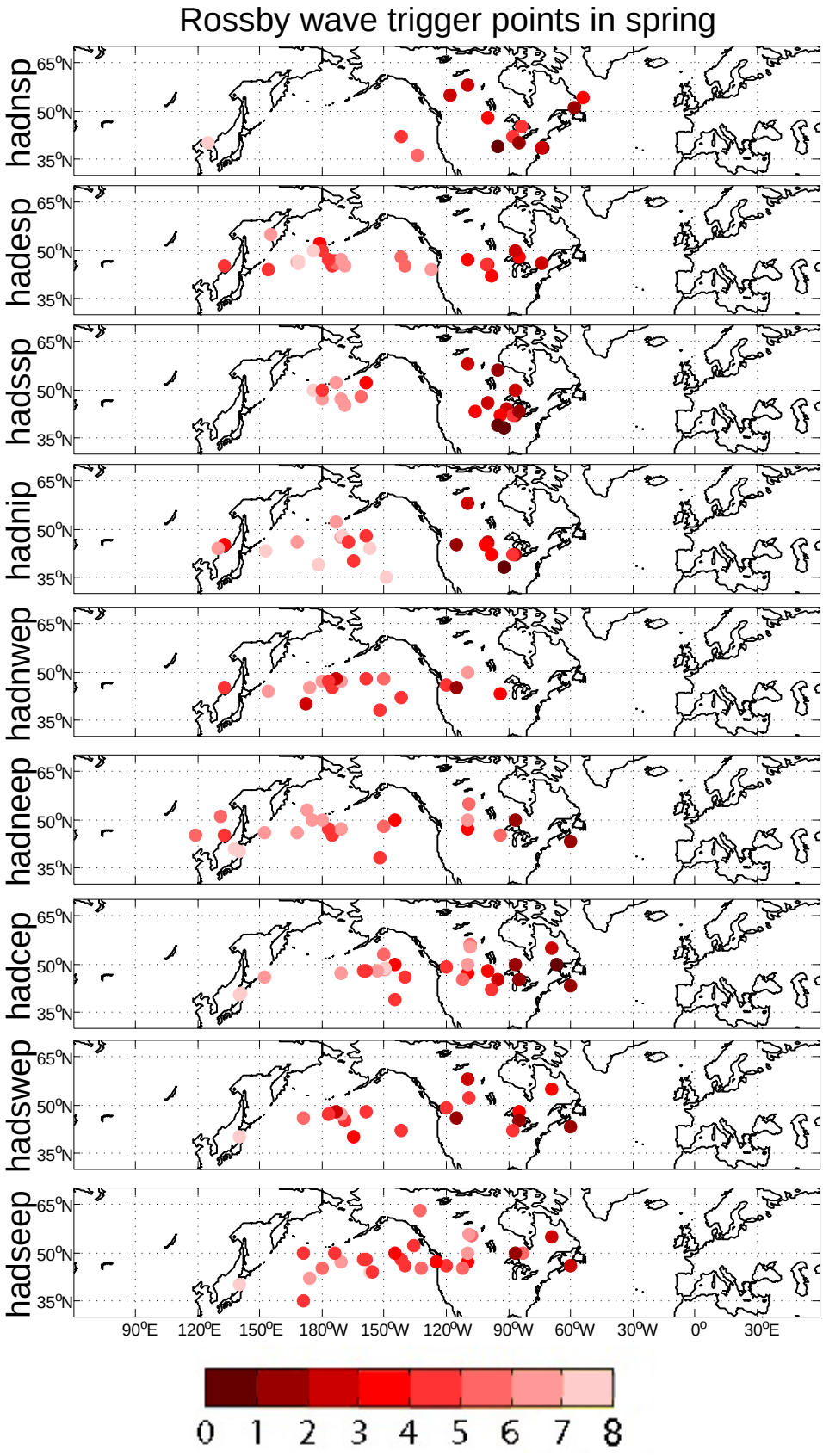

FIGURE B.3: Trigger points of Rossby wave trains preceding heavy precipitation events in the UK for spring (colours represent number of days prior to the heavy precipitation event).

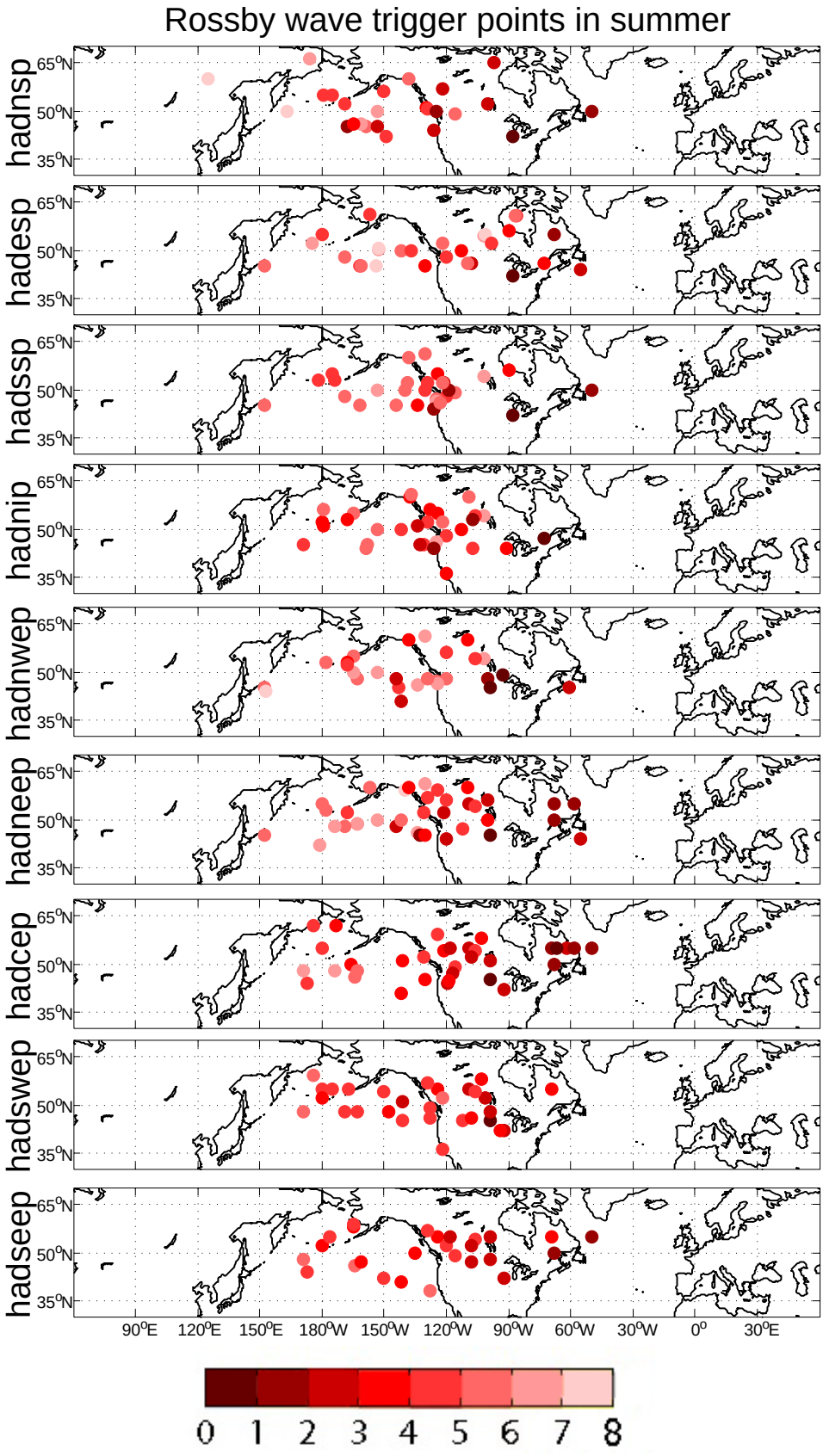

FIGURE B.4: Trigger points of Rossby wave trains preceding heavy precipitation events in the UK for summer (colours represent number of days prior to the heavy precipitation event).

Appendix C

Forecast quality and predictability of PV streamers

C.1 ECMWF deterministic forecasts

TABLE C.1: Case studies investigated

Heavy precipitation dates
20/10/2001
02/11/2002
16/11/2002
24/11/2002
25/11/2002
31/10/2003
27/11/2003
26/10/2004
01/11/2004
11/09/2005
02/10/2005
17/09/2006
03/10/2006

C.2 TIGGE forecasts

TABLE 1. Characteristics of the nine EPSs used in this study. The abbreviations used in the table are as follow: SV, singular vector; BV, bred vector; ET, ensemble transform; EnKF, ensemble Kalman filter; ETKF, ensemble transform Kalman filter; EOF, empirical orthogonal function; NH, Northern Hemisphere; SH, Southern Hemisphere; TR, tropics; GenSI, generalized multivariate statistical interpolation; 3-/4DVAR, 3-/4-dimensional variational data assimilation; GSI, gridded statistical interpolation; Tx, spectral triangular truncation at total wavenumber x; and TLx, spectral triangular truncation at total wavenumber x with linear grid.

Center	Horizontal resolution	No. of levels	No. of members	Initial perturbation	Perturbation model physics	Forecast length (days)	Forecast frequency (UTC)	Data assimilation
BoM	TL119 (1.5°)	19	32	SVs (NH, SH)	No	10	0000, 1200	GenSI
CMA	T213 (0.5625°)	31	14	BVs (globe)	No	10	0000, 1200	GSI
CMC	TL149 (1.2°)	28	20	EnKF (globe)	Yes	16	0000, 1200	4DVAR
ECMWF	TL399 (0.45°), TL255 (0.7°)	62	50	SVs (globe)	Yes	0–10 10–15	0000, 1200	4DVAR
JMA	TL319 (0.5625°)	60	50	SVs (NH, TR)	No	9	1200	4DVAR
KMA	T213 (0.5625°)	40	16	BVs (NH)	No	10	0000, 1200	3DVAR
NCEP	T126 (0.9474°)	28	20	ET (globe)	No	16	0000, 0600, 1200, 1800	GSI
UKMO	1.25° × 0.83°	38	23	ETKF (globe)	Yes	15	0000, 1200	4DVAR
CPTEC	T126 (0.9474°)	28	14	EOF (45°S–30°N)	No	15	0000, 1200	NCEP analysis

FIGURE C.1: Differences in the TIGGE ensemble prediction systems from Froude (2010)

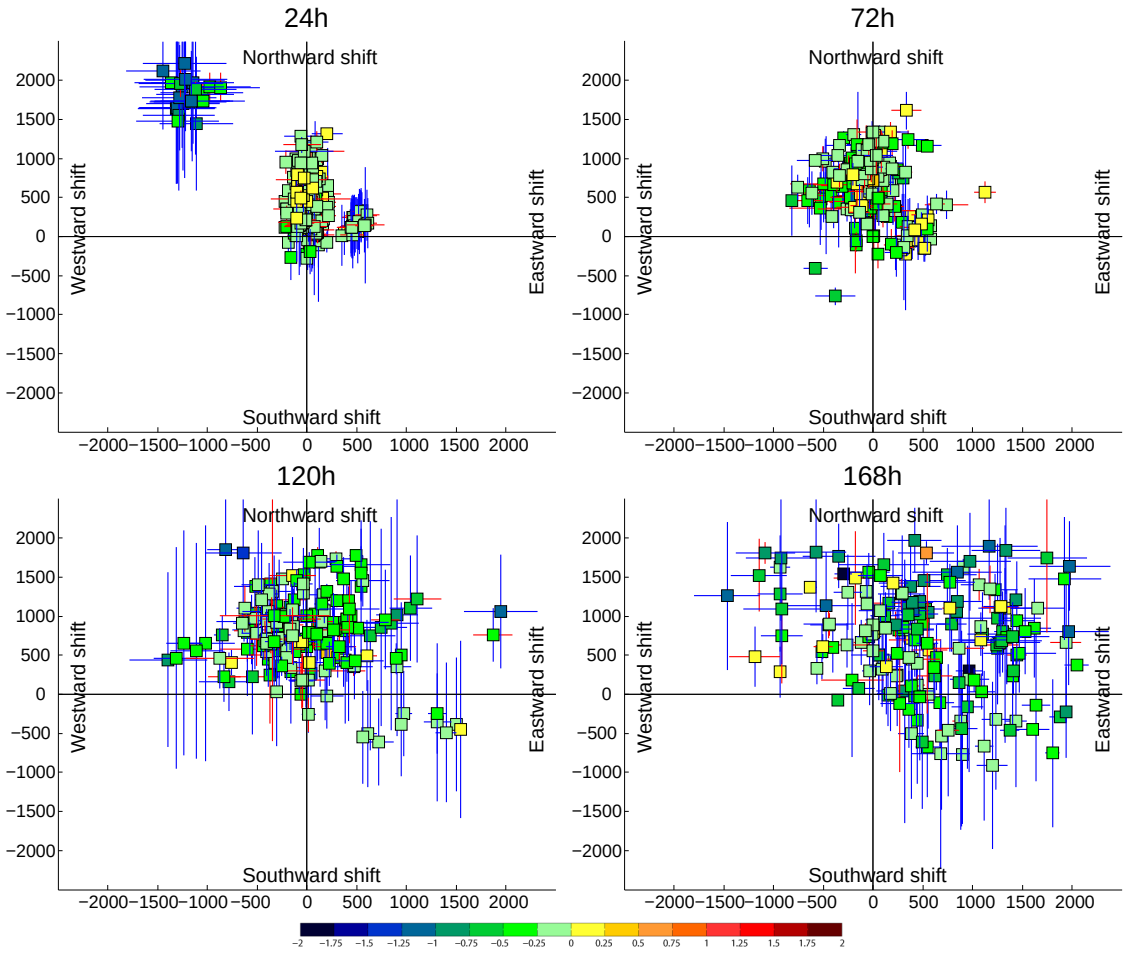

FIGURE C.2: Difference of forecast in relation to analysis streamer in 24, 72, 120 and 168-h lead times for all nine TIGGE ensemble systems. Differences in elongation (vertical lines) and width (horizontal lines) are displayed, red shows positive values (wider or longer streamers) while blue indicates negative changes (shorter or narrower). Colour of square illustrates mean UPV difference (forecast − analysis.

References

Aebischer, U. and C. Schär: 1998, Low-level potential vorticity and cyclogenesis to the lee of the Alps. *Journal of Atmospheric Sciences*, **55**, 186–207.

Akahori, K. and S. Yoden: 1997, Zonal flow vacillation and bimodality of baroclinic eddy life cycles in a simple global circulation model. *J. Atmos. Sci.*, **54**, 2349–2361.

Alexander, L. and P. Jones: 2001, Updated precipitation series for the U.K. and discussion of recent extremes. *Atmospheric Science Letters*, **358**, 570–572.

Altenhoff, A. M., O. Martius, M. Croci-Maspoli, C. Schwierz, and H. C. Davies: 2008, Linkage of atmospheric blocks and synoptic-scale Rossby waves: A climatological analysis. *Tellus*, **60A**, 1053–1063.

Anwender, D., P. A. Harr, and S. C. Jones: 2008, Predictability associated with the downstream impacts of the extratropical transition of tropical cyclones: case studies. *Monthly Weather Review*, **136**, 3226–3247.

Appenzeller, C. and H. C. Davies: 1992, Structure of stratospheric intrusions into the troposphere. *Nature*, **358**, 570–572.

Appenzeller, C., H. C. Davies, and W. A. Norton: 1996, Fragmentation of stratospheric intrusions. *J. Geophys. Res.*, **101**, 1435–1456.

Athanasiadis, P. J. and J. M. Wallace: 2010, Patterns of wintertime jet stream variability and their relation to the storm tracks. *Journal of the Atmospheric Sciences*, **67**, 1361–1381.

Barry, R. G. and A. M. Carleton: 2001, *Synoptic and Dynamic Climatology*. Routledge.

Barry, R. G. and R. J. Chorley: 2003, *Atmosphere, weather and climate*. Routledge, 8th edition.

Bigg, G.: 2003, Lecture 7: The general circulation of the atmosphere. University of East Anglia, http://www.uea.ac.uk/-e930/e174/l7-atmc.html.

Blackburn, M., J. Methven, and N. Roberts: 2008, Large-scale context for the UK floods in summer 2007. *Weather*, **63**, 280–288.

Bluestein, H. B.: 1993, *Synoptic Dynamic Meteorology in Midlatitudes*. Oxford University Press.

Brennan, M. J., G. M. Lackmann, and K. M. Mahoney: 2007, Potential vorticity (PV) thinking in operations: the utility of nonconservation. *Weather and Forecasting*, **23**, 168–182.

Browning, K. A.: 2004, The sting at the end of the tail: Damaging winds associated with extratropical cyclones. *QJRMS*, **130**, 375–399.

Browning, K. A. and M. Field: 2004, Evidence from Meteosat imagery of the interaction of sting jets with the boundary layer. *Meteor. Appl.*, **11**, 277–289.

Buizza, R.: 2006, *Predictability of Weather and Climate*, Cambridge University Press, chapter The ECMWF Ensemble Prediction System. 459–488.

Caracena, F., A. Marroquin, and E. Tollerud: 2001, A PV-streamer's role in a succession of heavy rain-producing MCSS over the central U.S. *Physics and Chemistry of the Earth*, 26–29.

Chang, E. M. and D. B. Yu: 1999, Characteristics of wave packets in the upper troposphere. part I Northern Hemisphere winter. *Journal of Atmospheric Science*, **56**, 1708–1728.

Danielson, R., J. Gyakum, and D. Straub: 2004, Downstream baroclinic development among forty one cold-season eastern North Pacific cyclones. *Monthly Weather Review*, **131**, 2824–2837.

Dirren, S., M. Didione, and H. C. Davies: 2003, Diagnosis of "forecast-analysis" differences of a weather prediction system. *Geophysical Research Letters*, **30**, 2060.

Eliassen, A. and E. Kleinschmidt: 1957, *Dynamic Meteorology*. Springer, 1-154 pp.

Errico, R.: 1997, What is an adjoint? *Bulletin of American Meteorological Society*, **78**, 2577–2591.

Errico, R. and K. D. Raeder: 1999, An examination of the accuracy of the linearization of a mesoscale model with moist physics. *QJRMS*, **125**, 169–195.

Ertel, H.: 1942, Ein neuer hydrodynamischer Wirbelsatz. *Meteor. Z.*, **59**, 277–281.

Esler, J. G. and P. H. Haynes: 1999, Baroclinic wave breaking and the internal variability of the tropospheric circulation. *J. Atmos. Sci.*, **56**, 4014–4031.

Fehlmann, R. and H. C. Davies: 1999, Role of salient PV-elements in an event of frontal-wave cyclogenesis. *Quart. J. Roy. Meteor. Soc.*, **125**, 1801–1824.

Fehlmann, R. and C. Quadri: 2000, Predicability issues of heavy Alpine south-side precipitation. *Wea. and Forecasting*, **72**, 223–231.

Fehlmann, R., C. Quadri, and H. C. Davies: 1999, An Alpine rainstorm: Sensitivity to the mesoscale upper-level structure. *Wea. and Forecasting*, **15**, 4–28.

Field, C., V. Barros, T. Stocker, D. Qin, D. Dokken, K. Ebi, M. Mastrandrea, K. Mach, G. Plattner, S. Allen, M. Tignor, and P. Midgley: 2011, Summary for Policymakers. *Intergovernmental Panel on Climate Change special report on managing the risks of extreme events and disasters to advance climate change adaptation.*, IPCC, Cambridge University Press.

Frhlich, L. and P. Knippertz: 2008, Identification and global climatology of upper-level troughs at low latitudes. *Meteorol. Z.*, **17**, 565–573.

Froude, L. S. R.: 2010, TIGGE: Comparison of the prediction of Northern Hemisphere extra-tropical cyclones by differenct ensemble prediction systems. *Weather and Forecasting*, **25**, 819–836.

Gheusi, F. and H. C. Davies: 2004, Autumnal precipitation distribution on the southern flank of the Alps: A numerical model study of the mechanisms. *QJRMS*, **130**, 2125–2152.

Glatt, I., A. Dornbrack, S. Jones, J. Keller, O. Martius, A. Muller, D. W. Peters, and V. Wirth: 2011, Utility of Hovmöller diagarams to diagnose Rossby wave trains. *Tellus*, **63A**, 991–1006.

Grams, C. M., H. Wernli, M. Bottcher, J. Campa, U. Corsmeier, S. Jones, J. H. Keller, C. Lenz, and L. Wiegand: 2011, The key role of diabatic processes in modifying the upper-tropospheric wave guide: a North Atlantic case-study. *QJRMS*, **137**, 2174–2193.

Grazzini, F.: 2007, Predictability of a large-scale flow conducive to extreme precipitation over the western Alps. *Meteorol. Atmos. Phys.*, **95**, 123–138.

Grazzini, F. and G. Van der Grijn: 2003, Central European floods during summer 2002. *ECMWF Newsletter*, 18–28.

Gregory, J. M., P. D. Jones, and T. M. Wigley: 1991, Precipitation in Britain: An analysis of area-average data updated to 1989. *Int. J. Climatol.*, **11**, 331–345.

Griffiths, M., A. J. Thorpe, and K. A. Browning: 2000, Convective destabilization by a tropopause fold diagnosed using potential-vorticity inversion. *QJRMS*, **126**, 125–144.

Hakim, G. J.: 2005, Vertical structure of midlatitude analysis and forecast errors. *Monthly Weather Review*, **133**, 567–575.

Hall, J. W., P. B. Sayers, and R. J. Dawson: 2005, National-scale assessment of current and future flood risk in England and Wales. *Natural Hazards*, **36**, 147–164.

Hand, W. H.: 2004, Climatology of shower frequency in the British Isles at 5km resolution. *Weather*, **60**, 153–158.

Hand, W. H., N. I. Fox, and C. G. Collier: 2005, A study of twentieth-century extreme rainfall events in the United Kingdom with implications for forecasting. *Meteorological Applications*, **11**, 15–31.

Harr, P. A. and J. M. Dea: 2009, Downstream development associated with the extratropical transition of tropical cyclones over the western north Pacific. *Monthly Weather Review*, **137**, 1295–1319.

Haylock, M. R., N. Hofstra, A. M. G. K. Tank, E. J. Klok, P. D. Jones, and M. New: 2008, A European daily high-resolution gridded data set of surface temperature and precipitation for 1950-2006. *Journal of Geosphysical Reasearch*, **113D**.

Haynes, P. H. and M. E. McIntyre: 1987, On the evolution of isentropic distributions of potential vorticity in the presence of diabatic heating and frictional or other forces. *J. Atmos. Sci.*, **44**, 828–841.

Hennon, C.: 2007, Lecture: Atmospheric kinematics and dynamics - Rossby waves. University of North Carolina, http://facstaff.unca.edu/chennon/classes/atms310/pdf/rossby-waves.pdf.

Hogan, T. and T. E. Rosmond: 1991, The description of the Navy Operational Global Atmospheric Prediction System's spectral forecast model. *Monthly Weather Review*, **119**, 1786–1815.

Hoinka, K. P. and H. C. Davies: 2007, Upper tropospheric flow features and the Alps: an overview. *QJRMS*, **133**, 847–865.

Holton, J.: 2004, *An introduction to dynamic meteorology*. Elsevier Academic, 4th edition.

Homar, V. and D. J. Stensrud: 2004, Sensitivities of an intense Mediterranean cyclone: Analysis and validation. *QJRMS*, **130**, 2519–2540.

Hoover, B. T.: 2009, Comments on "Interaction of Typhoon Shanshan (2006) with the mid-latitude trough from both adjoint-derived sensitivity steering vector and potential vorticity perspectives". *Monthly Weather Review*, **137**, 2761–2775.

Hoover, B. T. and M. C. Morgan: 2010, Validation of a tropical cyclone steering response function with a barotropic adjoint model. *Journal of Atmospheric Science*, **67**, 1806–1816.

— 2011, Dynamical sensitivity analysis of tropical cyclone steering using an adjoint model. *Monthly Weather Review*, **139**, 1806–1816.

Hoskins, B.: 2006, *Predictability of Weather and Climate*, Cambridge University Press, chapter Predictability from a dynamical meteorological perspective. 30–39.

Hoskins, B. J.: 1991, Towards a PV-θ view of the general circulation. *Tellus*, **43AB**, 27–35.

Hoskins, B. J. and T. Ambrizzi: 1993, Rossby wave propagation on a realistic longitudinally varying flow. *Journal of Atmospheric Science*, **50**, 1661–1671.

Hoskins, B. J. and D. J. Karoly: 1981, The steady linear responses of a shperical atmosphere to thermal and orographic forcing. *Journal of Atmospheric Science*, **38**, 1179–1196.

Hoskins, B. J., M. E. McIntyre, and A. W. Robertson: 1985, On the use and significance of isentropic potential vorticity maps. *Quart. J. Roy. Meteor. Soc.*, **111**, 877–946.

Hovmöller, E.: 1949, The trough and ridge diagram. *Tellus*, **1**, 62–66.

Isotta, F., O. Martius, M. Sprenger, and C. Schwierz: 2008, Long-term trends of synoptic-scale breaking Rossby waves in the Northern Hemisphere between 1958 and 2001. *International Journal of Climatology*, **28**, 1551–1562.

Jacobeit, J.: 1987, Variations of trough positions and precipitation patterns in the Mediterranean area. *Journal of Climatology*, **7**, 453–476.

Jenkner, J., C. Frei, and C. Schwierz: 2008, Quantile-based short range QPF evaluation over Switzerland. *Meteor. Z.*, **17**, 827–848.

Jones, S. C., P. Harr, J. Abraham, L. Bosart, P. Bowyer, J. Evans, D. Hanley, B. Hanstrum, F. Lalaurette, M. Sinclair, R. Smith, C. Thorncroft, and R. Hart: 2003, The extratropical transition of tropical cyclones: forecast challenges, current understanding, and future directions. *Weather and Forecasting*, **18**, 1052–1092.

Juckes, M. and R. K. Smith: 2000, Convective destabilization of upper-level troughs. *QJRMS*, **126**, 111–123.

Karoly, D. J.: 1983, Rossby wave propagation in a barotropic atmosphere. *Dynamics of Atmospheres and Oceans*, **7**, 111–125.

Klein, H., N. S., W. Haunold, U. Bundke, B. Nillius, M. Ebert, S. Weinbruch, L. Schuetz, Z. Levin, L. A. Barrie, and H. Bingemer: 2010, Saharan dust and ice nuclei over central Europe. *Atmospheric Chemistry and Physics*, **10**, 10211–10221.

Kleist, D. and M. C. Morgan: 2005a, Application of adjoint-derived forecast sensitivities to the 24-25 January 2000 US east coast snowstorm. *Monthly Weather Review*, **133**, 3148–3175.

— 2005b, Interpretation of the structure and evolution of adjoint-derived forecast sensitivity gradients. *Monthly Weather Review*, **133**, 466–484.

Knippertz, P. and A. H. Fink: 2006, Synoptic and dynamic aspects of an extreme springtime Saharan dust outbreak. *Quart. J. Roy. Meteor. Soc.*, **132**, 1153–1177.

Krichnak, S. O., P. Alper, and M. Dayan: 2004, The role of atmospheric processes associated with hurricane Olga in the December 2001 floods in Israel. *Journal of Hydrometeorology*, **5**, 1259–1270.

Krishnamurti, Y., T. S. V. vijaya Kumar, K. Rajendran, and A. Hopkins: 2003, Antecedents of the flooding over south-eastern England during October 2000. *Weather*, **58**, 367–370.

Lamb, H. H.: 1950, Types and spells of weather around the year in the British Isles: annual trends, seasonal structure of the year, singularities. *QJRMS*, **76**, 393–429.

Langland, R. H., R. L. Elsberry, and R. M. Errico: 1995, Evaluation of physical processes in an idealized extratropical cyclone using adjoint sensitivity. *Quart. J. Roy. Meteor. Soc.*, **121**, 1349–1386.

— 1996, Adjoint sensitivity of an idealized extratropical cyclone with moist physical processes. *QJRMS*, **122**, 1891–1920.

Langland, R. H. and R. M. Errico: 1996, Comments on "Use of an adjoint model for finding triggers for Alpine lee cyclogenesis.". *Monthly Weather Review*, **124**, 757–760.

Lazear, R. A.: 2007, *The effects of diabatic heating on upper-tropospheric anticyclogenesis*. Master's thesis, University of Wisconsin - Madison.

Lutgens, F. K. and E. J. Tarbuck: 2004, *The Atmosphere: An Introduction to Meteorology*, Pearson Education Ltd, chapter Circulation of the atmosphere. 9th edition, 191–226.

Lynch, A. H. and J. J. Cassano: 2006, *Applied atmospheric dynamics*. Wiley.

Maraun, D., T. J. Osborn, and N. P. Gillett: 2008, United Kingdom daily precipitation intensity: Improved early data, error estimates and an update from 2000 to 2006. *International Journal of Climatology*, **28**, 833–842.

Maraun, D., T. J. Osborn, and H. Rust: 2011, The influence of synoptic airflow on uk daily precipitation extremes: Part I: observed spatio-temporal relations. *Climate Dynamics*, **36**, 261–275.

Maraun, D., H. W. Rust, and T. J. Osborn: 2009, The annual cycle of heavy precipitation across the UK: a model based on extreme value statistics. *International Journal of Climatology*, **29**, 1731–1744.

Martin, A., R. Romero, V. Homar, A. De Luque, S. Alonso, T. Rigo, and M. Llasat: 2007, Sensitivities of a flash flood event over Catalonia: A numerical analysis. *Monthly Weather Review*, **135**, 651–669.

Martin, J. E.: 2006, *Mid-Latitude Atmospheric Dynamics: A First Course*. Wiley.

Martius, O.: 2005, Climatological aspects of wave disturbances on the tropopause and links to extreme weather in Europe. Dissertation ETH, eTH No. 16152.

Martius, O., C. Schwierz, and H. C. Davies: 2006a, A refined Hovmoller diagram. *Tellus*, **58**, 221–226.

— 2007, Breaking waves at the tropopause: Climatological analyses of the orientation and theoretical LC1/2 classification. *Journal of the Atmospheric Sciences*, **64**, 2576–2592.

— 2008, Far-upstream precursors of heavy precipitation events on the Alpine south-side. *Quarterly Journal of the Royal Meteorological Society*, **134**, 417–428.

— 2010, Tropopause-level waveguides. *Journal of the Atmospheric Sciences*, **67**, 866–879.

Martius, O., E. Zenklusen, C. Schwierz, and H. C. Davies: 2006b, Episodes of Alpine heavy precipitation with an overlying elongated stratospheric intrusion: A climatology. *International Journal of Climatology*, 1149–1164.

Massacand, A., H. Wernli, and H. C. Davies: 1998, Heavy precipitation on the Alpine southside: An upper-level precursor. *Geophys. Res. Letters*, **25**, 1435–1438.

Massacand, A. C., H. Wernli, and H. C. Davies: 2001, Influence of upstream diabatic heating upon an Alpine event with heavy precipitation. An upper level precursor. *Monthly Weather Review*, **129**, 2822–2828.

Mayes, J. C.: 1991, Regional airflow patterns in the British Isles. *International Journal of Climatology*, **11**, 473–491.

McIntyre, M. E. and T. N. Palmer: 1983, Breaking planetary waves in the stratosphere. *Nature*, **137**, 189–206.

Meier, F. and P. Knippertz: 2009, Dynamics and predictability of a heavy dry-season precipitation event over west Africa - sensitivity experiments with a global model. *Monthly Weather Review*, **305**, 593–600.

MIDAS: 2007, Met office MIDAS surface data users guide. UK Meteorolocical Office, http://badc.nerc.ac.uk/data/surface/ukmo-guide.html.

Murcia, R., D. Amodeo, M. Robbiano, and F. Fresia: 2008, Analis dell'evento alluvionale che ha interessato il Piemonte nel maggio 2008. Meteonetwork, http://www.meteo.it/Clima-Statistiche/Analisi-delle28099eventoalluvionale-che-ha-interessato-il-Piemonte-nel-maggio-2008/content/it/1-695-305427-57756.

Pelly, J. L. and B. J. Hoskins: 2003, How well does the ECMWF Ensemble Prediction System predict blocking? *QJRMS*, **129**, 1683–1702.

Plumb, A. R.: 2003, Atmospheric and oceanic circulations. Massachusetts Institute of Technology, http://ocw.mit.edu/NR/rdonlyres/Earth–Atmospheric–and-Planetary-Sciences/12-333Spring-2004/5B8025C8-7133-4B64-A4E3-B819C8B0A59C/0/full.pdf.

Postel, G. A. and M. H. Hitchman: 1999, A climatology of Rossby wave breaking along the subtropical tropopause. *Mon. Wea. Rev.*, **129**, 2555–2569.

Richardson, D., R. Buizza, and R. Hagedorn: 2005, Tigge. *Final report of the 1st Workshop on the THORPEX Interactive Grand Global Ensemble (TIGGE).*, WMO, tD-1273 WWRP/THORPEX Rep.5, 39pp.

Riemer, M. and S. C. Jones: 2010, The downstream impact of tropical cyclones on a developing baroclinic wave in idealized scenarios of extratropical transition. *QJRMS*, **136**, 617–637.

Riemer, M., S. C. Jones, and C. A. Davis: 2008, The impact of extratropical transition on the downstream flow: An idealized modelling study with a straight jet. *QJRMS*, **134**, 69–91.

Roberts, N. M.: 2000, The relationship between water vapour imagery and thunderstorms. *JCMM internal report*, 40pp.

Romero, R., G. Sumner, C. Ramis, and A. Genoves: 1999, A classification of the atmospheric circulation patterns producing significant daily rainfall in the Spanish Mediterranean area. *International Journal of Climatology*, **19**, 765–785.

Rosmond, T. E., J. Teixeira, M. Peng, T. Hogan, and R. Pauley: 2002, Navy Operational Global Atmospheric Prediction System (NOGAPS). *Oceanography*, **15**, 99–108.

Rossby, C. G.: 1939, Relation between variations on the intensity of the zonal circulation of the atmosphere and the displacements of the semi-permanent centers of action. *J. Mar. Res.*, **2**, 38–55.

— 1940, Planetary flow patterns in the atmosphere. *Quart. J. Roy. Meteor. Soc.*, **66**, 68–87.

Rosting, B. and J. E. Kristjansson: 2008, A successful resimulation of the 7-8 January 2005 winter storm through inital potential vorticity modification in sensitivie regions. *Tellus*, **60A**, 604–619.

Sardeshmukh, P. D. and B. J. Hoskins: 1988, The generation of global rotational flow by steady idealised tropical divergence. *Journal of Atmospheric Science*, **45**, 1228–1251.

Schlemmer, L., O. Martius, M. Sprenger, C. Schwierz, and A. Twitchett: 2010, Disentangling the forcing mechanisms of a heavy precipitation event along the Alpine south side using potential vorticity inversion. *Monthly Weather Review*, **138**, 2336–2353.

Schwierz, C., S. Dirren, and H. C. Davies: 2004, Forced waves on a zonally aligned jet stream. *Journal of the Atmospheric Sciences*, **61**, 73–87.

Shapiro, M. A. and A. J. Thorpe: 2004, *THORPEX International Science Plan*. version 3 edition.

Shapiro, M. A., H. Wernli, J. W. Bao, J. Methven, X. Zou, J. Doyle, T. Holt, E. Donall-Grell, and P. Neiman: 1998, *The Life Cycles of Extratropical Cyclones*, Amer. Meteor. Soc., chapter A Planetary-scale to mesoscale perspective of the life cycles of extratropical cyclones: the bridge between theory and observations. 139–185.

Slingo, J. M.: 1998, Extratropical forcing of tropical convection in a northern winter simulation with the UGAMP GCM. *Quart. J. Roy. Meteor. Soc.*, **124**, 27–51.

Sodemann, H., A. S. Palmer, C. Schwierz, M. Schwikowski, and H. Wernli: 2006, The transport history of two Saharan dust events archived in an Alpine ice core. *Atmospheric Chemistry and Physics*, **6**, 667–688.

Stoelinga, M. T.: 1996, A potential vorticity-based study of the role of diabatic heating and friction in a numerically simulated baroclinic cyclone. *Monthly Weather Review*, **124**, 849–874.

Szunyogh, I., H. Wernli, J. Barkmeijer, C. H. Bishop, E. Chang, P. Harr, S. Jones, T. Jung, N. Kitabatake, P. Knippertz, S. Maeda, S. Majumdar, C. Schwierz, O. talagrand, and F. Vitart: 2011, Recent developments in predictability and dynamical processes (PDP) research: A report by the THORPEX PDP working group. *BAMS*, submitted.

Thorncroft, C. D., B. J. Hoskins, and M. E. McIntyre: 1993, Two paradigms of baroclinic-wave life-cycle behaviour. *Quart. J. Roy. Meteor. Soc.*, **119**, 17–56.

Thorpe, A. J. and K. A. Emanuel: 1985, Frontogenesis in the presence of small stability to slantwise convection. *J. Atmos. Sci.*, **42**, 1809–1824.

Torn, R. D.: 2010, Diagnosis of the downstream ridging associated with extratropical transition using short-term ensemble forecasts. *Journal of Atmospheric Science*, **67**, 817–833.

Tripoli, G. J., C. M. Medaglia, S. Dietrich, A. Mugnai, G. Panegrossi, S. Pinore, and S. E. A.: 2005, The 9-10 November 2001 Algerian flood. *Bulletin of the American Meteorological Society*, **86**, 1229–1235.

Vukicevic, T. and K. Raeder: 1995, Use of an adjoint model for finding triggers for Alpine lee cyclogenesis. *Monthly Weather Review*, **123**, 800–816.

Wernli, H. and C. Schwierz: 2006, Surface cyclones in the ERA-40 dataset (1958-2001). Part i: Novel identification method and global climatology. *J. Atmos. Sci.*, **63**, 2486–2507.

Wernli, H. and M. Sprenger: 2007, Identification and ERA15 climatology of potential vorticity streamers and cut-offs near the extratropical tropopause. *J. Atmos. Sci.*, **64**, 1569–1586.

Wiegand, L., A. Twitchett, C. Schwierz, and P. Knippertz: 2011, Heavy precipitation at the Alpine south side and Saharan dust over central Europe: A predictability study using TIGGE. *Weather and Forecasting*, **26**, 957–974.

Wigley, T. M. L., J. M. Lough, and P. D. Jones: 1984, Spatial patterns of precipitation in England and Wales and a revised, homogeneous England and Wales precipitation series. *Journal of Climatology*, **4**, 1–25.

Wu, C. C., J. H. Chen, P. H. Lin, and K. H. Chou: 2007, Targeted observations of tropical cyclone movements based on the adjoint-derived sensitvity steering vector. *Journal of the Atmospheric Sciences*, **64**, 2611–2626.

Wu, C. C., S. G. Chen, J. H. Chen, K. H. Chou, and P. H. Lin: 2009, Interaction of Typhoon Shanshan (2006) with the midlatitude trough from both adjoint-derived sensitivity steering vector and potential vorticity perspectives. *Monthly Weather Review*, **137**, 852–862.

Zdunkowski, W. and A. Bott: 2004, *Dynamics of the Atmosphere: A course in theoretical meteorology*. Cambridge University Press.

Zou, X. and Q. Huang, W. adn Xiao: 1998, A User's guide to the MM5 adjoint modeling system. NCAR Tech., note NCAR/TN-437+IA.

Zou, X., F. Vandenberghe, M. Pondeca, and Y. H. Kuo: 1997, Introduction to adjoint techniques and the MM5 adjoint modeling system. NCAR Tech., note NCAR/TN-435+IA.